ERRATA

DP 1579

NUMERICAL SIMULATION OF EARTHQUAKE EFFECTS ON TUNNELS FOR GENERIC NUCLEAR WASTE REPOSITORIES

BY

K. K. Wahi, B. C. Trent, D. E. Maxwell, R. M. Pyke,
C. Young, and D. M. Ross-Brown

Table 1 (p. 57) lists the peak velocities of the mine tremor (East Rand Proprietary Mines) as 1.47, 0.97, and 1.23 cm/sec; however, the velocity used for excitation of the model was higher by a factor of about 100, as it was entered as m/sec. The actual recording was for an aftershock (M=1.45) which provided the velocities given in the table. The main event was thought to be magnitude 3.7 and it is conceivable would have had a velocity history very similar to the one that was actually used to excite the model. Thus the effects obtained should more properly be associated with an earthquake of magnitude 3.7 rather than with M=1.45.

This error was discovered and confirmed by C. H. Dowding, R. M. Pyke, and K. K. Wahi.

IWM:pmc
Disc 7

DP-1579
Distribution Category UC-70

NUMERICAL SIMULATIONS OF EARTHQUAKE EFFECTS ON TUNNELS FOR GENERIC NUCLEAR WASTE REPOSITORIES

by

K. K. Wahi, B. C. Trent, D. E. Maxwell, R. M. Pyke,
C. Young, and D. M. Ross-Brown

Science Applications, Inc.
Fort Collins, Colorado

A report prepared for the Savannah River Laboratory.

Approved by

E. L. Albenesius, Research Manager
Waste Disposal Technology

Publication Date: December 1980

E. I. du Pont de Nemours & Co.
Savannah River Laboratory
Aiken, SC 29808

PREPARED FOR THE U. S. DEPARTMENT OF ENERGY UNDER CONTRACT DE-AC09-76SR00001

PREFACE

The National Waste Terminal Storage (NWTS) program of the Department of Energy (DOE) has the goal of locating, developing, and operating several underground repositories for the permanent disposal of nuclear waste from commercial nuclear power reactors. As part of this program the Savannah River Laboratory (SRL), operated by E. I. du Pont de Nemours and Company, is conducting several programs of geologic research that are of generic applicability. Some of these studies are on the subsurface effects of earthquakes, particularly for a mined opening. Reports on two such studies in this program conducted by Terra Tek, Inc. have already been published.

1. Pratt, H. R., W. A. Hustrulid, and D. E. Stephenson. "Earthquake Damage to Underground Facilities," USDOE Report DP-1513, E. I. du Pont de Nemours & Co., Savannah River Laboratory, Aiken, South Carolina (1978).

This report documents reported damage to tunnels and shallow underground openings, mines and deep openings, and wells and vertical openings. Its general conclusion is that underground damage due to earthquakes is significantly less than surface damage for the same size earthquake.

2. Pratt, H. R., G. Zandt, and M. Bouchon. "Earthquake Related Displacement Fields Near Underground Facilities," USDOE Report DP-1533, E. I. du Pont de Nemours & Co., Savannah River Laboratory, Aiken, South Carolina (1980).

This report discusses block motion-displacement phenomena, joint displacement as a function of angle and distance from the focus of an earthquake, magnitude of displacement as a function of depth and distance from the focus, and the effect of the medium on displacement spectra.

Although damage in the ordinary sense of the word, i.e., roof falls, broken machinery, broken pipe lines, etc., will be of interest during the operational phase of the repository, in the long term, greater interest will be in seismic damage that causes cracks that may enhance the permeability and the potential movement of ground water. As a result of this interest, the Savannah River Laboratory (SRL) contracted with Science Applications, Inc. (SAI) to begin with state-of-the-art numerical techniques and develop a numerical method of simulating the seismic effects of several selected earthquakes on repository tunnels in selected rock types -- salt, granite, and shale. This study emphasizes fracturing in the adjacent rock, although it also predicts deformation and displacement at the tunnel walls.

A two-volume report (Volume I - Main Report; Volume II - Appendices) presenting the results of the numerical simulation of earthquake effects on waste repository tunnels was completed by SAI in February, 1980. That report contains full details of the material models used, the numerical simulations performed, and the analysis of the results. It is expected to be of interest to rock mechanics and numerical modeling specialists.

This report is an abbreviated version of that two-volume report and is designed for the more general reader. The assumptions, input data, material properties, and the results are included in reasonable detail, while the calculational techniques and modeling effort are only briefly described. If after reading this abbreviated report more information is required, reference should be made to the more detailed report which is available from the SRL Technical Information Service group.

The study was performed in two phases. Linear elastic calculations were performed in Phase I to develop the necessary boundary conditions for accurately transmitting the seismic waves across the calculational mesh and for obtaining information on the response of the tunnel to different types of motions. Although these Phase I calculations were a necessary stepping stone to the fully nonlinear simulations carried out in Phase II, they are only briefly referred to in this abbreviated version of the report. This report, therefore, concentrates on the Phase II nonlinear calculations for waste repositories in the three different rock types considered.

I. Wendell Marine, Senior Research Associate, Geology

E. I. du Pont de Nemours & Co.
Savannah River Laboratory
Aiken, SC 29808

ABSTRACT

The objectives of this generic study were to use numerical modeling techniques to determine under what conditions seismic waves generated by an earthquake might cause instability to an underground opening, or cause fracturing and joint movement that would lead to an increase in the permeability of the rock mass.

Three different rock types (salt, granite, and shale) were considered as host media for the repository located at a depth of 600 meters. Special material models were developed to account for the nonlinear material behavior of each rock type. The sensitivity analysis included variations in the <u>in situ</u> stress ratio, joint geometry, pore pressures, and the presence or absence of a fault. Three different sets of earthquake motions were used to excite the rock mass.

The calculations were performed using the STEALTH codes in a three-stage process as follows:

a. An excavation and heating phase to load the model with the correct thermomechanical stress history (quasi-static; involving several years of simulated time).

b. A stabilizing stage to bring the model into equilibrium prior to the earthquake.

c. An earthquake phase (dynamic, with time increments that were less than a milli-second).

It was concluded that the methodology is suitable for studying the effects of earthquakes on underground openings. In general, the study showed that moderate earthquakes (up to 0.41 g) did not cause instability of the tunnel or major fracturing of the rock mass.

A rock-burst tremor with accelerations up to 0.95 g, however, was found to be amplified around the tunnel, and fracturing occurred as a result of the seismic loading in salt and granite. In shale, even moderate seismic loading resulted in tunnel collapse. Other questions appraised in the study include the stability of granite tunnels under various combinations of joint geometry and <u>in situ</u> stress states, and the overall stability of tunnels in shale subject to the thermomechanical loading conditions anticipated in an underground waste repository.

CONTENTS

LIST OF TABLES

LIST OF FIGURES

LIST OF FIGURES (Cont'd)

LIST OF FIGURES (Cont'd)

LIST OF FIGURES (Cont'd)

NUMERICAL SIMULATIONS OF EARTHQUAKE EFFECTS ON TUNNELS FOR GENERIC NUCLEAR WASTE REPOSITORIES

I. INTRODUCTION

General

The geologic environment offers a potential for isolating radioactive waste from the biosphere for the centuries that the waste remains hazardous. In designing and engineering a nuclear waste repository in the geologic environment, many geotechnical factors have to be considered. Included in these considerations are the response of the subsurface facility to mechanical, thermal, and seismic stresses. Geohydrology is an important geotechnical consideration because movement of ground water offers the largest potential for transport of radioactive species away from the confines of the repository.

Designs currently under consideration for a nuclear waste repository incorporate a multiplicity of barriers to insure geologic and hydrologic containment. The succession of independent engineered barriers includes the waste form, the canister, the backfill, and the host rock. Of these, engineering will have the least effect on the host rock properties. Extensive geotechnical studies will qualify the site and region in terms of present and anticipated conditions. As part of these studies the subsurface effects of earthquakes need to be better understood.

Hazards Due to Earthquakes

To date very little is known about the effects that an earthquake might have on the rock mass surrounding an underground opening. For instance, it is possible that the passage of seismic waves could cause additional fracturing and/or small displacements along existing fractures. In mining, such changes would be insignificant when compared to the changes brought about by the extraction process itself. Consequently, the problem has received virtually no attention to date.

The effects of earthquakes can be divided into short-term effects (during the operational phase of the repository) and long-term effects (after decommissioning). The worst case, during the operational phase, would be the collapse of the underground tunnels or shafts leading to accidents, loss of life, and possible radioactive leakage from damaged canisters. After decommissioning, the worst case would probably be the creation of new fractures or the opening of existing ones that might adversely affect the ground water flow patterns as well as cause breakdown of one or more of the engineered barriers.

Purpose of the Study

The objectives of this generic study were to use numerical modeling techniques to determine the conditions under which seismic waves generated by an earthquake might:

1. Cause collapse or other structural failure of underground openings.

2. Create new fractures or affect old fractures in the rock mass surrounding a repository in such a way as to increase permeability and water circulation.

Scope of Work

Three different host-rock materials were specified for consideration: namely, salt, granite, and shale. The repository was considered to be located at a depth of about 600 meters, and it was required that three different earthquake motions would be selected for the study. Two in situ stress conditions were specified, namely, lithostatic loading, and loading with the maximum or minimum stress in the horizontal direction. The analysis required accurate modeling of the rock-mass response with and without existing fractures, and with and without water saturation.

The study was divided into two phases. The first phase included the modeling of an opening in each of the three rock types assuming conditions of a homogeneous, unfractured, linear-elastic, unsaturated rock mass. These models were subject to free-field accelerations using an actual earthquake record.

In the second phase, nonlinear material behavior was taken into account. In salt, creep and tensile fracture were included as part of the material behavior. In granite and shale, joint slip as well as tensile fracture were allowed. Material anisotropy of shale was also included. An appropriate plasticity model was defined in each of the rock types. The sensitivity analysis consisted of three different earthquake records, variations in the in situ stress ratio, presence or absence of a shear zone, presence or absence of a heat source, joint-geometry variations, and variations in pore pressure.

Previous Investigations

A fairly comprehensive field study of earthquake damage to underground structures was completed by Rozen (1976). After examining the data from more than seventy case histories, Rozen found that there was no damage with peak accelerations up to 0.19 g, and only occasional minor damage up to accelerations of 0.25 g. Even above 0.25 g, damage appeared to be minor (falling of loose stones, cracking of bricks and concrete linings) up to an acceleration of 0.7 g. No case of collapse was associated with accelerations of up to 0.7 g. In general, distortions and local collapse were observed to be associated with fault displacement and by landslides close to the tunnel portals.

Additional case histories of damage to underground mines and wells were included in a study by Pratt et al. (1978). In addition to extending the data base, the report considers the various response mechanisms of underground openings to seismic waves. The conclusions with regard to reported damage of underground openings are similar to those reached by Rozen (1976).

An analytical study concerning the dynamic response of underground cavities to earthquake loads was carried out by Glass (1973). To our knowledge, prior to the present study, no attempt has been made to model the response of an underground opening using actual earthquake records (two components) and nonlinear material models.

II. PROBLEM DEFINITION

General

The intent of this study is to employ state-of-the-art modeling techniques to simulate underground repository response for the first five years or so of the life of a repository that is also subjected to a seismic event. A number of assumptions and idealizations are necessary to quantify the physical problem into a numerical model that can then be used for various parametric evaluations. The definition of the problem for the purpose of modeling consists of choosing representative:

1. Geometry.
2. Material property descriptions.
3. Initial conditions and boundary conditions.
4. Failure mechanisms.
5. Seismic motions.

Earthquake Motions

Because earthquakes are random events, a considerable amount of judgment is involved in obtaining a suitable set of input motions for a specific design. The strong motions reaching a site are dependent on many factors such as the source mechanism, the propagation path geology, and the local site conditions.

After a certain amount of research, three records from rock sites were selected as input for this study. For each record, the vertical velocity history together with the horizontal velocity history (with the greater maximum amplitude) was used to excite a 52 m x 52 m grid containing an idealized, 8 m x 8 m underground opening.

Selection of Input Motions For This Study

In choosing appropriate acceleration histories, particular consideration was given to the presence of higher frequencies, because sample calculations showed that for the dimensions of the tunnels considered in this study, it is the higher frequency motions that are more apt to cause damage. Then, assuming that it is possible to identify all possible sources of larger magnitude earthquakes and site the repository away from them, it is the smaller magnitude, close-in earthquakes that are of most concern, as these will have a relatively large high-frequency content. From the available strong-motion acceleration histories, the following three records were chosen as candidates for use in this study:

1. The Temblor record of the 1966 Parkfield, California, earthquake.

2. The CDMG-6 record of an aftershock of the 1975 Oroville, California, earthquake.

3. One of a number of mine tremors recorded early in 1978 at the East Rand Proprietary Mines (ERPM) in South Africa by A. McGarr of the U.S. Geological Survey.

Note that both the Temblor and the Oroville records were obtained at stations located on rock. Because there were no satisfactory records of the main Oroville event, the best of the Oroville aftershocks was chosen. The aftershocks were recorded as result of subsequent instrumentation installed by the California Division of Mines and Geology (CDMG).

Information regarding these records is summarized in Table 1. As part of this study, velocity histories and Fourier spectra were computed from the acceleration histories. The acceleration histories for the respective records are shown in Figures 1-3. Note there are different scales for both ordinate and abscissa for several of the figures.

The mine tremors recorded by McGarr were recorded using accelerometers having better high-frequency response characteristics than standard strong-motion accelerometers. Peak accelerations of up to 5 g were recorded at high frequencies, and the peak accelerations for the record used in this study are of the order of 1 g. The corresponding peak velocities and displacements are quite small, but it is believed that these records may provide an upper boundary for the high frequency content. It has previously been reported (Spottiswoode and McGarr, 1975) that mine tremors appear to have the same characteristics as natural crustal earthquakes.

The three records listed in Table 1 are considered to be representative of the earthquake motions that are likely to produce the most severe loading on an underground facility with relatively small shaft and tunnel sizes.

In the Phase 1 work, only the Oroville aftershock record was used. The larger horizontal component and the vertical component were applied to the numerical model of the tunnel and surrounding rock mass as planar waves representing P- and S-waves, respectively.

In the Phase 2 studies, the tunnel in salt was excited using all three records (i.e., the Oroville, Temblor, and ERPM records), the granite was excited by means of the Oroville and ERPM records, and shale was excited by means of the Oroville record. The actual components used are listed below:

Oroville Aftershock:	S55E	(P-wave)
	Vertical	(S-wave)
Temblor (Parkfield):	S25W	(P-wave)
	Vertical	(S-wave)
ERPM Mine Tremor:	Longitudinal	(P-wave)
	Vertical	(S-wave)

The ERPM mine tremor was baseline corrected for this study by a frequency-domain technique developed by Lysmer (1979) at the University of California at Berkeley. The Oroville and Parkfield records were corrected for instrument characteristics and baseline, with procedures developed at the California Institute of Technology.

Underground Geometry

From the draft Generic Environmental Impact Statement (draft GEIS) prepared by the Office of Waste Isolation (ONWI, 1978), an 8-m x 8-m square opening was selected as being typical of the various repository designs, and this geometry was incorporated into the explicit, finite-difference, numerical simulations of the earthquake response in all three rock types. The floor of the tunnel was located at a depth of 600 m below the surface.

Geology and Material Properties

Three different rock types were specified for evaluation in this study, namely: salt, granite, and shale. Information contained in the draft GEIS (OWI, 1978) was used as a basis for the material property data.

Although most material properties are temperature dependent to some extent, the data base is generally poor. Hence, with the exception of thermal conductivity, temperature effects on material properties were not accounted for during this study. The variation of mechanical properties with temperature is very important, however, the degradation of mechanical properties with increasing temperature is very likely to be within the scatter of the available data at a given temperature.

In Situ Stress

The vertical overburden stress was calculated using a value of 2.3×10^4 Pa per meter of depth (approximately 1 psi per foot of depth). The density of the particular rock type being modeled was used to compute the vertical stress gradient within the mesh. The horizontal stress (initial and boundary) was prescribed to be a function of the vertical stress according to the following equation:

$$\sigma_H = f \times \sigma_V$$

where f was 0.5, 1.0, 1.5, or 2.0 depending on the particular case being analyzed.

Geothermal Gradient

A geothermal gradient of 0.033°C per meter of depth was used to obtain an average ambient temperature of 35°C throughout the mesh, assuming a surface temperature of 15°C.

Thermal Source Description

The waste was assumed to be 10-year-old spent fuel (SURF). A thermal load density of 60 kW/acre was employed. If the center-to-center distance between tunnels is 52 m and the canisters are rated at 5 kW, the canisters would be spaced 6.5 m apart down the centerline of the tunnel floor.

A plane-strain assumption in all the simulations implied a continuous heat source. A square cross-section, represented by four contiguous zones, described the heat-source region. The heat generation rate for each of these zones was such that the total heat output was equivalent to an infinite number of 5 kW canisters placed 6.5 m apart. The decay rate is defined by:

$$\dot{Q}/\dot{Q}_o = [(559 - 19.6t) + 0.52t^2]/558$$

where t is time in years, and $\dot{Q}$ and $\dot{Q}_o$ are the instantaneous and the initial heat generation rates, respectively.

Pore Pressures

Both dry and wet conditions were simulated in the study. Pore pressures were assumed to reach equilibrium at the time of excavation in these calculations.

Sequence of Events

The following sequence of events was assumed in the fully nonlinear calculations:

(a) The tunnel is excavated instantaneously and the appropriate in situ boundary stress conditions are applied. The model begins to come to equilibrium under the applied stresses.

(b) The canisters are emplaced 6 months after tunnel excavation.

(c) The earthquake hits the tunnel 4.5 years after waste emplacement (i.e. total elapsed time = 5.0 years), when the stress gradients (rather than absolute temperature) are likely to be approaching their maximum. This is also within the retrievability period, so that the tunnel is not backfilled. There is no ventilation through the tunnel for the purpose of these calculations.

Anticipated Response Mechanisms

In the nonlinear calculations, the principal stress difference, $\Delta\sigma_p$ and deviatoric stress tensor, $\sqrt{J_2'}$, were chosen as a measure of the "potential for fracture" of the rock mass. These are defined below:

$$\Delta\sigma_p = |\sigma_1 - \sigma_3|$$

$$\sqrt{J_2'} = \frac{3}{2} \left[(S_{xx}^2 + S_{yy}^2 \quad S_{zz}^2) + 3\tau_{xy}^2\right]^{1/2}$$

where σ_1 is the maximum principal stress.

σ_3 is the minimum principal stress

τ_{xy} is the shear stress in the xy plane

S_{xx} etc. are the stress deviators

In addition to $\Delta\sigma_p$ and $\sqrt{J_2'}$, other parameters were used to provide a more direct measure of failure (or potential failure). For instance, certain variables of the CAVS Tensile Model that indicate the number of cracks as well as the void strain in 3 orthogonal directions, and certain variables in the Joint Slip Model provided other forms of damaged criteria. Thus, the repository response evaluation was performed by analyzing the data for velocity, $\sqrt{J_2'}$, $\Delta\sigma_p$, the CAVS parameters, and the joint slip parameters.

III. CALCULATIONAL TECHNIQUES USED

General

The general philosophy with respect to the numerical calculations in Phase 1 was to utilize linear-elastic material properties and observe concentrations of certain stress-related variables that may lead to nonlinear behavior in real materials. The computer codes used are explicit finite-difference programs. Explicit refers to the method of solution of the equations of motion for a given grid point within the calculational mesh. Only grid points and zones immediately adjacent to the grid point in question influence its subsequent response. This may be contrasted to implicit solutions which require the simultaneous solution of many or all of the motion (or energy) equations for the entire grid.

Because the problem of modeling acceleration time histories is in the time domain rather than the frequency domain, explicit formulations are preferable. Further, explicit finite-difference techniques are better suited for nonlinear material modeling. In Phase 2, the material models are nonlinear in general, and failure criteria are also applied so that parameters other than stress (or stress-dependent quantities) can be used to evaluate and analyze the results.

The LESS Code

The numerical code LESS 2-D (Linear Elastic Small Strain) was used in the Phase 1 test calculations. It is a much smaller and faster version of STEALTH 2-D, (Hofmann, 1976), because the the general equations of continuum mechanics for a two-dimensional (2-D) formulation are significantly simplified for linear-elastic, small-strain, constitutive models.

The STEALTH Code

After some preliminary test calculations, the numerical code STEALTH (Solids and Thermal-Hydraulics code for EPRI Adapted from Lagrange TOODY and HEMP) was utilized for the more comprehensive analyses. The principal reason for using STEALTH was its ability to simulate nonlinear material behavior accurately and to provide simultaneous thermal and mechanical solutions. The STEALTH code makes no simplifying assumptions about the strains having to be small.

The necessary material models for the STEALTH calculations are: an equation-of-state (mean properties), a strength model (deviatoric mechanical properties), and heat transfer properties.

Extensive output and display capabilities are available to be used in conjunction with STEALTH. A sophisticated plotting package called GRADIS (GRAphic DISplay) can provide time histories, spatial snapshots, mesh configuration plots, and contour, vector, and tensor plots. Several modes of printed output are also available.

Boundary Conditions

The simulation of earthquake response in this investigation was essentially a problem of establishing the appropriate mechanical boundary conditions. The influence of thermal loading is a relatively straightforward modification to STEALTH. One effective way of modeling an open structure within a continuum is to place the boundaries of the mesh far enough from the opening such that the assumed, idealized, boundary conditions introduce a negligible error in the simulated response. Another way would be to attempt to emulate a nonreflecting boundary without using large overall dimensions. Two different methods were utilized for the two codes, LESS 2-D and STEALTH 2-D, as described in the next subsection.

Simulation of Earthquake Motions

After the boundary isolation problem had been resolved, the motion of the boundary then had to be determined. Two types of motion were studied in this investigation: 1) simple harmonic oscillation representing frequencies of interest, and 2) actual earthquake velocity history data. Type 1 consisted of a simple trigonometric function, while Type 2 was defined by a tabular relationship between velocity and time. The velocity-time history information was obtained by integrating actual accelerograms recorded from seismic events.

Time-Step Scaling

In Phase 2, all calculations involve a heating phase (with the exception of Case 4 in salt, which is a sensitivity case to analyze the absence of thermal loading) to simulate the heat released by the buried waste for approximately five years. In that period, the high-frequency response is not of interest, but instead the quasistatic response due to the changing thermal stress environment is desired. For that reason and to keep the computational costs to a reasonable limit, a time-step scaling technique is employed, in which a pseudo time-step is defined that is used in the equations of motion. Unlike density scaling, time-step scaling allows temporal as well as spatial variation in the effective scale-factor. However, an upper limit to the magnitude of scaling is imposed due to the thermal diffusion process which must occur on a real-time scale. In general, the computed thermal time-step is several orders of magnitude higher than the mechanical time-step for a given zone dimension. It was neither necessary nor desirable to use time-step scaling in the second (equilibrium) or the third (earthquake) phase of each calculation.

Dynamic Relaxation

Whether time-step scaling is used or not, it is customary in quasi-static calculations to use some form of damping that will either critically damp or slightly underdamp the system response. In the STEALTH codes, this damping is applied to the velocity calculation. The magnitude of the damping frequency can be obtained analytically for simple geometries. For complex geometries, an auxiliary simulation without damping is first run long enough to obtain the fundamental frequency from which a damping frequency is determined. This damping frequency can then be used in the simulation.

In these calculations, dynamic relaxation was applied in the first and second phase of each calculation. The earthquake phase was not damped because the dynamic response was desired in that instance.

IV. REPOSITORY SIMULATIONS

Calculations Assuming a Linear-Elastic Rock Mass

Linear elastic stresses were calculated with the LESS code for each rock type during the early stages of the study. These calculations developed the necessary boundary conditions to transmit accurately the seismic waves across the mesh, and to obtain desired information on the response of the tunnel to different types of motions. The results of this work (Phase 1) can be summarized as follows:

1. A philosophy was developed with regard to the selection of input motions, and three strong motion records recorded in rock or on rock outcrops were selected for the study.

2. The LESS and STEALTH codes were modified to simulate earthquake propagation accurately through a two-dimensional (2-D) grid.

3. The LESS code was used to scope the response of single and multiple openings to different kinds of artificial motions, including some at high frequencies.

4. The Oroville aftershock record of August 11, 1975, was used in linear elastic STEALTH formulations, representing openings in salt, granite, and shale.

5. The effect of the earthquake on the opening was monitored by a series of snapshots of the spatial distribution of the maximum principle stress difference, $\sigma_1 - \sigma_3$, and the second invariant of stress, I_2. The results demonnstrated that the methodology is suitable for studying the effects of earthquake motions on the rock mass surrounding an underground opening.

Nonlinear Simulations with STEALTH 2-D

The objective of the second phase of the progrem was to apply the methodology developed in Phase 1 to study the potential contributors to repository failure using fully nonlinear material models. This involved developments in several areas, the most important being:

1. Development of representative material models and failure criteria for salt, granite, and shale.

2. Introduction of thermal heating effects, including stress field perturbations and material property degradations, into the models.

3. Introduction of fluid pore-pressure effects into the material and failure models.

4. Development of criteria for evaluating the impact of nonlinear behavior upon overall repository performance and possible failure of the repository.

Each case investigated involves three phases. The first phase is quasi-static, in which heat from the buried waste (SURF) is the driving force for a number of years. The second phase is an equilibrium phase in which the residual velocity field at the end of the heating phase is nearly eliminated. The third phase is the dynamic response due to an earthquake. In all phases, the appropriate nonlinear material models are included. For example, in salt the CAVS Tensile Failure and the Creep models are applied.

The complexity of the nonlinear calculations was at least an order of magnitude higher than that of the linear elastic case for which sensitivity analyses were relatively simple and quick to perform. Additional complexities were introduced by heating and pore-pressure effects.

Assumptions Common to All Rock Types

The calculational grid is shown in Figure 4, and the assumptions common to all rock types are summarized in Table 2.

Development of Material Models

A simplified flow-chart for STEALTH is shown in Figure 5. For this project, major changes were made only to the Stress-Strain Constitutive Equations, i.e., to that part of the calculational sequence that relates the Strain Tensor to the Stress Tensor.

Figure 6 is an enlarged picture of the area between the Strain Tensor and the Stress Tensor in Figure 5. It shows how the calculations are broken up into two parts according to changes brought about by the mean stress and the stress deviator components. Figure 6 also shows how these components are affected by temperature and dilatancy.

An enlargement of the "Stress Deviator Update" box of Figure 6 is shown as Figure 7. It includes seven material models, all or some of which can be used to describe the geologic material(s) in a nuclear waste repository.

Referring to the material models shown in Figure 7, the Isotropic Elastic Material Model is generally used to model the elastic behavior of materials. An Anisotropic Elastic Material Model, however, was developed as part of this project for application to materials such as shale.

Isotropic Plastic Material Models are already incorporated into STEALTH. (Although an Anisotropic Plastic Material Model was developed for shale, it was not used because it had not been tested sufficiently).

The joint geometry for the Joint Slip Model consists of an orthogonal jointing system in the calculational plane, which is defined by the following three parameters (see Figure 8):

β_1 Orientation of Joint Set 1 (the second joint set has an orientation of (β_1 + 90°).

h_1 Spacing of Joint Set 1

h_2 Spacing of Joint Set 2

Because STEALTH is a continuum code, only the <u>effect</u> of joints can be modeled. This is achieved by adjusting the stresses in the direction of the joint orientations to simulate the effect of discontinuities. The model simulates slip along the joints and takes dilation effects into account. It also distinguishes between initial slip and subsequent slip, and keeps track of the total and relative displacement of each joint as the blocks move back and forth.

The CAVS Tensile Failure Model allows new cracks to initiate and propagate, and also monitors the opening and closing of the existing and the new cracks. This model is also a mathematical tool which allows discontinuous behavior to be modeled within STEALTH. The combinations of material models (Figure 7) that represent each rock type are listed below:

SALT

A. Isotropic Elastic
C. Isotropic Plastic
F. CAVS Tensile
G. Creep

(It is assumed that initially there are no joints in the salt, but tensile cracking can occur as the calculation proceeds. Pore pressures do not exist.)

GRANITE

A. Isotropic Elastic
B. Isotropic Plastic
E. Joint Slip
F. CAVS Tensile

(The granite has an initial joint pattern. For the cases that model pore-pressure effects, the joints are assumed to be saturated and have a hydrostatic pressure; near the tunnel, however, the pressures are reduced according to the proximity to a free surface. Creep does not occur.)

SHALE

B. An Isotropic Elastic
C. Isotropic Plastic
E. Joint Slip
F. CAVS Tensile

(Assumptions are similar to those for granite, with the addition of anisotropic material and joint properties parallel and normal to bedding.)

Modeling of Discontinuities

Any rock mass that contains discontinuities is significantly more complicated to model than an homogeneous, isotropic, rock mass such as dome salt or even bedded salt formations. Our philosophy in modeling the more complicated rock types was to isolate the physical mechanisms that are thought to influence rock mass behavior significantly. One of these mechanisms, namely tensile failure, is accounted for in the CAVS submodel which has been successfully used as a failure model in other calculations. At the time of this investigation, CAVS was still in a developmental stage. The only input parameters to this model were an intact rock tensile strength and a propagation strength. The crack initiation strength was taken directly from the draft GEIS

(OWI, 1978), and an arbitrary value (one-half of the initiation strength) was chosen for the propagation strength.

In addition to tensile failure, a model was included that would simulate joint-slip along prescribed joint sets. No such model existed that was appropriate for an explicit finite-difference code; therefore, all aspects of the new submodel had to be developed anew. The quantitative reliability of the model was limited due to a limited data base. The Joint Slip submodel was tested with simple test geometries to provide a comparison with direct shear experimental data. The emphasis was to keep the model relatively simple and yet include all the important features. The chosen parameters appear to be reasonable for the selected rock types.

Material Properties for Salt

The material properties and in situ stresses in the salt calculations are shown in Table 3.

Values for the Elastic Modulus and Poisson's ratio were taken from the draft GEIS (OWI, 1978), and converted into the Bulk Modulus and Shear Modulus values (given in Table 3) for input into the STEALTH code.

To describe plastic flow of a material it is necessary to have: (i) a yield function, (ii) a yield criterion, and (iii) a flow rule.

The yield function for most rocks can be represented by a Mohr-Coulomb type of yield surface. For salt, a constant yield function was chosen,

$$Y = 1 \times 10^8 \text{ Pa}$$

where Y is the yield stress in Pa. Plastic flow is allowed to occur when the equivalent stress exceeds the yield stress; this is a statement of the von Mises yield criterion (see Main Report, Vol. II). When the yield criterion is exceeded, stresses have to be adjusted (i.e., lowered) according to some flow rule such that the adjusted state of stress coincides with the yield surface. The flow rule chosen in these calculations is the nonassociated Prandtl-Reuss flow rule (see Main Report, Vol. II). In applying this flow rule, one effectively multiplies each component of the deviatoric stress tensor by the ratio of the yield stress to the equivalent stress. This ratio must be less than (or equal to) one in order for plastic flow to occur.

The CAVS submodel utilized a tensile strength of 1.55×10^6 Pa for the initiation of new cracks in salt. Once a crack had been started, it was assumed to propagate if the tensile stress across that crack remained in excess of 0.78×10^6 Pa. These data are summarized in Table 3.

The main feature of salt behavior, especially at elevated temperatures, is its ability to undergo creep. SAI, as part of an ongoing study for the Office of Nuclear Waste Isolation (Battelle Columbus), has developed a creep model which has been successfully used in the simulation of the Project Salt Vault experiment. It is a purely phenomenological model and is based on the laboratory experiments of Lomenick (1971) for determining the primary creep of salt. It does not have a wide range of proven applicability. Also, it does not account for tertiary creep, dilatancy, and any associated effects that may exist. The form of the model, however, does provide a framework from which a more complete model can be developed at a later stage. For the purpose of the present calculations, the creep model included in Table 3 appears to be quite adequate.

Material Properties for Granite

The material properties for granite, together with joint geometry and other data specific to the granite simulations, are given in Table 4.

From the draft GEIS (OWI, 1978), the following two elastic constants representative of the granite rock mass were taken:

Elastic Modulus: 2.5×10^6 psi (= 1.729×10^{10} Pa)

Poisson's Ratio: 0.18

These constants were converted into the Bulk Modulus and Shear Modulus quoted in Table 4.

For the Isotropic Plastic Model, the following yield model was chosen for granite:

$$Y = \max(0); \min (1.0 \times 10^8, 2.83 \times 10^7 + 1.4 P)$$

where Y is the yield stress in Pa, and P is the pressure (or mean stress) in Pa.

The parameters used in the Joint Slip Model are summarized in Table 4 and discussed in Section 8.3 of the Main Report.

As previously indicated, only two input parameters were required for the CAVS model in addition to the two elastic constants which have already been defined. The appropriate virgin (initiation) tensile strength would be that for intact granite, and a value of 7×10^6 Pa was taken from the draft GEIS (OWI, 1978). The ratio of initiation-to-propagation strength was arbitrarily chosen to be 2, which is thought to be a reasonable value.

Material Properties for Shale

The material properties for shale are summarized in Table 5. The main features of shale behavior that have been taken into account in the shale calculations are the existence of bedding plane joints (represented by closely-spaced, near-horizontal joints), the generally lower strength of the intact material, and the anisotropic behavior usually exhibited by shales.

An anisotropic elastic model was specifically developed for this study. A suitable anisotropic plastic model has not been developed yet; therefore, the isotropic plastic model specified in Table 5 was used. It is unlikely that a change in the plastic model from isotropic to anisotropic will have much of an effect on the results, because most of the anisotropic effects are taken into account in the Joint Slip Model.

Much of the discussion of the granite model applies to shale, for the same type of parameters are required for each rock type. Shale is a sedimentary rock and, as such, typically displays bedding plane joints and often one or two sets of cross-bedding joints. It must be emphasized at this point that material variability for shale is much greater than that for granite. Material property description of shale, therefore, requires a much higher degree of engineering judgment than that of granite. This should be kept in mind when interpreting the results of the shale calculations. Moderate changes in a few key parameters could probably change an unstable structure into a stable one and vice versa while keeping well within allowable values.

The Anisotropic Elastic Model for shale is fully described in Section 7.7 of the Main Report.

The discussion of the salt plasticity model applies here as well. The yield function chosen for shale is:

$$Y = \max (0), (3.0 \times 10^7 + 1.4P)$$

where P is in units of Pa.

Consistent with the discussion above concerning the extreme variability and complexity of shale as a material, the Joint Slip Model was made anisotropic in the sense that the two different joint sets were allowed to have different numerical values for the joint slip parameters (Table 6, and Section 7.7 of the Main Report).

The two elastic constants required in the CAVS Tensile Failure Model are a bulk modulus and a shear modulus. To be exact, one would have to use directonal moduli for an anisotropic material. However, isotropy was assumed with respect to tensile failure, and the following values were chosen.

Bulk modulus 1.65×10^9 Pa

Shear modulus 8.99×10^8 Pa

The initiation strength was taken from the intact shale properties in the draft GEIS (ONWI, 1978) to be 1.38×10^6 Pa. The ratio of initiation-to-propagation strength was taken to be 2, as for granite.

Representation of a Large Shear Zone in the STEALTH Code

A large shear zone was modeled (in a non-sophisticated manner) in one of the salt calculations. In Figure 9, the zones marked with x's represent the location of the shear zone. For these special zones, the following procedures were applied:

1. Stresses were rotated to the shear zone.

2. The shear stress in the shear zone was set equal to zero and the stresses were rotated back to the x-y plane.

3. The "CAVS" model was by-passed for these zones.

Criteria for Failure, Damage, and Permeability Enhancement

Failure and damage are terms that may be defined in several different ways, because there are no universal criteria or threshold limits applicable to the design of underground tunnels. The criteria will vary from problem to problem depending on the size of the tunnel, the *in situ* stress condition, the rock type, and the use to which the tunnel is put.

The primary criterion relates to whether the tunnel remains stable or not - this is referred to as the *failure criterion*, and is defined by relative displacement of the tunnel walls, roof, or floor.

The secondary criteria are damage criteria. Damage may be due to a number of causes such as fracturing, slippage along joints, or opening of existing joints or new cracks. Damage may be local and occur within a calculational zone or element (with dimensions of 2 m x 2 m for these calculations), or may occur on a regional-scale covering several zones. Major damage generally manifests itself as displacement of the tunnel walls. Damage need not necessarily lead to failure and may not be a cause for concern. Failure in its present context, however, cannot occur without damage due to one or more of the causes mentioned above.

For this particular application of repository tunnels, a third criterion, namely a permeability criterion is utilized. This is necessary to limit the flow of groundwater towards the waste canister and to inhibit the transport of radionuclides away from the canister, should the integrity of the canister be breached.

For the purpose of these calculations the failure, damage, and permeability criterion are defined as follows:

Failure occurs when the tunnel becomes unstable and starts to collapse. Failure is defined in terms of the displacement of the walls, roof, or floor in relation to the tunnel dimension being considered. It has been chosen as 5% for this study, i.e., if displacement of the tunnel dimension exceeds 5%, the tunnel has failed. In some of the calculations, there was a tendency towards accelerated slip, in which the tunnel walls would not have reached equilibrium again. This situation was considered as failure; if the calculations had been continued long enough, the failure criterion defined in terms of relative displacement would have been exceeded.

Damage refers to deleterious changes in the rock mass, which may or may not lead to failure of the tunnel. Three sub-criteria were used in the present analysis:

1. Damage caused by fracturing occurs on a local scale when at least one new throughgoing crack is formed within a zone. The new crack must cross the zone, i.e,. be at least 2 m long. (Note that by this definition, several small cracks would not constitute damage.)

2. The threshold for damage caused by slipping along joints has been chosen as 10 mm of slip per joint. This is based on our experience with these calculations which show that slipping in excess of 10 mm is required for failure of the tunnel to occur. (Note that any slipping of the joints will cause joint dilation and some damage

to the joint asperities; this small-scale damage is considered elsewhere and is related to the Maximum Joint Asperity Energy Damage in the Joint Slip Model.)

3. Damage caused by opening of joints or cracks occurs when any crack opening exceeds 2 mm (calculated from 0.1% void strain in a single crack within a given zone). Opening of the joints or cracks may occur due to dilation during slip of a single joint or due to tensile or shear forces within the rock mass.

The permeability criterion states that there should be no significant change in the permeability of the rock mass away from the immediate vicinity of the tunnel. This has been arbitrarily defined as "no permeability enhancement," because a 0.1% additional void strain or crack opening strain at two tunnel diameters (i.e., the rock mass more than 16 m away from the tunnel walls) is required. In addition, no new throughgoing cracks (even with zero permeability) are allowed to extend beyond this 16-m zone for the permeability criterion to be met.

Matrix of Calculations Performed

The matrix of calculations performed for salt is given in Table 6. Comparison runs were made for cases with and without heat, with and without a shear zone, and for three different sets of earthquake motions.

For the granite runs (Table 7), three different porepressure assumptions were applied, five different *in situ* stress states were analyzed, and data from two different earthquakes were applied.

The calculational matrix for shale is shown in Table 8, and it includes two pore-pressure assumptions.

V. DISCUSSION OF RESULTS

General

The results from the various cases analyzed in each of the three rock types are presented below. It should be kept in mind that all three materials have a tensile fracture criterion. Creep is allowed in salt only, and joint-slip is modeled in granite and shale. Repository evaluation is primarily based on slip response and fracture response, because they influence potential permeability changes.

A traveling seismic wave bundle that induces significant failure in a geologic medium must undergo substantial alteration by dispersion. A modified wave form that survives to travel large distances can, therefore, not induce failure in the medium until a discontinuity such as an underground opening is encountered. The earthquake boundary conditions that were applied in this study were applied without regard to compatibility with the media. Thus, failure regions near the boundaries of the computational grid probably indicate a non-real case. For example, if there is more salt creep or more joint slip at the boundaries than in the regions in the vicinity of the opening, then the assumed seismic boundary conditions are improbable for the selected medium.

The presence of joints generally reduces the tendency for additional tensile failure in the vicinity of an underground opening. This is particularly true for potential tensile failures normal to the joint planes. In this case, the compressive stress clamping the joint must go to zero before tensile failure can occur. The deviatoric stress is then reduced by the joint-slip motion. This decrease in deviatoric stress drives all the stress components near the value of the mean stress, which is almost always compressive due to the overburden contribution. There can be local exceptions due to geometric discontinuities such as at the corners of the openings.

In the following discussion, void volume refers to the difference between the total volume of a calculational zone and the volume of rock within the same zone. Void strain is the ratio of the void volume to the total volume ($V_S = V_V/V_T$). Dilatancy is the increase (or decrease) of volume associated with the shear deformation of rock joints.

The SI system of units has been used in these calculations. On the computer generated plots, SI units are implied unless stated otherwise. Furthermore, an exponent to the base ten is expressed as an 'E' followed by that exponent. For example, the number 1.5×10^3, 1.5E3, and 1500 are all equivalent.

Salt

Case 1 in salt is considered as the reference case for that material (see Table 6). A temperature contour map is shown in Figure 10. As expected, temperatures are essentially unchanged during the three seconds of the earthquake motion. Some cracks develop around the cavity during the heating phase. The crack distribution remains unchanged following the passage of the earthquake (Oroville record). A slight increase in the void strain associated with the cracks does occur as a consequence of the earthquake. An increase in the magnitude of void strain corresponds to an increase in permeability. Two locations at the tunnel surface have been chosen to compare the x- and the y-velocity histories of the various cases. Location 1 is the center of the roof (y-velocity at I = 14 and J = 16), and Location 2 is the center of the right wall (x-velocity at I = 16 and J = 14) as indicated on Figure 11. Both boundary velocity signals pass through the repository relatively unperturbed, suggesting that the response is essentially linear and no failure has occurred. The term "unperturbed" is used to imply that the input motion signal and the response signal at an arbitrary location are the same. Time histories of $\sqrt{J_2'}$ (second invariant of the deviatoric stress tensor) in Figures 12 and 13 are typical of the $\sqrt{J_2'}$ response at these locations in most cases.

In Case 2, the Temblor record of the Parkfield earthquake replaced the Oroville record with all other conditions being the same. The peak velocities in the Tremblor record occurred between four and five seconds. The simulation was carried out for the first five seconds of the earthquake motion. No new cracks were formed as a result of the passage of the Temblor record. As in Case 1, the response motion was very similar to the input motion, indicating that the overall response in Case 2 also was essentially linear elastic.

The ERPM earthquake motion was used as the boundary velocity input in Case 3 of salt, all other input being identical to that of Case 1. The duration of this record was 0.58 s. Considerable damage occurred in the first tenth of a second and the calculation was stopped after 0.138 s due to excessive displacement at the tunnel walls. Peak input velocities occurred at about 0.09 s and were of the order of 1.5 m/s.

At Location 2, the peak velocities were a factor of two higher than the peak input velocities. The y-velocity response at

Location 1 was much more catastrophic than the x-velocity response at Location 2. Extensive cracking in the regions adjacent to the tunnel permitted high velocity amplitudes at the tunnel walls. The degree of cracking prior to the earthquake was very minor, as seen in Figure 14. However, after 0.138 s of earthquake motion, a substantial amount of cracking was indicated (see Figure 15). All zones adjacent to the tunnel had at least one throughgoing crack, some had as many as 15 new throughgoing cracks! Whereas the void strains in all other cases considered for salt were negligible, they were very large in Case 3 (as much as 90% of the zone size). Figure 16 shows the mesh configuration just prior to the earthquake for Cases 1, 2, and 3.

The displacement at the tunnel walls following the passage of the Oroville aftershock (Case 1) and the Temblor record (Case 2) was relatively small. In Case 3, very large displacements were predicted even before the entire motion was passed through the mesh. This is illustrated in Figure 17 which is a mesh plot at 0.138 s into the ERPM earthquake. Although collapse was not modeled as such in these calculations, failure of the tunnel is indicated when deformations such as those shown in Figure 17 occur.

Compared to Cases 1, 2, 4, and 5 of salt, significantly higher levels of stress are encountered in Case 3. The results indicate a potential hazard to the repository due to an earthquake or blast similar to the ERPM record.

Except for the absence of a heat source in Case 4, Case 1 and Case 4 are exactly the same in terms of input conditions. Cracks formed prior to or following the earthquake in and around the tunnel in Case 4. The slight increase in permeability that occurred in Case 1, did not occur in Case 4. The $\sqrt{J_2'}$ contours at a time of 0.5 s are compared in Figure 18 for Cases 1 and 4, and it is clear that the thermal stresses introduced by the heat source give rise to steeper stress gradients in the mesh. However, salt creep and the relatively high thermal conductivity are mitigating factors that prevent higher stress concentrations around the tunnel.

A 45° shear zone, diagonally across the mesh, was defined in Case 5. All other input was identical to Case 1. No new cracks formed as a result of the passage of the Oroville record for Case 5. Apparently no damage occurred due to the earthquake.

Generally speaking, the stress perturbations due to the Oroville aftershock or the Temblor record are less than ten percent of the equilibrium stress values and, as such, have little influence on the stability or integrity of the repository.

The permeability changes in Cases 1, 2, 4, and 5 are either non-existent or very small and do not affect the rock more than one tunnel diameter away. Significant permeability changes can be expected for Case 3. More important than the potential permeability increase is the fact that the tunnel configuration is unstable when subjected to the ERPM motion.

Granite

Of the eight cases considered in granite (Table 7), it was possible to carry six of the simulations through the earthquake phase. Cases 3 and 7 were unstable, even prior to any seismic activity, for reasons that will be discussed later. In Cases 1, 2, 4, and 5, no new cracks were formed, nor was there any void strain associated with the existing cracks. Varying amounts of joint slip and associated dilatancy occurred in all the granite cases.

Consider Case 1 to be the baseline case for granite. The velocity response at the two representative locations is presented in Figure 19, which indicates that the signal passes through the repository without much attenuation or dispersion. However, some slip does occur.

Case 2 of granite has in situ horizontal stresses that are one-half the overburden stress. The joint slip is much more prevalent in this case as compared to Case 1. The velocity histories at the representative locations, once again, are nearly identical to the input histories at the boundary. Contours of $\sqrt{J_2'}$ at 0.5 and 1.5 s are presented in Figure 20. Whereas these contours were approximately circular in Case 1 ($\sigma_H = \sigma_V$), they are not circular in Case 2 of granite. The non-hydrostatic nature of the in situ stresses ($\sigma_H = 1/2\sigma_V$) in Case 2 allows a higher fractional change of the horizontal stress component due to thermal stressees and due to the earthquake motion. This is also the explanation for more slip in this case as compared to Case 1.

The horizontal stresses were prescribed to be twice the overburden stress in Case 3 of granite. Therefore, a much higher absolute differential stress was operating on the joints and resulted in accelerated slip that gave rise to an unstable configuration even prior to the start of the earthquake motion. It should be recalled that each complete calculation has three phases: 1) a heating phase (~4.5 years of real time); 2) an intermediate phase to equilibrate the stresses for a given temperature distribution at the end of the heating phase; and 3) an earthquake motion phase (3 seconds of real time for the Oroville aftershock).

Case 3 of granite could not be brought to equilibrium in the second phase. This suggests that the opening would undergo significant slip deformation through the heating phase, and that conditions are unstable even without the earthquake. Therefore, it was thought that simulating the third phase for this case would be a futile exercise, because the residual velocities prior to the earthquake were of the order of peak velocities that would be experienced during the earthquake motion. To ascertain that the joint slip was responsible for the instability, the Joint Slip Model was inactivated and the second phase repeated. With the slip in an inactive mode, indeed, the calculation becomes stable. This is graphically illustrated in Figure 21 which is a time-history of the kinetic energy of the mesh during the second phase (with and without slip).

Cases 4 and 5 of granite are different from Case 1 in that they have a pore-pressure distribution (see Table 4). As expected, the pore-pressure makes it easier for slip to occur. Case 4 slip is lesser in magnitude and extent than Case 5 slip, which is also consistent with the pore-pressure distribution in the two cases. Conceivably, it is also easier to initiate cracks when a finite pore-pressure exists, because that pressure acts to reduce the normal stress across the joint (i.e., make it relatively more tensile). However, no new cracks formed in Case 4 or Case 5 of granite. It is possible that the tensile strength specified may have been too high for new cracks to initiate, even with non-zero pore pressure.

Except for the type of earthquake motion, the input conditions for Case 6 of granite were identical to the input conditions for Case 1. Therefore, the same heating and equilibrium phases were utilized in the two cases. The ERPM record was used in Case 6, and the response indicates that the repository configuration was not stable with respect to the prescribed input motion. The duration of the ERPM record is roughly 0.6 s. However, by a simulation time of only 0.16 s, the deformations at the tunnel walls were too large to justify further computation. As in Case 3 of salt, extensive cracking and large void strains occurred near the tunnel walls, and a factor of two (or more) amplification of the peak input velocity at approximately 0.08 s was predicted.

In Case 7 for granite, the _in situ_ horizontal stress, (σ_{xx}) in the plane of calculation was twice the overburden stress. The other _in situ_ horizontal stress (σ_{zz}') normal to the plane of calculation was equal to the overburden. The response in this case was unstable, similar to Case 3 where both _in situ_ horizontal stresses (σ_{xx} and σ_{zz}') were twice the overburden stress. It was not possible to bring the calculation to a state of equilibrium prior to the time when seismic activity was imposed on the boundaries. Although the extent of slip and cracking for Case 7 was somewhat lower than for Case 3, it was still higher than for other cases in granite at the end of the heating phase. As in Case 3, the residual velocity field prior to any seismic activity was comparable to (or higher than) the peak velocity motions that would be imposed by the Oroville earthquake motion. The explanation given earlier for the instability of Case 3 holds true for Case 7 as well.

The two in situ horizontal stresses, σ_{xx} and σ_{zz}, were fifty percent higher than the overburden stress σ_{yy} for Case 8 of granite. Unlike Case 3 and Case 7, which also had unequal in situ principal stresses, Case 8 turned out to be a stable configuration. The kinetic energy of the system during the equilibrium phase is compared between Cases 7 and 8 in Figure 22. Clearly, the slip process is not as active in Case 8 as it is in Case 7 (or Case 3). Some cracking occurred in the floor and the ceiling for Case 8 during the heating phase, but was less predominant than the cracking in Case 7 for a comparable period. Further, no new cracks were formed by the passage of the Oroville motion in Case 8.

The permeability changes in granite resulted primarily from dilatancies associated with joint slip. As is clear from the data presented earlier in this section, joint slip is generally concentrated in the regions surrounding the tunnel opening. The average dilatancy in the vicinity of the tunnel, in Case 1, is approximately 2.11×10^{-4} m (i.e., 0.0211%), which corresponds to a joint opening of 0.2 mm for each of the joints. Also, joint slip away from the cavity is non-existent. Case 2 joint slip is much more extensive than that in Case 1, and the average dilatancy around the tunnel is 1.98×10^{-4} m, which also corresponds to a joint opening of roughly 0.2 mm. Dilatancies are present away from the tunnel as well, although their magnitude is somewhat lower. By the end of the heating phase, Case 3 shows joint slip and associated dilatancies everywhere in the mesh. The dilatancies near the tunnel are three to four times those found in Cases 1 and 2, meaning that even prior to the passage of an earthquake, the joint-openings are 0.6 to 0.8 mm as compared to 0.2 mm for Cases 1 and 2. Cases 4 and 5 gave joint slips that are more extensive than for Case 1, but comparable to Case 2. The average dilatancy in the vicinity of the tunnel is 1.62×10^{-4} m for Case 4, and 1.68×10^{-4} m for Case 5. Even though lower average dilatancies (and hence lower permeability changes) near the tunnel wall are observed in Cases 4 and 5 compared to Cases 1 and 2, it should be emphasized that Cases 2, 3, and 4 show dilatancies away from the tunnel as well, whereas Case 1 does not.

The presence of pore-pressure, therefore, appears to reflect a more diffuse permeability change, and without pore-pressure the permeability changes are restricted to the region near the tunnel walls. The dilatancies for Case 6 of granite prior to the earthquake are obviously the same as for Case 1. At 0.16 s into the ERPM, which is as long as the calculation was continued, dilatancy changes were large compared to other cases, and occurred everywhere in the mesh. The numerical values of dilatancy for Case 6 probably have less physical significance at this stage because the displacements at the opening indicate collapse.

The average dilatancy in the vicinity of the tunnel for Case 7, at the end of the heating period, is 3.42×10^{-4} m which corresponds to a joint opening of 0.34 mm. Dilatancies of magnitudes decreasing with distance from the tunnel center also occur in the vicinity of the diagonals going through the room corners, in proportion to the slip contours. The average dilatancy around the tunnel region for Case 8 after 3 s of earthquake motion is 4.06×10^{-4} m, corresponding to a joint opening of approximately 0.4 mm. No dilatancy beyond 6 m from the tunnel walls occurred in Case 8.

Shale

Two cases were attempted in shale. They were similar in that the shale was represented as a medium with an orthogonal jointing system with different (anisotropic) properties for the bedding plane joints and the cross-bedding joints. The only difference was in the pore pressure, which was absent in Case 1, but present in Case 2.

One of the shale cases was unstable even prior to the earthquake. Case 2, which uses a finite pore-pressure distribution, predicted deformations that were much greater than those predicted by Case 1. Mesh plots at the end of the heating phase are compared in Figure 23. Although relative equilibrium was achieved for Case 1 of shale (but not for Case 2 of shale), the residual velocities at the end of the equilibrium phase were an order of magnitude higher than those for granite or salt. The presence of pore-pressure in Case 2 obviously results in a less stable slip configuration.

The Oroville record was applied as boundary input for Case 1 of shale. However, the calculation was stopped after the first 0.5 s due to excessive deformation of the tunnel. Substantial cracking and accelerated slip appear to be the factors in causing the failure. All cases of granite and salt in which the Oroville record was used were stable. The relatively low tensile strength of shale causes it to fail at substantially lower levels of tensile stress. Likewise, the slip parameters for shale have lower thresholds compared to granite, and another failure mechanism (i.e., uncontrolled slip) is triggered at lower levels of stress. Tunnel deformations at the end of the five-year heating period for salt, granite, and shale are compared in Figure 24.

The presence or absence of a heat source appeared not to matter much, because a test run was made without the heat source and the solution was not altered significantly. Here, too, slip appeared to be the main contributing factor; because the second phase of Case 2 was repeated without slip and the results seem to approach equilibrium, which was not the case when slip was allowed. The kinetic energy in the mesh was plotted during the equilibrium phase for Case 2 (with and without slip) as in Figure 25. Another test run was made in which the friction angle was changed from 26° to 33° in Case 2 for shale. The results showed a retarded rate of slip, but the rate was not sufficient to achieve equilibrium. The orientation of the joints was certainly an influential factor contributing to slip in shale.

Material Sensitivity

In the first few decades of the life of a repository, the thermal conductivity of the medium plays an important role in the heat diffusion and the associated thermal stress dissipation or relaxation. From that point of view, salt is the most desirable of the three materials considered. Temperature-time histories adjacent to the heat source in each material are shown in Figures 26, 27 and 28 (note different scales for these figures). These figures show that the temperature buildup is the highest for shale and the lowest for salt, as expected. Higher temperature gradients imply higher thermal stress gradients that are potentially more harmful to the integrity of a repository. These effects probably do not impact the earthquake response that much, but the perturbations experienced due to an earthquake may be more apt to trigger failure in a repository with high thermal stresses than in to one with lower thermal stresses. This, of course, was not the case with salt where Case 1 had thermal stresses and Case 4 did not; and they both survived the Oroville aftershock.

The ERPM record, in particular, should only be considered be a limiting case of "earthquake" motion for the assumed seismic input. The reason for this is that the acceleration record was obtained in a competent quartzite which has superior characteristics with respect to transmission of seismic motion. In a less-competent rock mass, attenuation of the motion would be realized much more rapidly, particularly in the higher frequency range.

If any of the generic rock types had survived this severe loading, then it could be presumed to be quite stable under ordinary earthquake conditions. However, because all three rock types showed substantial damage from the ERPM loading, it is possible that such load levels represent unrealistic boundary conditions for the rock types considered. A more useful analysis might be provided by considering less severe boundary conditions that would be more representative of motions recorded in that environment. Only then can specific conclusions be drawn with respect to the relative stability or instability due to severe earthquake loading.

Given the qualification that uncertainties exist with regards to the material property data and the application of these particular seismic records to these particular geologies, it appears that salt and granite are competent host rocks for a nuclear waste repository that has a thermal loading of 60 kW/acre and is located at a depth of 600 m. This comment pertains to vulnerability to the Oroville and the Tremblor records, and is not valid for Cases 3 and 7 of granite, when $\sigma_{H_1} = 2\sigma_V$.

Assuming that the material property data used for shale are representative, the present analysis shows that an unsupported 8 m x 8 m opening in shale at the proposed depth may cause stability problems, particularly for saturated shales with finite pore pressures. The analyses presented in the next two sections support the findings of these shale calculations. More work is required to determine 1) whether this result is generally applicable to all shales that might be considered as a repository medium, and 2) if so, what degree of artificial support is required to produce a stable repository.

Output from the Joint Slip Model

The information presented in these next two sections is based on the same calculations already reported, but is presented with different plotting programs that show outputs from the Joint Slip Model and the CAVS Tensile Failure Model. The plots are complementary to the results presented earlier.

All the calculations in granite resulted in some joint slip near the primary opening. Only the relative slip of joints is accounted for, i.e, the rock on either side of the joint causes clockwise or counter-clockwise shear deformation. Only a small amount of slip actually occurred during the earthquake (~3 s in duration); typically less than five percent of the slip that occurred during the 5-year heating phase. Several joints indicated reversals and experienced dilation. Typical slip displacement values were less than 1 mm. The granite calculational results indicated only moderate damage to joints in certain zones near the opening, and no damage (no slip) in zones remote from the opening. The greatest joint damage occurred in the central zones immediately above the roof and immediately below the floor. Clearly, the orientation of these joints (45° from horizontal) is well suited to stability.

As previously noted, the calculations for shale indicated marginal or no stability even prior to the earthquake phase. Indeed, when compared to the granite calculations in terms of residual velocities and total kinetic energy, the shale case was unstable, even with no pore-pressure.

In spite of the stability questions in shale, the joint slip motion response was consistent with what one would expect it to be. Joints which appear to have low clamping stresses, i.e., the horizontal joints in the roof and floor and the vertical joints on the sides of the opening, did indeed experience significant slip. The joints normal to these were extremely stable and rarely indicated a tendency to slip, which is consistent with high normal stress influence. Accordingly, the stability or instability of the calculations with respect to joint slip is supported by reasonable arguments in all the cases of shale and granite.

Granite

Two types of plots have been developed to illustrate more clearly some of the output from the Joint Slip Model and the CAVS Model. Figure 29 illustrates the STEALTH mesh in the vicinity of the tunnel showing zones from I = 8 to 19, and J = 8 to 19; i.e., the interior 144 zones (out of a total of 676 zones). The zone boundaries are indicated by dotted lines. The two sets of joints in granite are shown by the solid lines at angles of 45° to 135° from the horizontal. Figure 30 indicates the net relative slip on each joint for all the affected joints in a clockwise or counterclockwise sense after the 5-year heating and transition phases, but before any seismic input occurs. If more than one joint per zone exists (as was the case for both joint sets in both shale and granite), then the total slip along a joint set in any zone (related to total dilation) is equal to the net relative slip times the number of joints per zone for that set.

Figure 31 indicates the net relative slip after the Oroville aftershock had been applied to the boundaries. As shown, very little difference exists when compared to Figure 30 indicating very little additional slip due to the earthquake. Basically, the granite case corresponds to four double direct-shear tests being carried out simultaneously as illustrated in Figure 32. Because the maximum shearing stress is always 45° to the principal stresses, slippage should be confined to this area if the joints are oriented along these planes. This is precisely what is observed in Figures 30 and 31. The maximum slip on any joint is printed above the figure and corresponds to the largest set of arrows in any zone. The slip in any other zone may be approximated by taking the ratio of the size (linear dimension) of the arrows in question to the largest arrow and multiplying that ratio by the maximum slip. For example, arrows which are one-half as long as the longest arrows in Figures 30 and 31 represent 0.60 mm of slip per joint in that zone. The case of the ERPM record applied to the granite model provided the only seismically induced instability for this rock type. The resultant slip pattern is illustrated in Figure 33, and at least some slip on both joint sets occurred in nearly every zone.

Three cases of high horizontal stress were investigated in granite. The first case (Case 3) had <u>in situ</u> horizontal stresses that were twice the overburden stress, i.e., a stress ratio of $\sigma_V:\sigma_{H_1}:\sigma_{H_2}$ of 1:2:2. This loading resulted in excessive slippage such that equilibrium could not be attained. The second case (Case 7) provided an in-plane horizontal stress of twice the vertical stress. The initial out-of-plane stress (contrained by the plane-strain assumption) was prescribed to be equal to the vertical stress. The resultant stress distribution was therefore $\sigma_V:\sigma_{H_1}:\sigma_H$ = 1:2:1. Figure 34 illustrates the relative slip on the two joint sets for this case at the end of the heating and transition phases.

In contrast to the more stable cases in granite, most of the slippage is located at the corners rather than the sides. The magnitude of the net relative slip is also quite large, even at one tunnel dimension away, indicating stability problems. While there may exist real cases in granite with stress ratios of 1:2:1 that are stable, the calculations with the assumed joint characteristics imply that with two orthogonal joint sets oriented at 45° and 135° from the horizontal (in a plane-strain geometry), the tunnel configuration is unstable for the first two high horizontal stress cases.

The third case of high horizontal stress utilized equal horizontal stresses which were one and a half times the vertical stress, i.e., a stress ratio of 1:1.5:1.5. The net relative slip after the heating and transition phases is shown in Figure 35. Several very interesting features may be noted, particularly the similarity to Figure 30 where the stress ratio was 1:1:1. The maximum slippage is limited to the top and bottom as in Figure 30; however, the effect of the higher horizontal stress is to produce less relative slip at the sides.

While less maximum slip was produced in the 1:1.5:1.5 case than for the other two high horizontal stress cases in granite (6 mm vs 30 mm), the maximum slip for the case of equal stresses is only 1.2 mm (Figure 30), i.e., a factor of 5 less slip. Therefore, in Figure 35, the arrows indicating slip should be magnified five times for direct comparison with Figure 30. If this were done, it would be seen that the effect of high horizontal stress (1:1.5:1.5) is to <u>increase</u> the slip in the roof and floor, while the slip in the sides of the tunnel remains about the same. This is consistent with the expected asymmetric response due to asymmetric loading.

Because Case 8 (the third of the three high horizontal stress cases) of granite appeared stable, the seismic record (Oroville aftershock) was passed through the mesh. As with all other cases in granite which were initially stable, the Oroville record did very little additional damage (as shown in Figure 36). The maximum slip displacement increased by only 0.1 mm (to 6.1 mm) during the three-second earthquake. Also, very little change in the overall slip pattern occurred. By contrast, the maximum slip displacement increased by 29 mm (to 30 mm) during the first 0.15 s of the ERPM motion of granite (Case 6).

Shale

Figure 37 shows the 144 interior zones (24 m x 24 m region) in shale, including the closely spaced bedding plane joints at 3° from the horizontal, and the cross-bedding joints at 93° from the horizontal. The zone boundaries are illustrated by dotted lines. Figure 38 illustrates the nominally stable shale slippage after the heating and transition phases. Again, the four double direct-shear test analogy is appropriate as shown in Figure 39. As no joints are available to allow slippage at 45° from the free surface (as in the case of granite), the problem degenerates into one of four pistons simultaneously approaching the center of the grid. The slight angle (3°) has the effect of "locking" the upper right and lower left corners with respect to vertical motion. This has the effect of severely shearing (in a clockwise sense) the zones indicated by asterisks in Figure 39. This effect can easily be understood by considering Figure 37, and agrees well with what is observed in Figure 38. At this point, the actual slip per joint is less in the nearly horizontal joints than in the nearly vertical joints, although more total slip (and therefore dilation) would be expected in the nearly horizontal joints because 5 times as many joints per zone exist for this orientation. Although virtually no damage occurred in granite or salt during the Oroville event, the shale model was unstable, in part due to extremely unfavorable joint orientation. Figure 40 shows substantial slippage in most zones for Case 1 in shale.

Output from the CAVS Tensile Failure Model

Void strain is a measure of crack opening, such that a void strain of one percent in each of the three orthogonal directions implies an increase in volume of three percent, exclusive of any elastic deformations in the intact material. The type of plot presented in this section illustrates the total void strain (for a given crack or joint orientation) in each zone. This is scaled to the maximum void-strain in the entire grid, which is printed above the figure in Figures 41 through 48 and corresponds to the largest void-strain vector in any zone. The direction of the line corresponds to the direction of the tensile stress, i.e., the line is perpendicular to the existing or induced crack.

No void strain occurred in any case of granite where the stress ratio was 1:1:1, except in Case 6 (with the ERPM record) as illustrated in Figure 41. In other cases (Cases 1, 2, 4, and 5), the perturbations due to the earthquake motion were simply not strong enough to cause a net tensile stress normal to the joints that was sufficiently large to open the cracks.

The unstable cases of high horizontal stress (stress ratio of 1:2:1 and 1:2:2) in granite indicated significant void strain at the end of the heating and transition phases, as illustrated in Figure 42 for the former case. The 3.5 percent maximum void strain is very large and appears to be located in the proximity of maximum slip, as shown in Figure 34.

The stable high horizontal stress case (Case 8 in granite) indicated one-tenth of the void strain after the heating and transition phases (Figure 43). All of the resultant void strain was located near the free surfaces of the tunnel. After the Oroville record had been passed through, the maximum void strain actually decreased from 0.36 percent to 0.21 percent for Case 8. The distribution of void strain at the end of the earthquake is shown in Figure 44.

The Case 1 shale calculation indicated significant void strain during the heating phase in (Figure 45). After the earthquake was applied, a great deal of additional cracking took place, principally in the roof and the right side of the opening. Figure 46 shows that the volume of some of the roof zones increases dramatically as a result of caving (implied by high void strain). Once the calculation begins to go unstable, the numerical values of certain parameters such as velocity are no longer valid. Nevertheless, qualitative collapse is indicated if the instability is initiated by the physics of the problem and not the numerics.

In the case of salt, which did not contain any pre-existing joints, only Case 3 produced significant void strains during the seismic phase (ERPM), as shown in Figure 47. Relatively small amounts of void strain occurred in the heating and transition phases of Cases 1 and 2 of salt as shown in Figure 48, and virtually no additional void strains occurred during the seismic phase (Oroville). No void strains occurred in Cases 4 and 5. The largest void strains in salt were also oriented in directions favoring cracking parallel to a free surface.

Empirical Investigations of Underground Openings

Numerical simulations are often used to help understand the behavior of a system under controlled, idealized circumstances. Whenever possible, the results of such calculations should be compared to solutions obtained by alternate methods in order to determine if the results are reasonable. Such techniques might include theoretical (analytical) and/or empirical (case history) investigations. Since tunnelling in rock is not an exact science, analytical methods are often lacking. In many cases, empirical formulations based on specific evidence of underground rock behavior are available. The present discussion is limited to a non-seismic environment, and is mainly concerned with a shale rock-type, because a greater degree of uncertainty exists in the shale data compared to the granite data. It is important to recognize that the shale-rock mass properties utilized in this investigation represent a closely jointed and only moderately strong rock at a depth of roughly 600 meters. In addition, no artificial support of any kind was modeled, and a span of 8 meters (26.2 feet) was defined for this generic study. All of these factors have unfavorable influences on stability, as explained below.

Barton (1975) has presented a classification system for rock masses to differentiate between self-supporting tunnels and those requiring support. The basis of his classification technique is a quantity, Q, representing "Rock Mass Quality" and is defined as:

$$Q = (RDQ/J_n) \cdot (J_r J_a) \cdot (J_w/SRF)$$

	Range
where RQD = rock quality designation	0 - 100
J_n = joint set number	0.5 - 20
J_r = joint roughness number	4 - 0.5
J_a = joint alteration number	0.75 - 20
J_w = joint water-reduction factor	1.0 - 0.05
SRF = stress-reduction factor	0.5 - 20

The following values were considered representative of the shale used in the calculations without pore pressures:

RQD = 80: At the lower range of the "good" category; representing 80% of core recovered from a borehole consisting of pieces 100 mm or longer.

J_n = 4: Representing two joint sets.

J_r = 1.5: A value of 2.0 represents smooth, undulating joints (crossbedding) and 1.0 represents smooth, planar joints (bedding).

J_a = 2.0: Slightly altered joint walls. Non-softening mineral coatings, sandy particles, clay-free disintegrating rock, etc.

J_w = 1.0: Dry excavations or minor inflow.

SFR = 5.0: Competent Rock, Rock Stress Problems: σ_c = 10,000 psi and σ_t = 200 psi.

Overburden: σ_1 = 2000 psi, $(\sigma_c/\sigma_1) \doteq 5.0$, and $(\sigma_t/\sigma_1 = 0.1$.

Closest to the range, $\sigma_c/\sigma_1 = 2.5$ to 5, and $(\sigma_t/\sigma_1 = 0.16$ to 0.33.

Values of SRF in this range are 5 to 10.

With these values, the rock mass quality is

$$Q = (80/4)\cdot(1.5/2.0)\cdot(1.0/5.0) = 3.0$$

Two fundamental quantities concerning the stability of underground openings are stand-up time and length of unsupported span. They only represent likely response based upon many factors, and should therefore only be used as an indication of reasonable behavior.

Figure 49 illustrates actual case histories of supported (open circle) and unsupported (solid circle) underground excavations. The ESR (Excavation Support Ratio) value ranges from 0.8 to 5 depending on the degree of safety required. Because this question was not addressed in this investigation, a value of 1.0 is assumed. A value of Q = 3.0 yields a maximum unsupported span length of approximately 3 meters, indicating that the proposed 8-meter span utilized in this study may very well be unstable.

Performing a similar analysis for granite, a rock-mass quality value may be calculated as follows:

RDQ = 95: 95% of core taken is in sections of 100 mm or longer.

J_n = 4: two existing joint sets

j_r = 3: rough undulating joints.

J_a = 1: unaltered joint walls, surface straining only

J_w = 1: dry excavations or minor inflow

SFR = 1: $(\sigma_c/\sigma_1) = 25000/2000 = 12.5$; $\sigma_t/\sigma_1 = 1000/2000 = 0.5$; at medium stress, SRF = 1.

Therefore, $Q = (95/4)\cdot(3/1)\cdot(1/1) = 71.25$.

The resultant maximum unsupported span for granite (Figure 49) is approximately 10 meters. This result is also consistent with the numerical calculations in granite which indicate no potential instability during the 5-year heating and transition phases for lithostatic states of stress.

Figure 50 provides estimates of stand-up time as a function of rock mass quality. The values for the generic shale and gran give stand-up times of 6 months and 10 years, respectively. Again, these values are only estimates based on specific assumptions.

Another classification system has been presented by Bieniawski (1973). In Figure 51, a spacing of 200 mm and σ_c = 69 MPa indicates that the shale is a very weak and fractured (intensely jointed) rock mass. The granite with a 1-m joint spacing is classified as a strong rock mass that is only little-to-moderately jointed. Clearly, a different response would be expected from each of the two rock types.

Bieniawski does not indicate likely stability for any rock type with an unsupported span of greater than 8 meters. The case histories indicate that for granite, the stand-up time is 50 years for an unsupported span of 6 m. For a clayey shale, on the other hand, values of only 3 weeks of stand-up time and 2 meters of unsupported span are indicated, as shown in Figure 52.

Certain other factors also influence stability. Figure 53 indicates that square tunnels are less stable than circular ones, and that excavation techniques can also influence stability.

To summarize, the above empirical analysis supports the results and conclusions of the numerical calculations that were carried out for shale and granite.

VI. CONCLUSIONS AND RECOMMENDATIONS

Conclusions

The following conclusions can be drawn as a result of this study:

1. The STEALTH code was modified to simulate earthquake propagation accurately through a two-dimensional mesh. Material models were successfully developed to model the nonlinear behavior of salt, granite, and shale. A number of complex cases were modeled (in a three-stage calculational process) taking into account the effects of jointing, heating, water saturation, and different in situ stress combinations. The results demonstrated that the methodology is suitable for studying the effects of earthquake motions on underground structures.

2. Conclusions from the salt runs are as follows:

   a. During the heating phase, creep of the salt helped to relax the stress concentrations around the tunnel.

   b. The rock mass was able to withstand the Oroville and the Temblor earthquakes without significant fracturing or instability around the tunnel.

   c. The ERPM gold mine tremor was greatly amplified around the tunnel and fracturing occurred as a result of the seismic loading. This was the only case of salt that developed cracks as a direct result of the seismic motion. The higher frequency content of the ERPM motion is probably of the same magnitude as the natural frequency of the structure (in this case, an 8-m x 8-m tunnel) which would cause resonance and result in enhanced displacements of the tunnel walls. An evaluation of the salt results against the defined criteria is given in Table 9.

3. Conclusions drawn from the granite runs are listed below:

   a. During the heating phase, some slip occurred along the joints, and this was accompanied by occasional cracking of intact rock in the immediate vicinity of the opening. There was no tendency for major through-going cracks to form.

b. No cracks were developed as a result of passing the Oroville motions through the rock mass under hydrostatic loading conditions, although some additional slippage along joints occurred in zones which had already experienced slip during the heating phase.

c. For certain high horizontal stress scenarios (e.g., when one or both of the in situ horizontal stresses were twice the overburden), major slipping occurred along the joints even before the earthquake hit the tunnel. The effect of the earthquake was to exaggerate this slip. The inference is that the condition of high horizontal stress might pose problems for an underground waste repository under the assumed jointing and loading conditions. However, simply having in situ horizontal stresses that are higher than the overburden stress does not necessarily imply that problems are to be expected. For example, one case of granite was analyzed in which the horizontal stresses were fifty percent higher than the overburden, and yet the tunnel was stable.

d. The assumed pore-pressure distributions affect the stress distribution around the tunnel and the amount of joint slip. However, they do not appear to have very much influence on the transmission of the earthquake motions. Further work will be required to establish more realistic pore-pressure distributions and possibly to include a pore-pressure dissipation logic in the numerical code.

e. The ERPM motion causes the hypothetical repository configuration to become unstable. Large-scale deformation resulting from cracking and slippage causes this failure. The comment in Conclusion 2c applies here as well.

4. Conclusions drawn from the results of the shale runs are:

a. During the heating phase, heat was trapped near the cavity (due to the lower thermal conductivity of shale as compared to salt and granite) that led to higher stress gradients around the tunnel.

b. For the case in which a pore-pressure distribution existed, major slipping along joints occurred during the heating phase. Residual velocities, following the heating phase but prior to the earthquake, were of the order of the peak velocities that would be expected during the Oroville earthquake. Therefore, the earthquake effects would be small in comparison to the amount of slip driven by thermomechanical and in situ stresses. Large deformations at the tunnel occurred during the heating phase.

c. Application of the Oroville motion to the shale case in which no pore pressure existed resulted in tunnel instability after 0.5 s of the earthquake motion. It is likely that the tunnel was only marginally stable prior to the earthquake, because the Oroville motion is relatively weak and did not cause failure in either a granite or a salt repository. Also, the relative deformation in the mesh at the end of the equilibrium phase in shale was many times greater than in granite indicating incipient instability. The shale results are compared with the defined criteria in Table 11.

Detailed sensitivity analyses are required to determine the applicability of shale as a repository medium. Due to the wide variation in properties of shales encountered in the United States, it is likely that the more competent shales could be suitable host rocks. How competent must the shales be and/or how much artificial support is required, are questions that can only be answered by further investigation.

Recommendations

1. Validation of Material Models

   The material models used in the study have been designed to incorporate the known characteristics of the different rock types considered as host media. A conscientious effort has been made to fit the results of available laboratory and field tests to these models for each particular rock type. However, the data base for creating these models was generally poor. For instance, the Joint Slip Model has been developed to take account of rock strength, roughness characteristics, dilation, and different loading paths including multiple reversals. Although the model appears to be realistic for temperatures below 100°C, the joint behavior in some rock types will possibly change at higher temperatures. Because a data base for shear testing at elevated temperatures does not exist, this modification to shear behavior was not included in the Joint Slip Model.

2. Determine Seismic Criteria

Because this study has demonstrated that at least one set of seismic motions (the ERPM) could cause cracking and instability to an underground repository tunnel, the circumstances in which seismic motions are likely to cause problems must be defined more precisely. Considering the seismic environment (seismic source, distance from the source, and transmission path geology) and the characteristics of the earthquake motion (amplitude, frequency content, and acceleration), it would be be useful to define the specific seismic criteria in order to identify the potential problems for specific repositories.

3. Incorporate Fluid Flow into the Thermomechanical Models

This is desirable for proper coupling of the major components affecting the design of a nuclear waste repository. This refinement involves further development of the CAVS model, including definition of the relationship between permeability and opening width for jointed media from experimental data (to the extent that these data exist). This modification of the CAVS model is required to interpret what a given joint geometry and a specific void strain mean in terms of permeabilities and flow rates. The dilatancy associated with joint slip could also be coupled to the void strain induced by tensile stresses.

VII. REFERENCES

1. Barton, N. (1973). **A Review of the Shear Strength of Discontinuities in Rock Masses with Particular Reference to Slope Stability.** Internal Report. Norwegian Geotechnical Institute.

2. Barton, N. (1975). **Classification of Rock Masses to Distinguish Between Self-Supporting Tunnels from Those Requiring Support.** Presented at the SME Fall Meeting, Salt Salt Lake City, Utah, September 10-12, 1975.

3. Bienawski, A. T. (1973). Engineering Classification of Jointed Rock Masses. **Trans. S. Afr. Inst. Civil Eng.,** Vol. 15, No. 12, pp. 335-344, December, 1973.

4. Glass, C. E. (1973). **Seismic Considerations in Siting Large Openings in Rock.** Ph.D. Thesis, University of California, Berkeley.

5. Hofmann, R. (1976). **STEALTH, A Lagrange Explicit Finite-Difference Code for Solids; Structural and Thermohydraulic Analyses.** SAI Report EPRI NP-260, Vol. 1, User's Manual. Prepared by Science Applications, Inc. for Electric Power Research Institute, Palo Alto, California, August 1976.

6. Lomenick, T. F. (1971). "Laboratory Pillar Model Experiments." Chapter 12 of **Project Salt Vault,** USAEC Report ORNL-4555, Oak Ridge National Laboratory, Oak Ridge, Tennessee.

7. Lysmer, J. (1979). Personal Communication.

8. Maxwell, D. E., Hofmann, R., and Wahi, K. K. (1978). **An Optimization Study of the Explicit Finite-Difference Method for Quasi-Static Thermomechanical Simulations.** Document SAI-FR-921-3, prepared by Science Applications, Inc. for Union Carbide Corporation, Nuclear Division, under Contract Number W-7405-ENG-26.

9. OWI (1978). **Contribution to Draft Generic Environmental Impact Statement on Commercial Waste Management: Radioactive Waste Isolation in Geologic Formations.** USDOE Report Y/OWI/TM-44. Office of Waste Isolation, Union Carbide Co., Oak Ridge Tennessee.

10. Pratt, H. R., Hustralid, W. A. and Stephenson, D. E., (1978). **Earthquake Damage to Underground Facilities.** USDOE Document DP-1513, E. I. du Pont de Nemours & Co., Savannah River Laboratory, Aiken, South Carolina.

11. Rozen, A. (1976). **Response of Rock Tunnels in Earthquake Shaking.** M. S. Thesis, Mass. Inst. of Tech., Cambridge, Massachusetts.

12. Spottiswoode, S. M. and McGarr, A. (1975). Source Parameters of Tremors in a Deep-Level Gold Mine. **Bull. Seis. Soc. Amer.**, Vol. 65, No. 1, February, 1975, pp. 93-112.

TABLE 1

Summary of Selected Acceleration Histories

Event	Date	Local Magnitude	Focal Depth Km	Recording Site	Distance, km	Component Directions	Peak Acceleration, g	Peak Velocity, cm/sec	Peak Displacement, cm
Parkfield	June 27, 1966	5.6*	8.6*	Temblor	12† (fault)	S25W	0.35	22.5	5.5
						N65W	0.27	14.5	4.7
						VERT	0.13	4.9	1.4
Oroville Aftershock	Aug. 11, 1975	4.3	2.6**	CDMG-6	5† (epicenter)	N35E	0.29	7.7	0.7
						S55E	0.41	12.5	0.8
						VERT	0.23	6.9	0.3
Mine Tremor	April 21, 1978	1.45	2-3	ERPM	0.43	LONG.	0.95	1.47	0.03
						TRANS.	0.93	0.97	0.02
						VERT.	0.85	1.23	0.02

* Chang, F. K. (1978). "Catalog of Strong Motion Earthquake Records." **Miscellaneous Papers S-73-1, Report 9, U.S. Army Waterways Experiment Station**, Vicksburg, Mississippi.

** Seekins, L. C. and Hanks, T. C. (1978). "Strong Motion Accelerograms of the Oroville Aftershocks and Peak Acceleration Data." **Bulletin of the Seismological Society of America**, Vol. 68, No. 3, pp. 677-690, June 1978.

† Hanks, T. C. and Johnson, D. A. (1976) "Geophysical Assessment of Peak Acceleration." **Bulletin of the Seismological Society of America**, Vol. 66, No. 3, 959-968, June 1976.

TABLE 2

Assumptions Common to All Rock Types

1. Calculational Grid

   The calculational grid used for all runs (except the model with shear zone) is shown in Figure 4. The grid is 52-m x 52-m and contains a tunnel (or room) 8-m x 8-m.

2. Depth

   The bottom of the tunnel is 600 m below the surface; i.e., the top of the grid is 570 m below the surface.

3. Overburden Stress

   Vertical overburden stress is 23×10^3 Pa per meter of depth (approximately 1 psi per foot of depth); i.e., the vertical stress at the top of the grid is 1.3×10^7 Pa. The horizontal stress will be some fraction of the vertical stress; e. g.,

   $$\sigma_H = \sigma_V;\ \sigma_H = 1.5\ \sigma_V;\ \sigma_H = 0.5\ \sigma_V;\ \text{and}\ \sigma_H = 2\sigma_V$$

4. Geothermal Gradient

   The geothermal gradient is 1° per 30 m of depth. The mean surface temperature is assumed to be 15°C. Therefore, the natural rock temperature around the tunnel is 35°C (15° at the surface plus 20° geothermal increase).

5. Waste Emplacement

   The waste is assumed to be 10-year-old spent fuel (SURF). It is stored in 5-kW canisters, spaced 6.5 m apart down the centerline of the tunnel. If the tunnels are 52 m apart, the thermal loading is approximately 60 kW/acre.

6. Heat Dissipation

   Canisters are simulated by applying heat to four zones (marked by a cross in Figure 4). Heat applied is 5 kW every 6.5 m or 0.77 kW/m along the tunnel. Therefore, each of the four zones emits 192.5 W.

TABLE 2 (Contd)

7. Decay Rate for Heat

$$\text{Decay Rate} = [(558 - 19.6t) + 0.52t^2]/558$$

where t is in years [OWI (1978), Figures 9-11]

8. Temperature Effect on Material Properties

Most material properties are to some extent affected by temperature changes. Unfortunately, there is a lack of data. This, together with the fact that in this problem the canister is being simulated by adding heat to four zones of the rock material rather than modeling the canister itself, masks many of the property changes that might be caused by heat. For the duration of the earthquake, of course, any temperature changes will be minute.

In general, temperature effects on material properties are not accounted for in this study. All thermal properties are isotropic for all materials.

9. Pore Pressures

It is assumed that pore pressure will reach equilibrium within a year of excavating the tunnel. However, the code contains no pore pressure dissipation logic. Pore pressures are considered during the slip and dilatancy positions of the Joint Slip Model, but are not included in the CAVS Tensile Model.

10. Sequence of Events

(a) The tunnel is excavated instantaneously and the appropriate <u>in-situ</u> boundary stress is applied.

(b) The canisters are emplaced 6 months after tunnel excavation.

(c) The earthquake hits the tunnel 4.5 years after waste emplacement (i.e., total time = 5.0 years), when the stress gradients (rather than absolute temperatures) are likely to be approaching their maximum. This is also within the retrievability period, so that the tunnel is not backfilled.

TABLE 2 (Contd)

11. Boundary Conditions

(a) The mechanical boundary conditions are determined as if there were only a single tunnel, although 60 kW/acre assumption implies a tunnel spacing of 52 m. This is done to ascertain the effect of different ratios of horizontal-to-vertical stress.

(b) The base of the grid is a fixed boundary.

(c) The other boundaries are stress bondaries.

(d) Heat boundaries are isothermal top and bottom, and are adiabatic on the sides.

(e) No ventilation is assumed.

(f) During the earthquake, all four boundaries are velocity history boundaries.

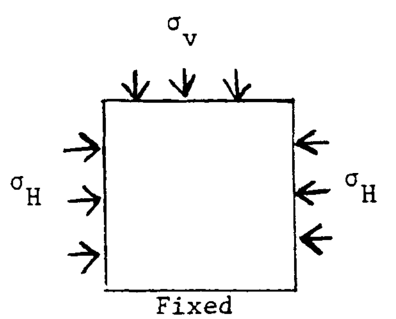

Stress Boundaries

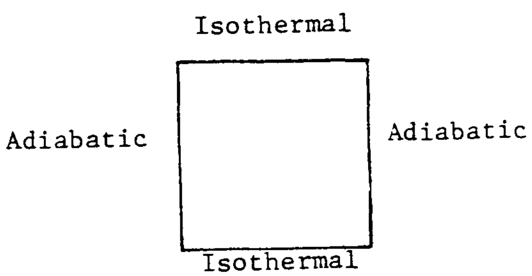

Thermal Boundaries

TABLE 3

Material Properties for Salt

A. JOINT GEOMETRY

No joints present

B. GENERAL

Rock Mass Density, $\gamma = 2130\ kg/m^3$

C. THERMAL PROPERTIES

Thermal Conductivity, $K = 6.1 - (2.5 \times 10^{-2}\ T) + (7.15 \times 10^{-5}\ T^2) - (8.3 \times 10^{-8} T^3)\ J/(s.m.°C)$

where T is temperature in °C.

Specific Heat Capacity, $C = 880\ J/(kg.°C)$

Coefficient of Linear Expansion, $\alpha = 4.0 \times 10^{-5} \left(\frac{m}{m}\right)/°C$

D. ISOTROPIC ELASTIC MODEL

Bulk Modulus, $K = 1.22 \times 10^{10}$ Pa

Shear Modulus, $G = 4.08 \times 10^{10}$ Pa

E. ISOTROPIC PLASTIC MODEL

Yield Model

$Y = 1 \times 10^8$ Pa

Yield Criterion

Von Mises as defined in STEALTH (Section 7 of the Main Report)

Flow Rule

Nonassociated Prantl-Reuss as defined in STEALTH (Section 7 of the Main Report)

F. JOINT SLIP MODEL

Not applicable

TABLE 3 (Contd)

G. CAVS TENSILE MODEL

Tensile Strength of Intact Rock = 1.55×10^6 Pa
(governs initiation of new cracks)

Tensile Strength of Dry Joint = 0.78×10^6 Pa
(governs propagation of existing cracks)

H. CREEP MODEL

The creep model is a generalized form of the Starfield-McClain equation (Section 7 of the Main Report) and can be expressed conveniently as follows:

$$\langle \dot{e}^{cr} \rangle = A_1 \cdot \Theta^{9.5} (T - \lambda)^{0.3} (\langle s \rangle)^3$$

where $\langle \dot{e}^{cr} \rangle$ is the generalized creep strain

$A_1 = 3.5 \times 1.5288^{-49}$

Θ is temperature in °K

T is time in seconds

$(T - \lambda)$ is a parameter with units of time

$\langle s \rangle$ is the equivalent deviatoric stress

I. PORE PRESSURES

Not applicable

J. IN SITU STRESSES

$\sigma_V = 1.3 \times 10^{-7}$ Pa at 570-m depth

σ_H is a fraction of σ_V

TABLE 4

Material Properties for Granite

A. JOINT GEOMETRY

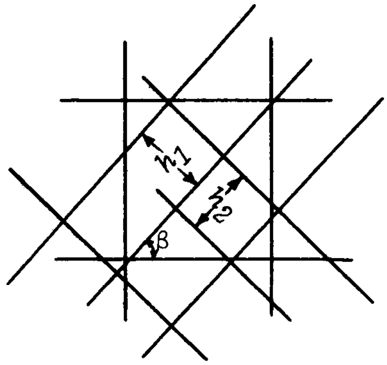

Type G_1

$\beta = 45°$

$h_1 = 1$ meter

$h_2 = 1$ meter

B. GENERAL

Rock Mass Density, $\gamma = 2640\ kg/m^3$

C. THERMAL PROPERTIES

Thermal Conductivity, $K = 2.85\ e^{(-0.001T)}/J(s.m.\ °C)$

where T is temperature in °C

Specific Heat Capacity, $C = 920\ J/(kg.\ °C)$

Coefficient of Linear Expansion $= 8.1 \times 10^{-6} \left(\frac{m}{m}\right)/°C)$

D. ISOTROPIC ELASTIC MODEL

Bulk Modulus $K = 8.98 \times 10^9$ Pa

Shear Modulus $G = 7.31 \times 10^9$ Pa

(Based on rock mass properties from the draft GEIS (OWI, 1978).

E. ISOTROPIC PLASTIC MODEL

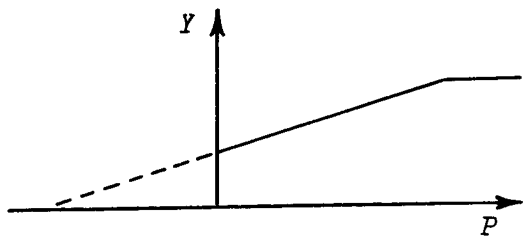

Yield Model

$Y = (1.4P + 4100)(6.895 \times 10^3\ Pa)$

Upper Yield Limit = 1×10^8 Pa (unlikely to be activated)

Lower Yield Limit = 0

TABLE 4 (Contd)

Yield Criterion

Von Mises as defined in STEALTH (Section 7 of Main Report).

Flow Rule

Nonassociated Prantl-Reuss as defined in STEALTH (Section 7 of Main Report)

F. JOINT SLIP MODEL

Compressive Strength of Intact Rock, $\sigma_c = 1.827 \times 10^8$ Pa

Angle of Internal Friction, $\phi = 30°$

DP1	=	0.00027 meter
DP2	=	0.00273 meter
DP3	=	3.4475×10^6 Pa
DP4	=	3
TIOVTR	=	0.2
TUOVTR	=	0.4
REDFTR	=	0.95
MINPK	=	1.2
QMAX	=	2×10^4 Pa·m
POW	=	1.0
$\frac{\text{DITCH}}{\text{DPEAK}}$	=	1.0

TABLE 4 (Contd)

G. CAVS TENSILE MODEL

Tensile Strength of Intact Rock = 7×10^6 Pa
(governs initiation of new crack)

Tensile Strength of a Dry Joint = 3.5×10^6 Pa
(governs propagation of existing cracks)

H. PORE PRESSURES

Pore pressure is assumed to increase linearly with distance from the tunnel wall until the hydrostatic condition is reached ('d' is in meters; 'P' is in Pa).

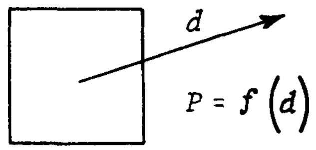

Type H1

1. if $d \leq 4$, P = 0

2. if $d \geq 30$, P = hydrostatic = 5.9×10^6 Pa

3. linear interpolation between d = 4 and d = 30

Type H2

1. if $d \leq 4$, P = 0

2. if $d \geq 12$, P = hydrostatic = 5.9×10^6 Pa

3. linear interpolation between d = 4 and d = 12

I. IN-SITU STRESSES

Assume density of overburden is about 22.7×10^3 Pa/m of depth; i.e., (approx. 1 psi per foot of depth)

$_V = 1.3\ 10^7$ Pa at 570 m depth

$_H$ is a fraction of $_V$

TABLE 5

MATERIAL PROPERTIES FOR SHALE

A. GEOMETRY

Type S_1 (OWI, 1978)

$\beta = 3^{o}$

$h_1 = 0.2m$

$h_2 = 1m$

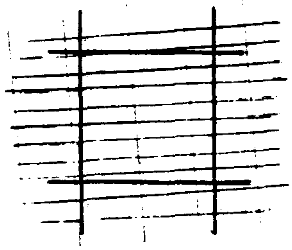

B. GENERAL

Rock mass density, $\gamma = 2560\ kg/m^3$

C. THERMAL PROPERTIES

Thermal conductivity, $K = 1.7e^{(-0.0008T + 0.0000012T^2)}\ J/(s.m.^{o}C)$
where T is temperature in ^{o}C.

Specific heat capacity $C = 840\ J(kg.^{o}C)$

Coefficient of linear expansion $\alpha = 12 \times 10^{-6} (\frac{m}{m})/^{o}C$

D. ANISOTROPIC ELASTIC MODEL

Given Constants (Based on OWI, 1978, Table 7-3)

$E_H = 6.0 \times 10^5\ lb/in^2 = 4.1370 \times 10^9\ Pa$

$E_v = 3.0 \times 10^5\ lb/in^2 = 2.0685 \times 10^9\ Pa$

$\nu_H - \nu_v = 0.15$

TABLE 5 (cont'd)

Derived Constants

$C_{11} = 4.52 \times 10^9$ Pa

$C_{12} = 0.923 \times 10^9$ Pa

$C_{13} = 0.817 \times 10^9$ Pa

$C_{33} = 2.31 \times 10^9$ Pa

$C_{44} = 0.899 \times 10^9$ Pa

Bulk Modulus $K_b = 1.65 \times 10^9$ Pa

E. ISOTROPIC PLASTIC MODEL

Yield Model

$Y = (1.4P + 3 \times 10^7)$ Pa

Upper Yield Limit = 1×10^8 Pa (unlikely to be activated)

Lower Yield Limit = 0

Yield Criterion

Von Mises as defined in STEALTH (Section 7 of Main Report).

Flow Rule

Non-associated Prandtl-Reuss as defined in STEALTH (Section 7 of Main Report).

TABLE 5 (cont'd)

F. JOINT SLIP MODEL

Compressive Strength of intact rock, $\sigma_c = 6.9 \times 10^7$ Pa
Angle of internal friction, $\phi = 26^o$.

Parameter	Bedding Joints	Cross-Joints
DP1	0.00101m	0.00060m
DP2	0.00499m	0.00340m
DP3	3.4475×10^6Pa	3.4475×10^6Pa
DP4	3.5	2.5
TIOVTR	0.5	0.4
TUOVTR	0.4	0.3
REDFTR	0.95	0.95
MINPK	1.05	1.1
QMAX	1×10^4Pa.m	1×10^4Pa.m
POW	1.0	1.0
$\frac{\text{DITCH}}{\text{DPEAK}}$	1.0	1.0

G. CAVS TENSILE MODEL

Tensile Strength of Intact rock = 1.4×10^6 Pa

Tensile Strength of Dry Joint = 0.7×10^6 Pa

H. PORE PRESSURES

Type H1

1. if $d \leq 4$, $P = 0$
2. if $d \geq 12$, P = hydrostatic = 5.9×10^6 Pa
3. linear interpolation between d = 4 and d = 12m

Type H2

1. if $d \leq 4$, $P = 0$
2. if $d \geq 6$, P = hydrostatic = 5.9×10^6 Pa
3. linear interpolation between d = 4 and d = 6m

I. *IN SITU* STRESSES

$\sigma_v = 1.3 \times 10^7$ Pa at 570 m depth

σ_h is a fraction of σ_v

TABLE 6

Calculational Matrix for Salt

Simulation / Property	Case 1	Case 2	Case 3	Case 4	Case 5
Joint Geometry	X	X	X	X	X
Pore Pressures	X	X	X	X	X
In Situ Stresses	$\sigma_H = \sigma_V$	$\sigma_H = \sigma_V$	$\sigma_H = \sigma_V$	$\sigma_H = \sigma_V$	$\sigma_H = \sigma_V$
Shear Zone	X	X	X	X	✓
Thermal Loading	✓	✓	✓	X	✓
Earthquake	Oroville (0.41g)	Parkfield (0.35g)	ERPM (0.95g)	Oroville (0.41g)	Oroville (0.41g)

X = None

✓ = Yes

TABLE 7

Calculational Matrix for Granite

Property \ Simulation	Case 1	Case 2	Case 3	Case 4	Case 5	Case 6	Case 7	Case 8
Joint Geometry	G_1	G_1	G_1	G_1	G_1	G_1	G_1	G_1
Pore Pressure	X	X	X	H1	H2	X	X	X
In Situ Stresses	$\sigma_H = \sigma_V$	$\sigma_H = \frac{1}{2}\sigma_V$	$\sigma_H = 2\sigma_V$	$\sigma_H = \sigma_V$	$\sigma_H = \sigma_V$	$\sigma_H = \sigma_V$	$\sigma_{H1} = 2\sigma_V$ $\sigma_{H2} = \sigma_V$	$\sigma_H = \frac{3}{2}\sigma_V$
Shear Zone	X	X	X	X	X	X	X	X
Thermal Loading	√	√	√	√	√	√	√	√
Earthquake	Oroville (0.41g)	Oroville (0.41g)	Oroville (0.41g)	Oroville (0.41g)	Oroville (0.41g)	ERPM (0.95g)	Oroville (0.41g)	Oroville (0.41g)

X = None

√ = Yes

TABLE 8

Calculational Matrix for Shale

Property \ Simulation	Case 1	Case 2
Joint Property	S_1	S_1
Pore Pressures	X	H1
In Situ Stresses	$\sigma_H = \sigma_V$	$\sigma_H = \sigma_V$
Shear Zone	X	X
Thermal Loading	√	√
Earthquake	Oroville (0.41g)	Oroville (0.41g)
Anisotropy	√	√

X = None

√ = Yes

TABLE 9

Results for Salt Compared with Defined Criteria

	Simulation / Property	Case 1	Case 2	Case 3	Case 4	Case 5
	Joint Geometry	X	X	X	X	X
	Pore Pressures	X	X	X	X	X
	In Situ Stresses	$\sigma_H = \sigma_V$	$\sigma_H = \sigma_V$	$\sigma_H = \sigma_V$	$\sigma_H = \sigma_V$	$\sigma_H = \sigma_V$
	Shear Zone	X	X	X	X	✓
	Thermal Loading	✓	✓	✓	X	✓
	Earthquake	Oroville (0.41g)	Parkfield (0.35g)	EPRM (0.95g)	Oroville (0.41g)	Oroville (0.41g)
CRITERIA	FAILURE CRITERION	0	0	FAILED (Earthquake Phase)	0	0
CRITERIA	DAMAGE CRITERIA	FRACTURING VOID STRAIN	0	FRACTURING VOID-STRAIN	0	0
CRITERIA	PERMEABILITY CRITERION	0	0	0	0	0

X = None, ✓ = Yes, 0 = Does not exceed criterion

TABLE 10

Results for Granite Compared with Defined Criteria

Property \ Simulation	Case 1	Case 2	Case 3	Case 4	Case 5	Case 6	Case 7	Case 8
Joint Geometry	G_1	G_1	G_1	G_1	G_1	G_1	G_1	G_1
Pore Pressure	X	X	X	H1	H2	X	X	X
In Situ Stresses	$\sigma_H = \sigma_V$	$\sigma_H = \frac{1}{2}\sigma_V$	$\sigma_H = 2\sigma_V$	$\sigma_H = \sigma_V$	$\sigma_H = \sigma_V$	$\sigma_H = \sigma_V$	$\sigma_{H1} = 2\sigma_V$ $\sigma_{H2} = \sigma_V$	$\sigma_H = \frac{3}{2}\sigma_V$
Shear Zone	X	X	X	X	X	X	X	X
Thermal Loading	✓	✓	✓	✓	✓	✓	✓	✓
Earthquake	Oroville (0.41g)	Oroville (0.41g)	Oroville (0.41g)	Oroville (0.41g)	Oroville (0.41g)	ERPM (0.95g)	Oroville (0.41g)	Oroville (0.41g)
FAILURE CRITERION	0	0	FAILED (Before Earthquake Phase)	0	0	FAILED (Earthquake Phase)	FAILED (Before Earthquake Phase)	0
DAMAGE CRITERIA	0	0	SLIP	0	0	FAILED (Earthquake Phase)	SLIP	0
PERMEABILITY CRITERION	0	0	EXCEEDED	0	0	EXCEEDED	EXCEEDED	0

X = None, ✓ = Yes, 0 = Does not exceed criterion

TABLE 11

Results for Shale Compared with Defined Criteria

	Property \ Simulation	Case 1	Case 2
	Joint Property	S_1	S_1
	Pore Pressures	X	H1
	In Situ Stresses	$\sigma_H = \sigma_V$	$\sigma_H = \sigma_V$
	Shear Zone	X	X
	Thermal Loading	√	√
	Earthquake	Oroville (0.41g)	Oroville (0.41g)
	Anisotropy	√	√
CRITERIA	FAILURE CRITERION	FAILED (Earthquake Phase)	FAILED (Heating Phase)
CRITERIA	DAMAGE CRITERIA	SLIP VOID-STRAIN	SLIP VOID-STRAIN
CRITERIA	PERMEABILITY CRITERION	EXCEEDED	EXCEEDED

X = None, √ = Yes, 0 = Does not exceed criterion

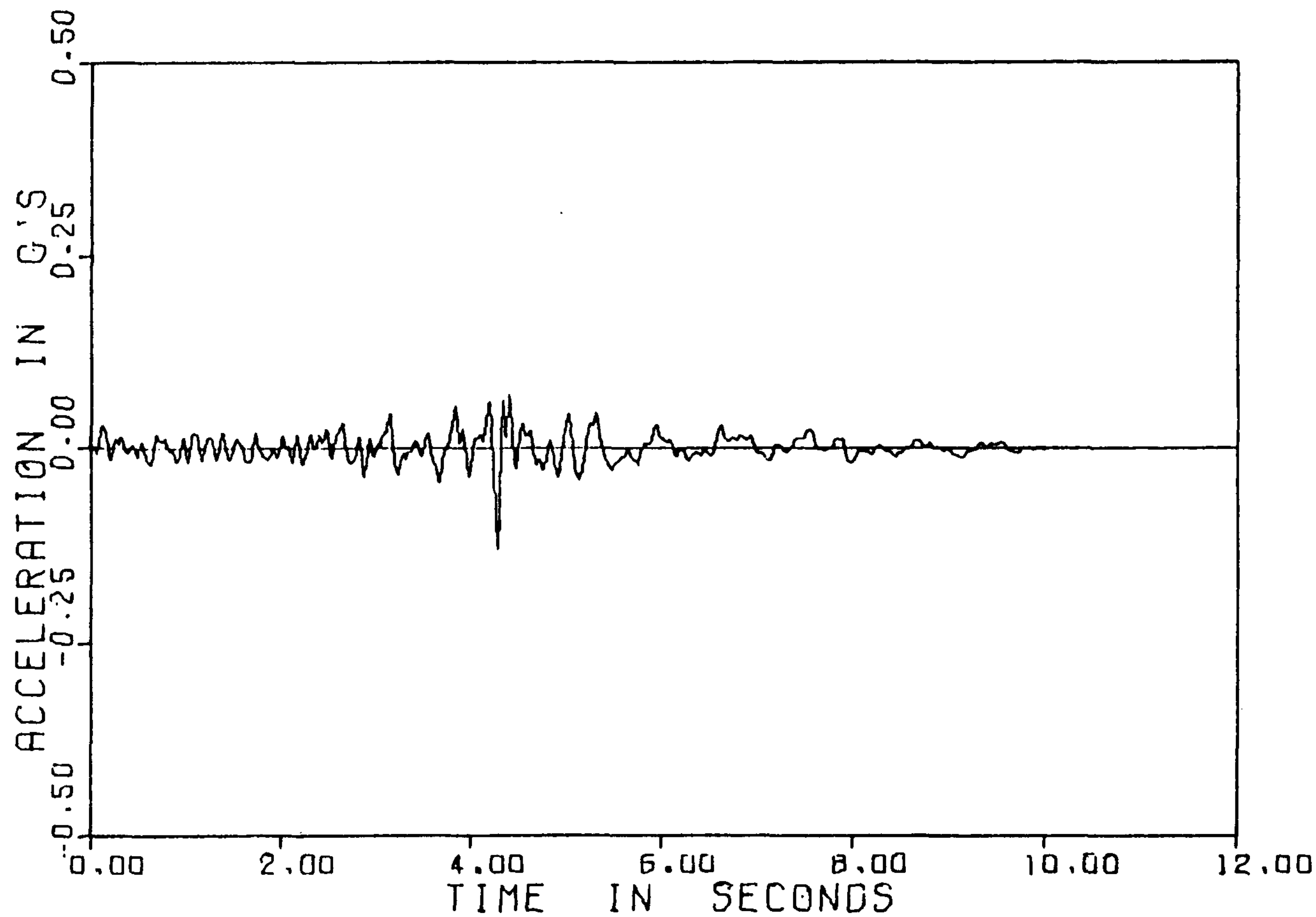

FIGURE 1a. Acceleration Record of Temblor, Parkfield (1966) - Vertical Component

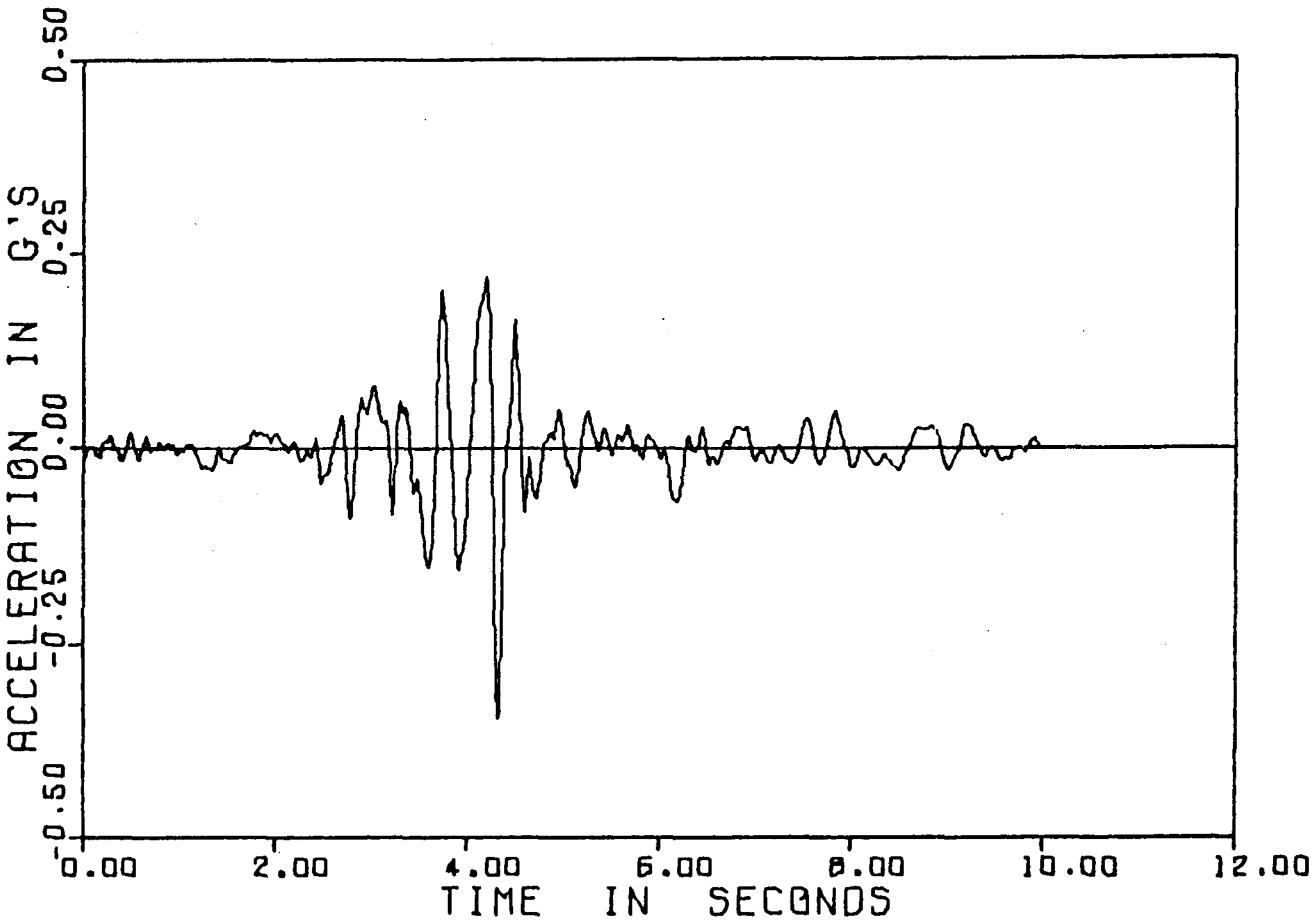

FIGURE 1b. Acceleration Record of Temblor, Parkfield (1966) – S25W Component

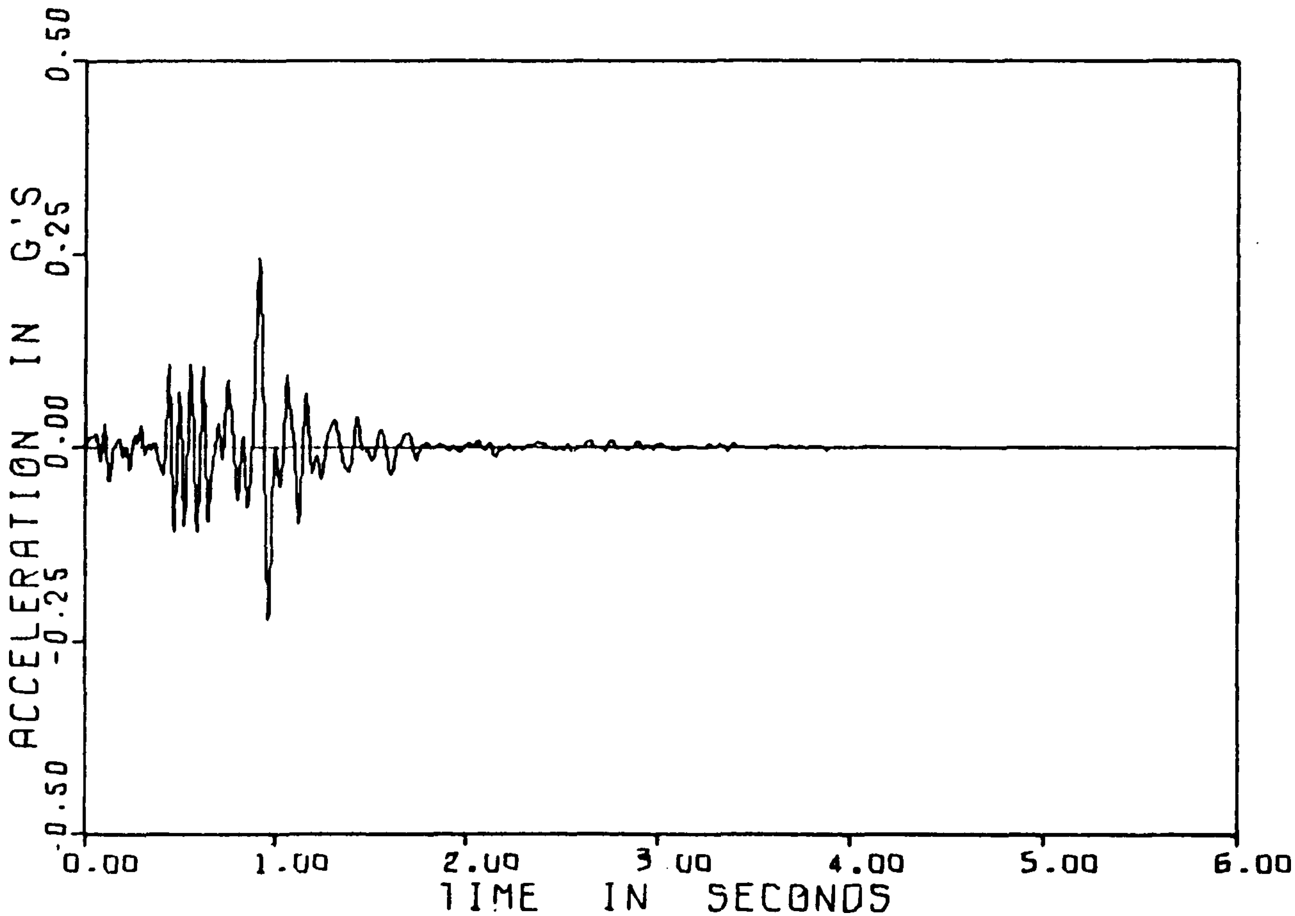

FIGURE 2a. Acceleration Record of CDMG-6, Oroville Aftershock (1975) - Vertical Component

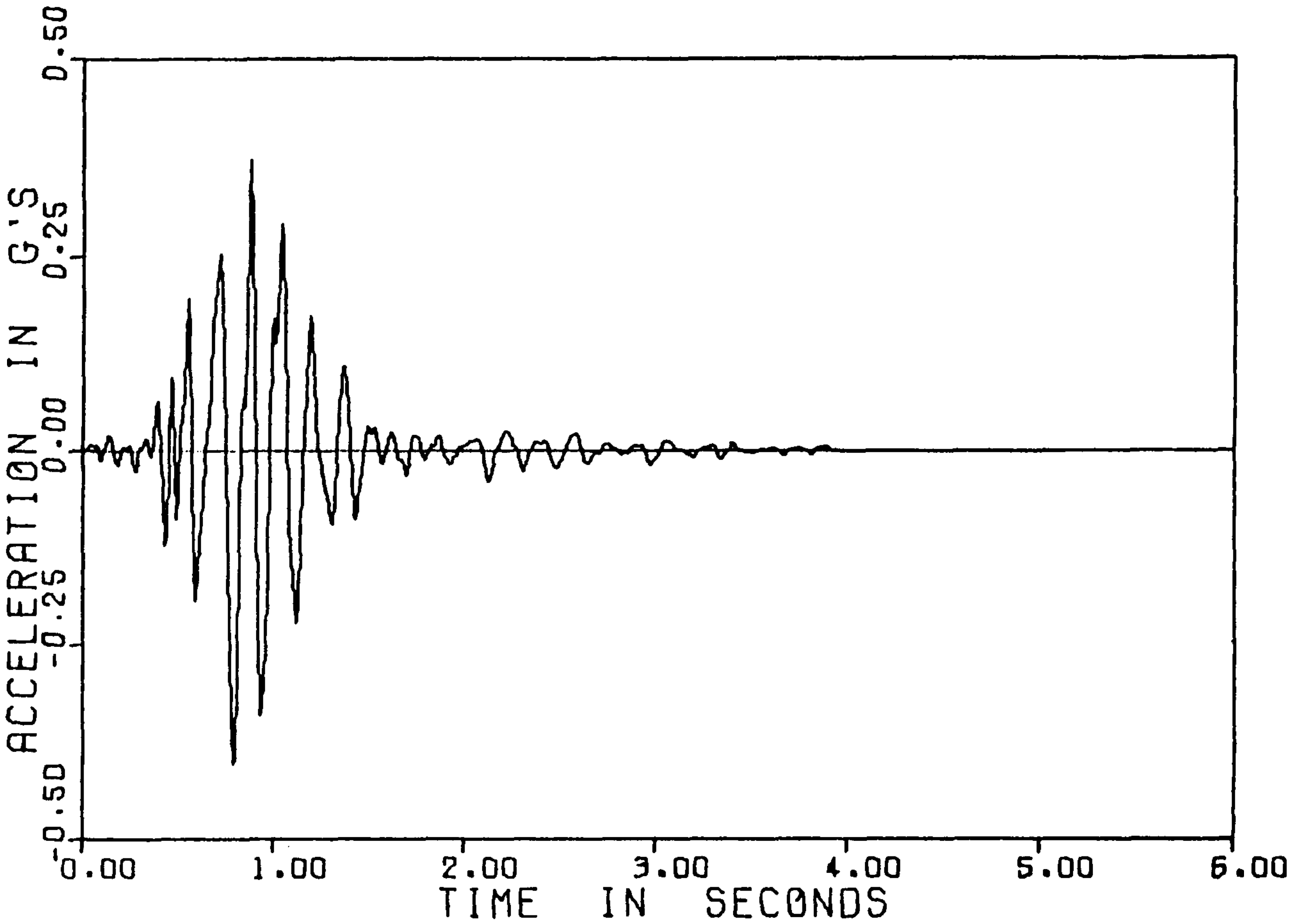

FIGURE 2b. Acceleration Record of CDMG-6, Oroville Aftershock (1975) - S55E Component

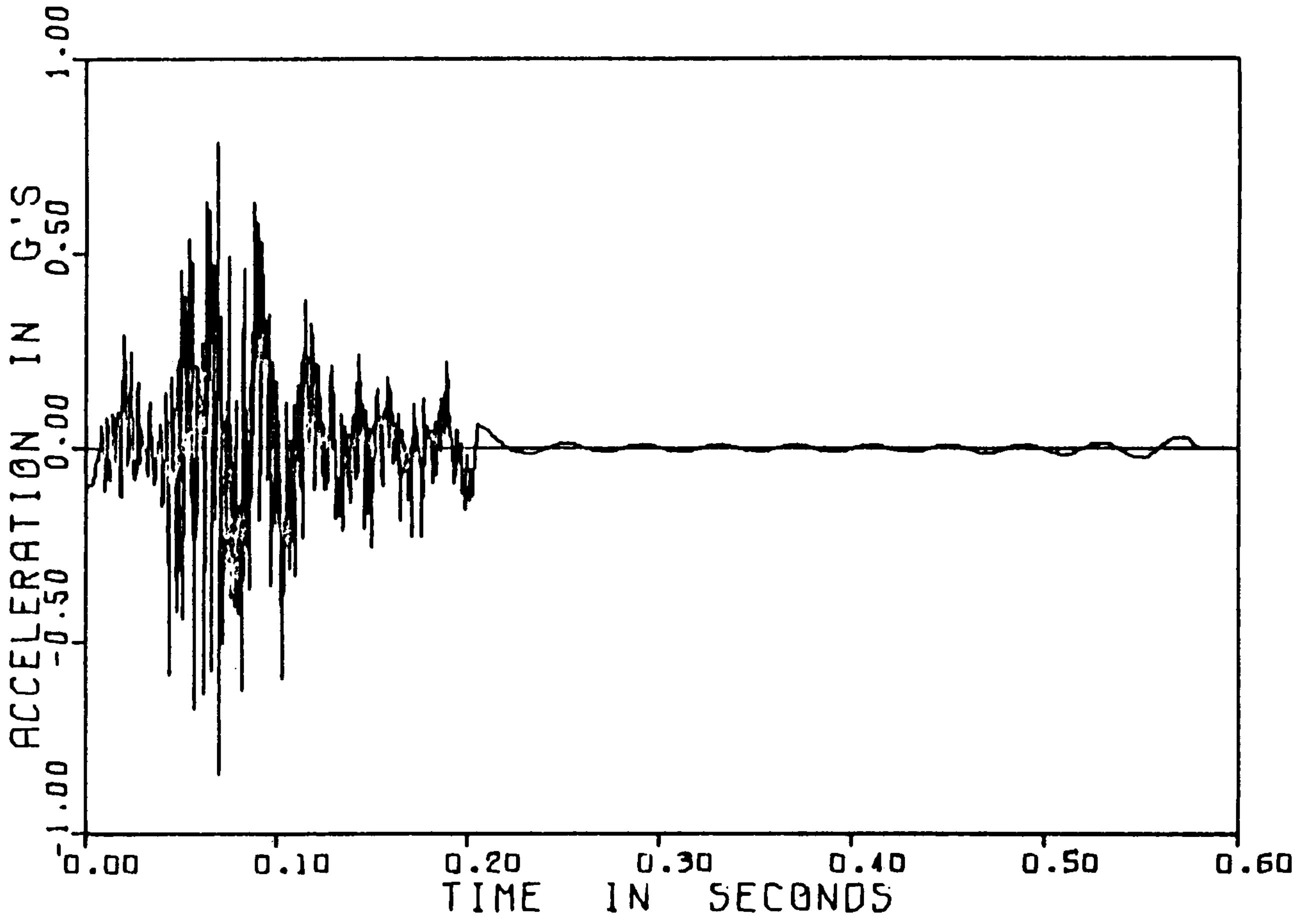

FIGURE 3a. Acceleration Record of the East Rand Proprietary Mines, South Africa (1978) - Vertical Component

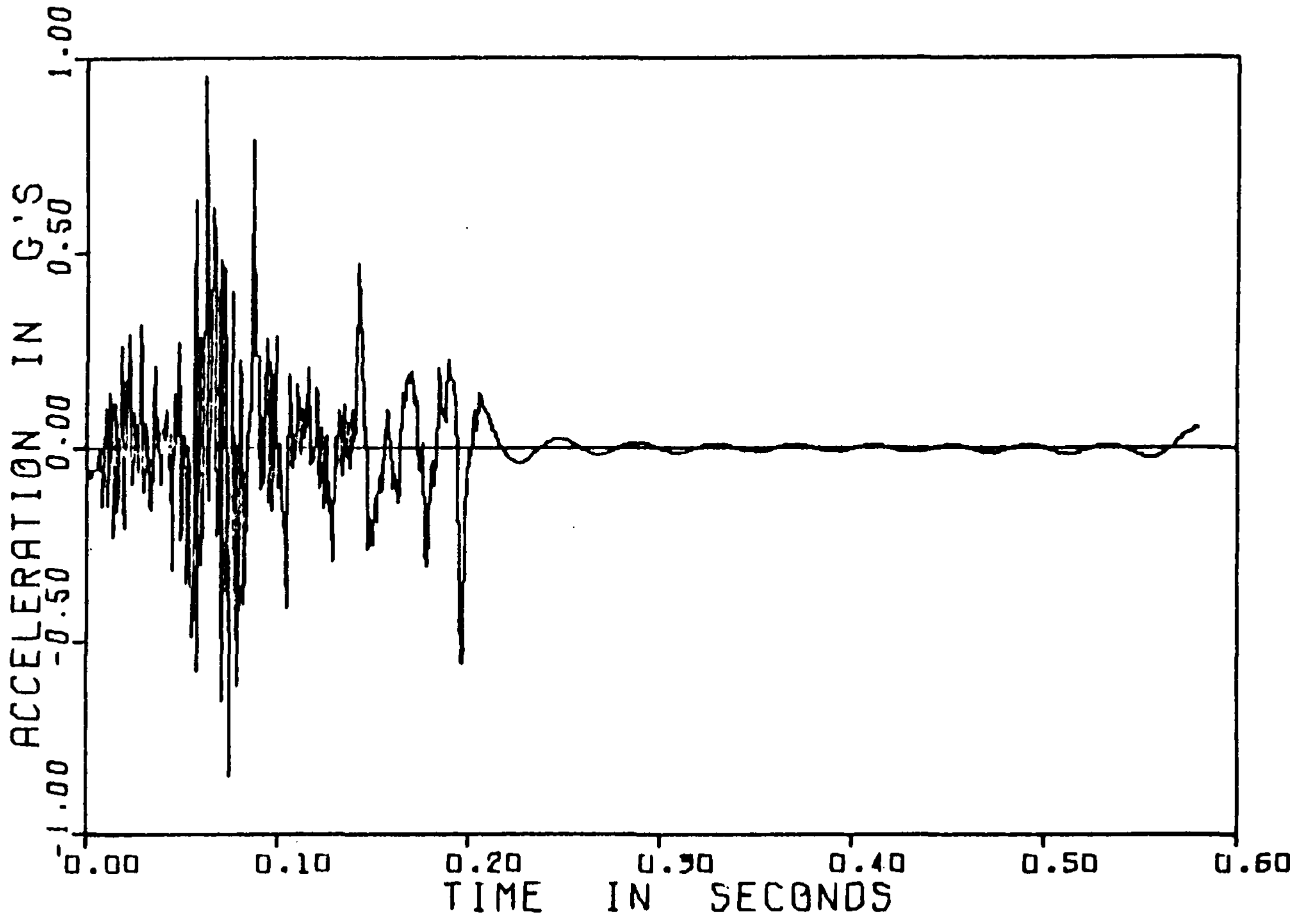

FIGURE 3b. Acceleration Record of the East Rand Proprietary Mines, South Africa (1978) - Longitudinal Component

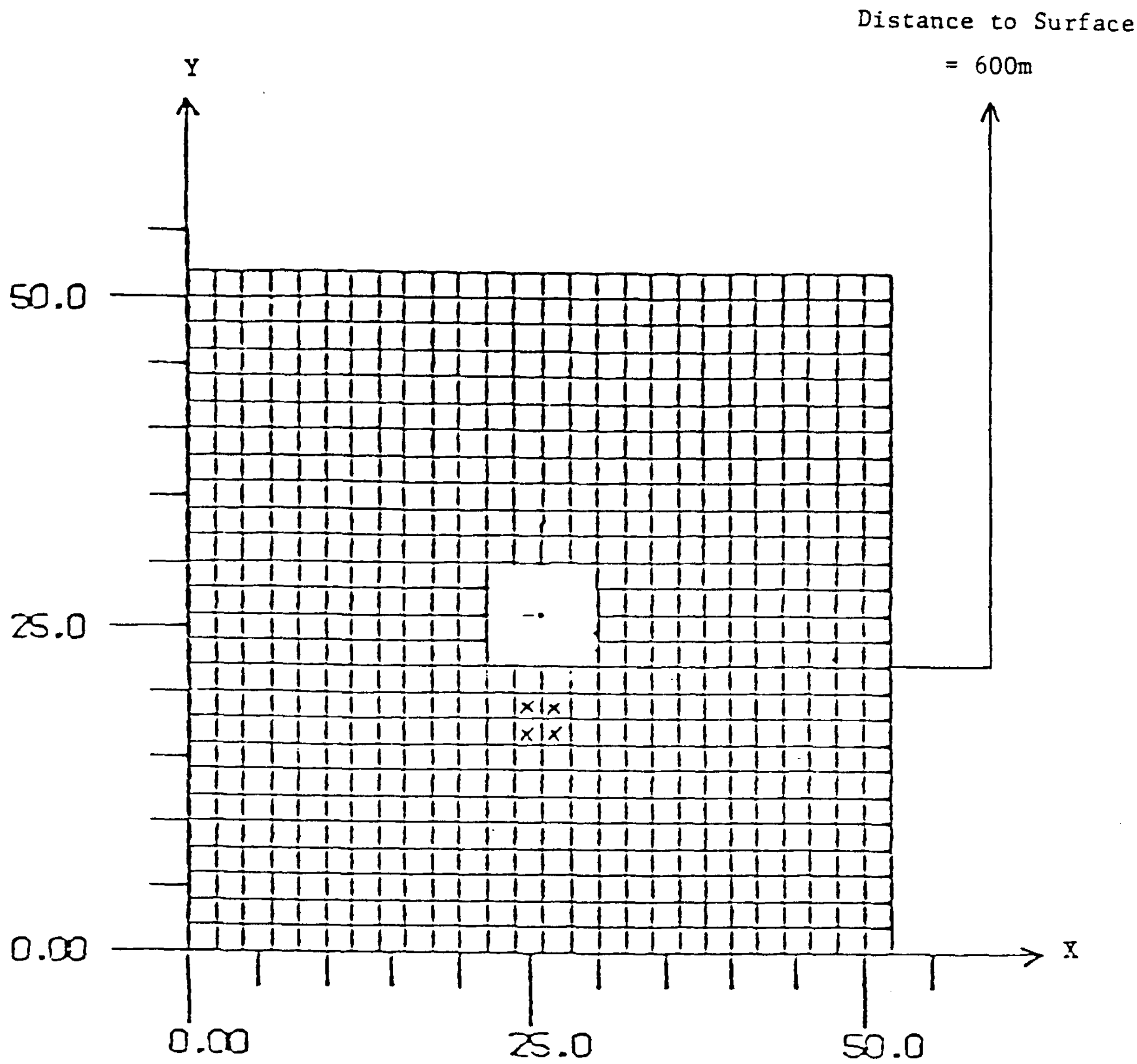

KEY

X Zones Simulating Canister Heating

Notes:

1) Tunnel (or room) dimensions are 8 m x 8 m.
2) Bottom of tunnel is 600 m below surface, i.e., top of grid is 570 m below the surface.

FIGURE 4. Calculational Grid Used for All Runs (except Model with Shear Zone)

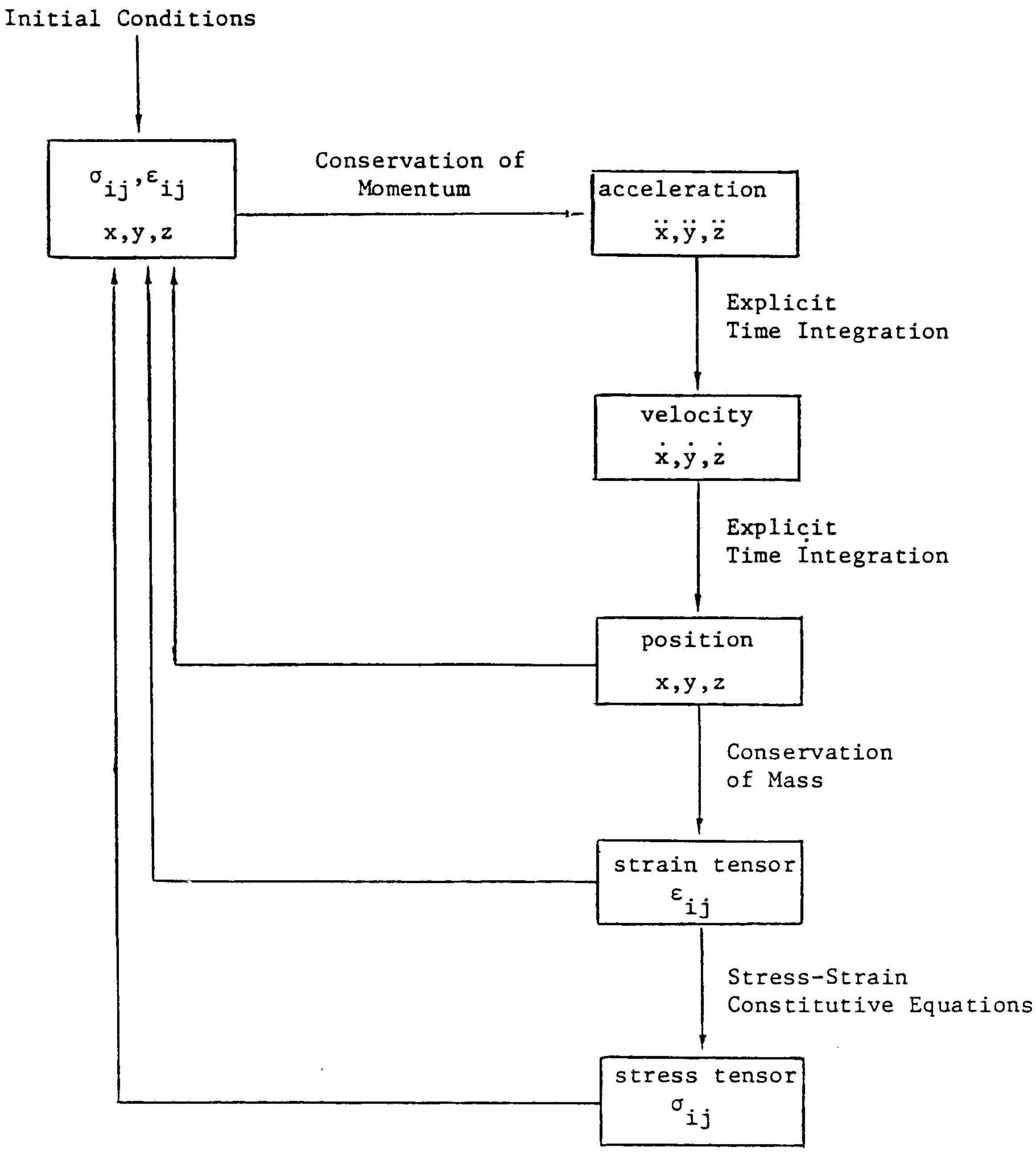

FIGURE 5. Calculational Sequence for STEALTH

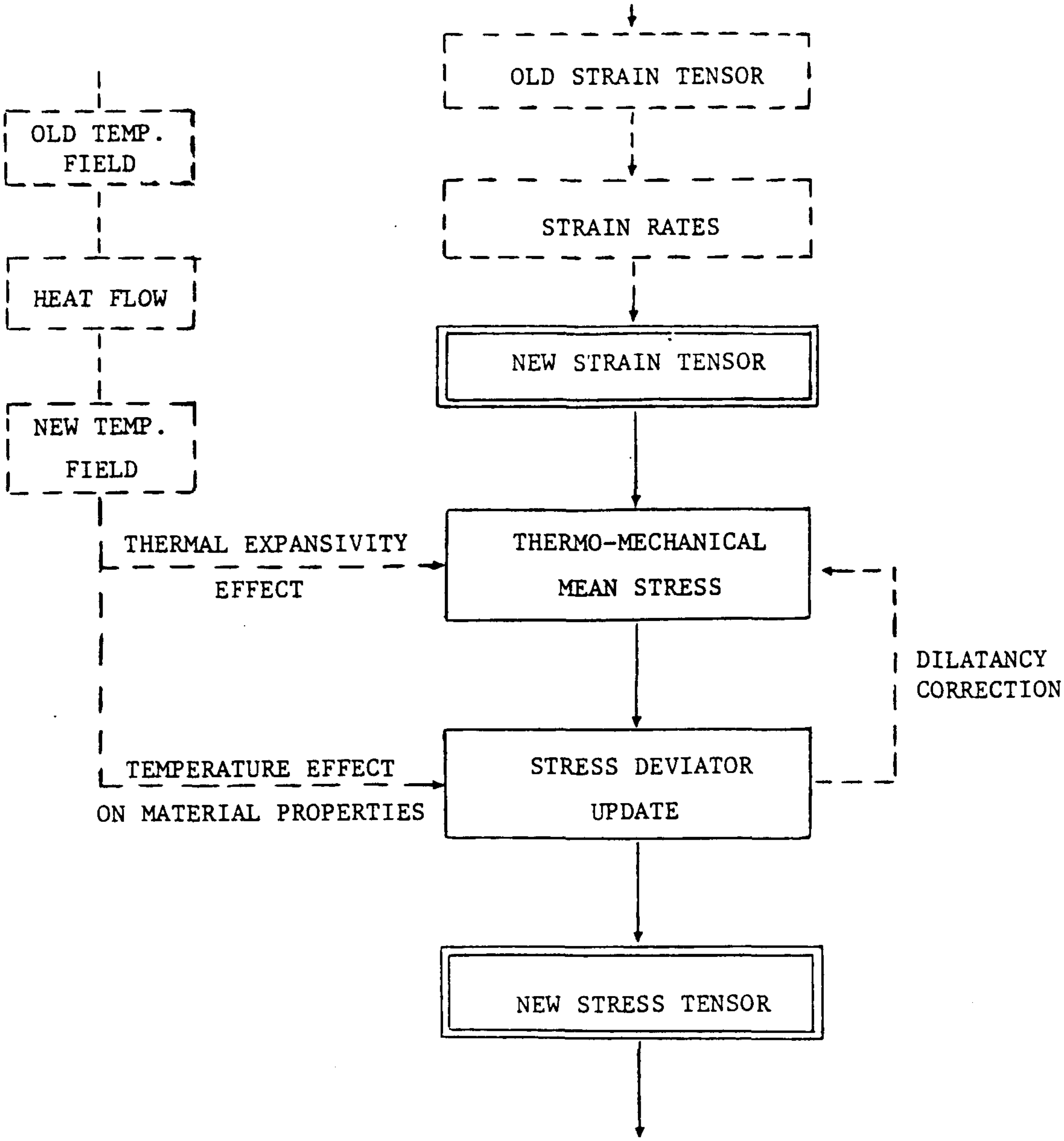

FIGURE 6. Calculational Sequence to Obtain New Stress Tensor

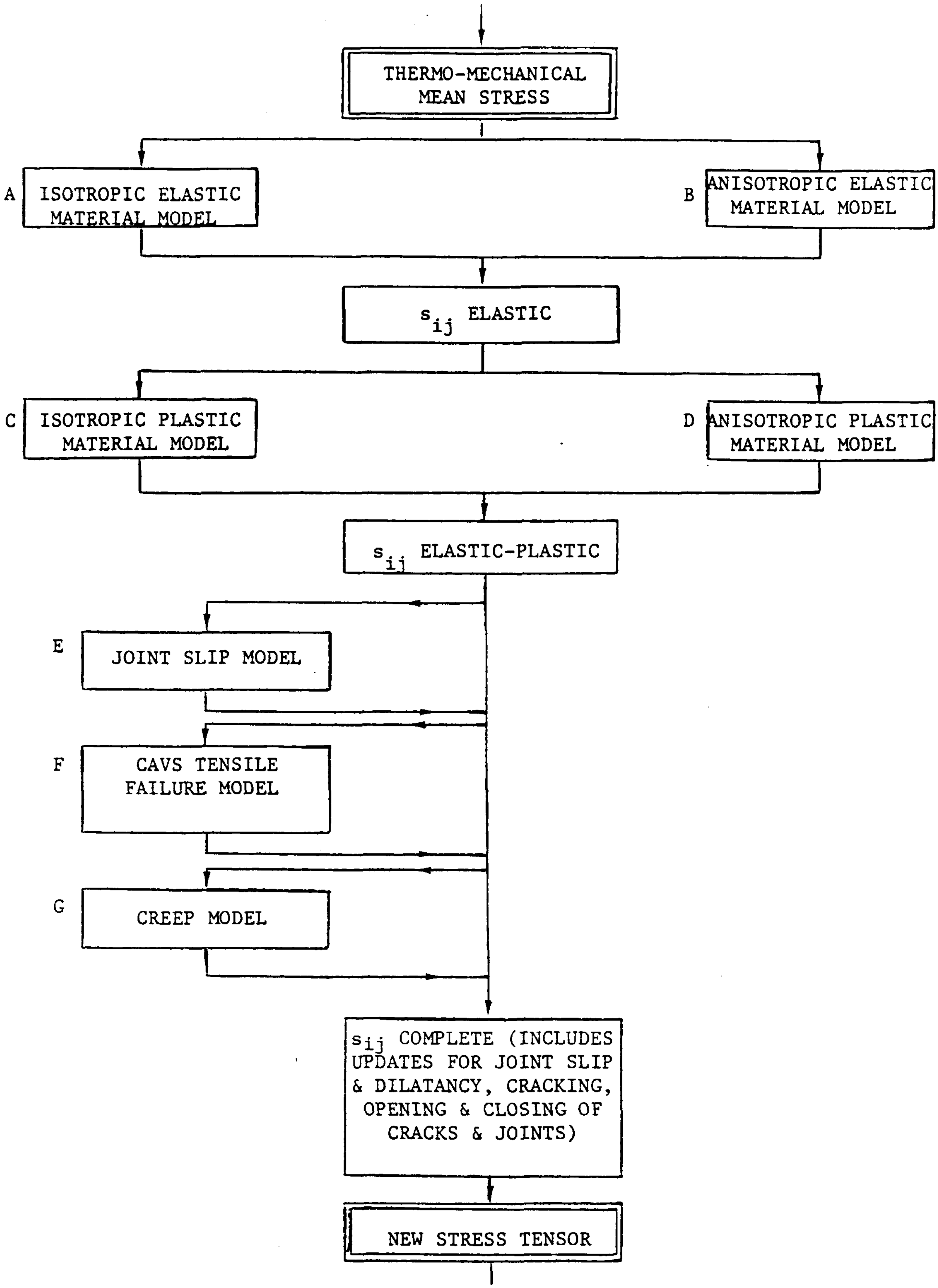

FIGURE 7. Calculational Sequence to Update Stress Deviators (s_{ij})

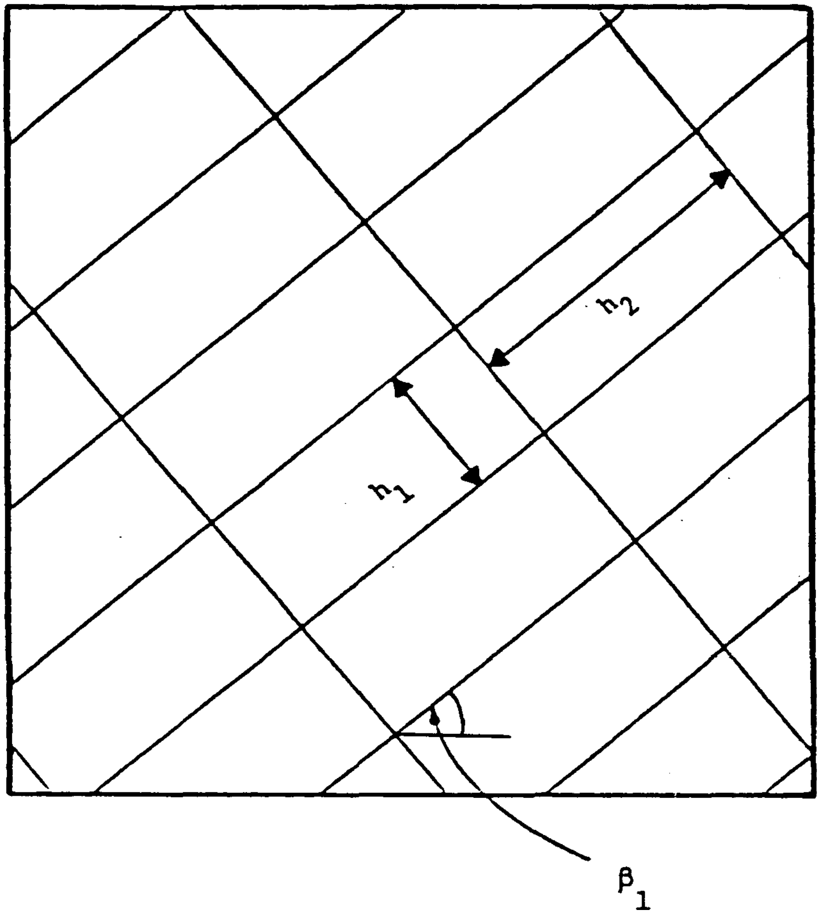

FIGURE 8. Definition of Orthogonal Jointing System Used in the Joint Slip Model

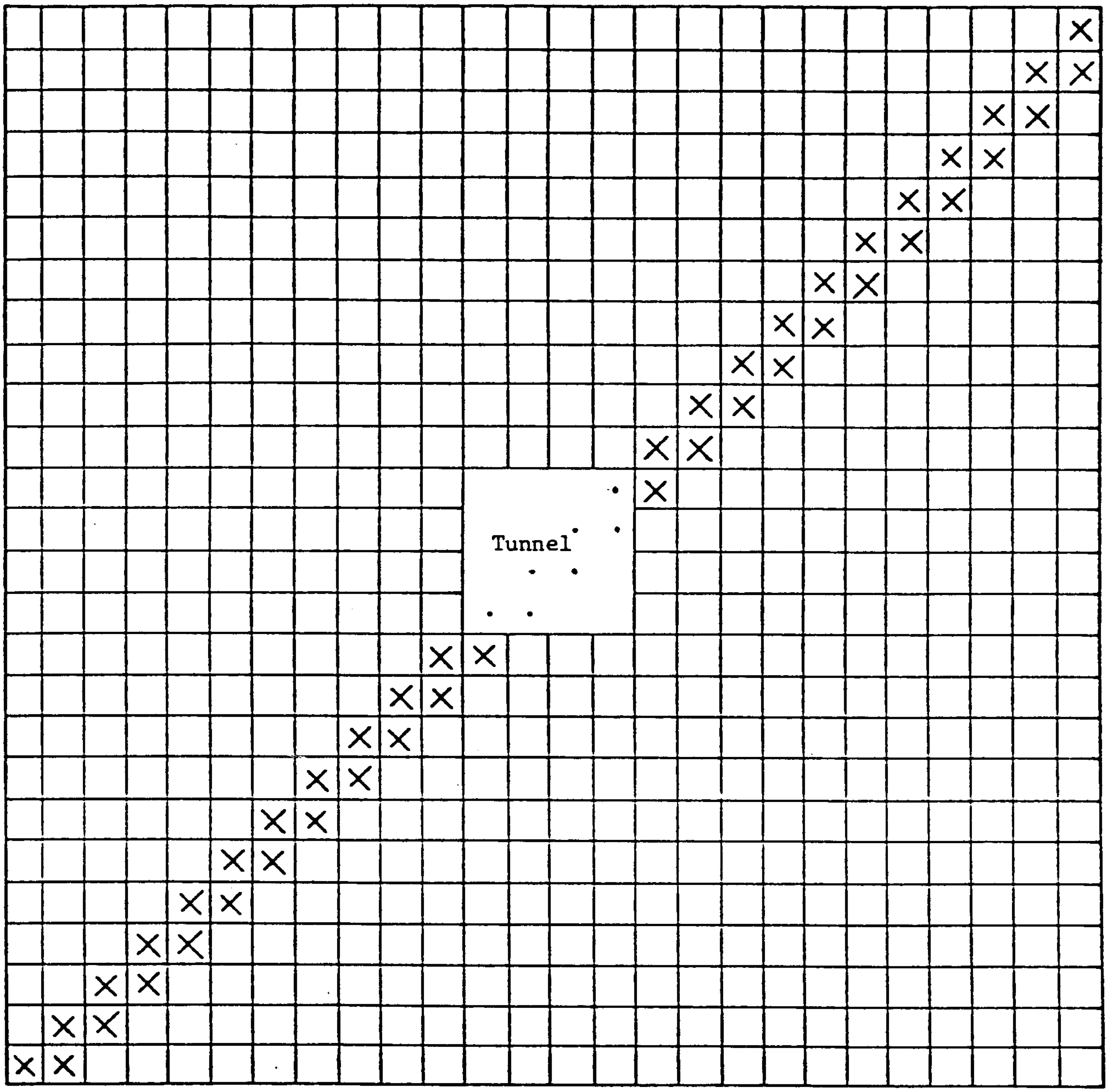

FIGURE 9. Representation of a Shear Zone in the STEALTH Calculations

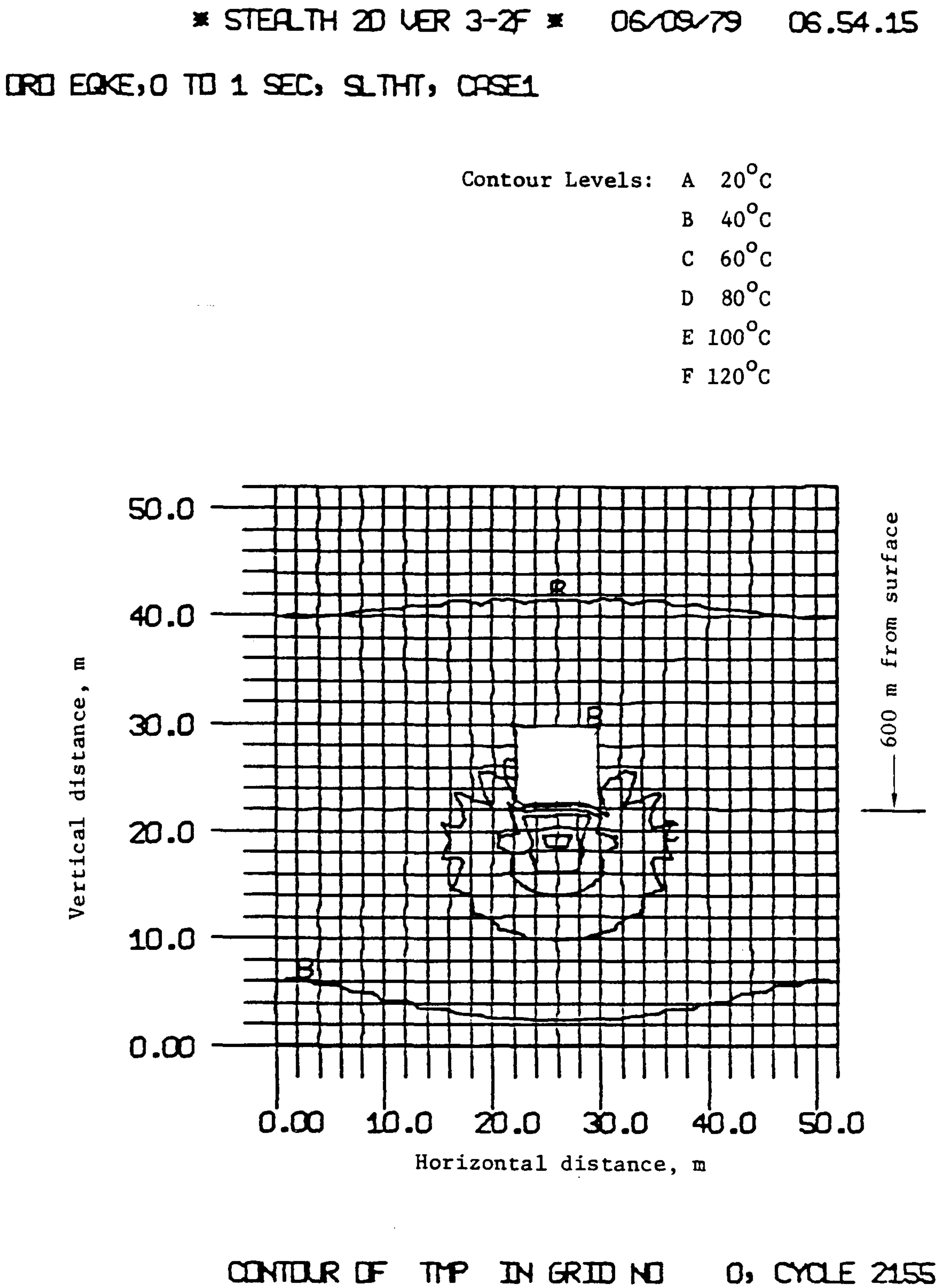

FIGURE 10. Temperature Contours (°C) in Salt at the End of the Heating Phase

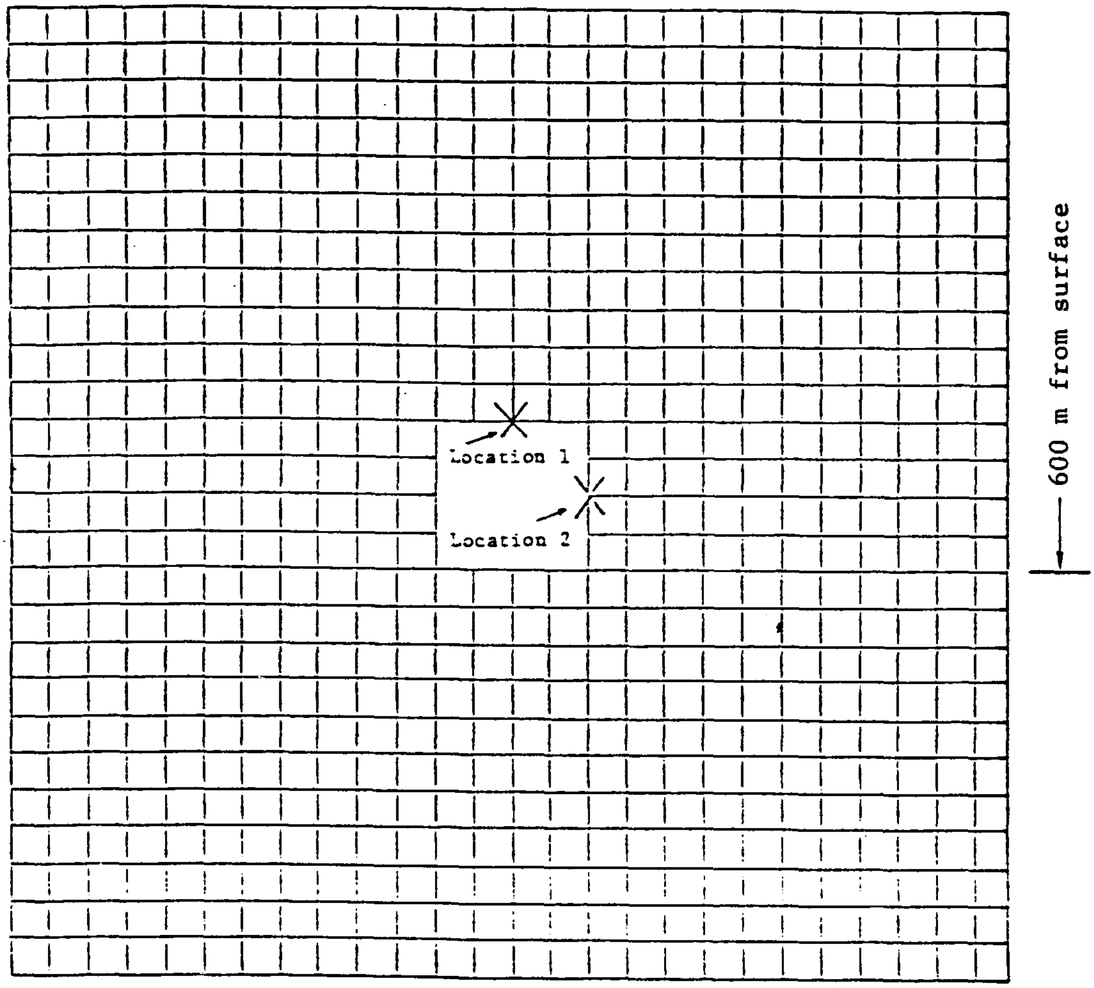

FIGURE 11. **Finite-Difference Mesh Showing Location 1 and Location 2**

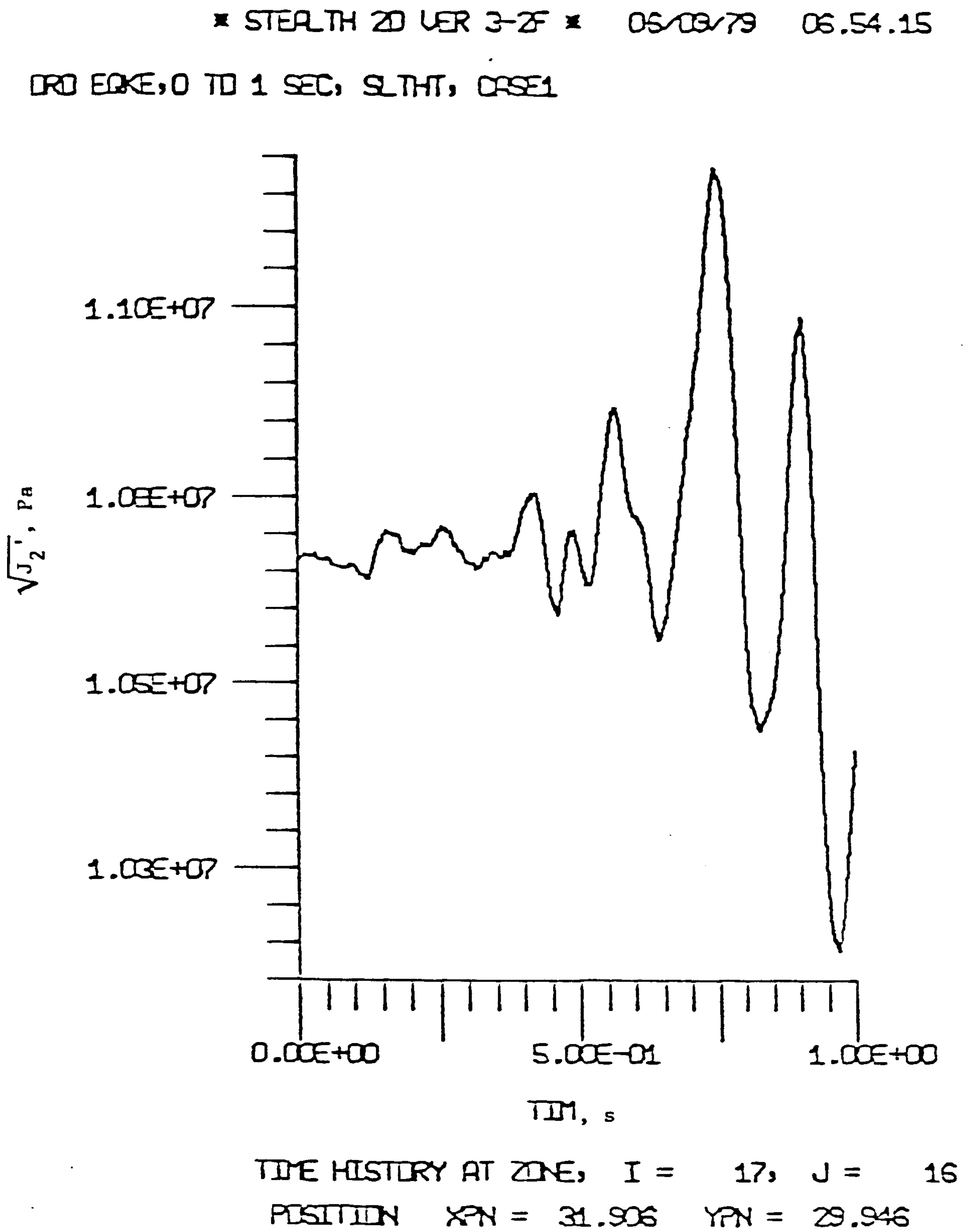

FIGURE 12. A Time History of $\sqrt{J_2'}$ (Second Invariant of the Deviatoric Stress Tensor) Near the Upper Right Hand Corner of the Tunnel, Salt, Case 1

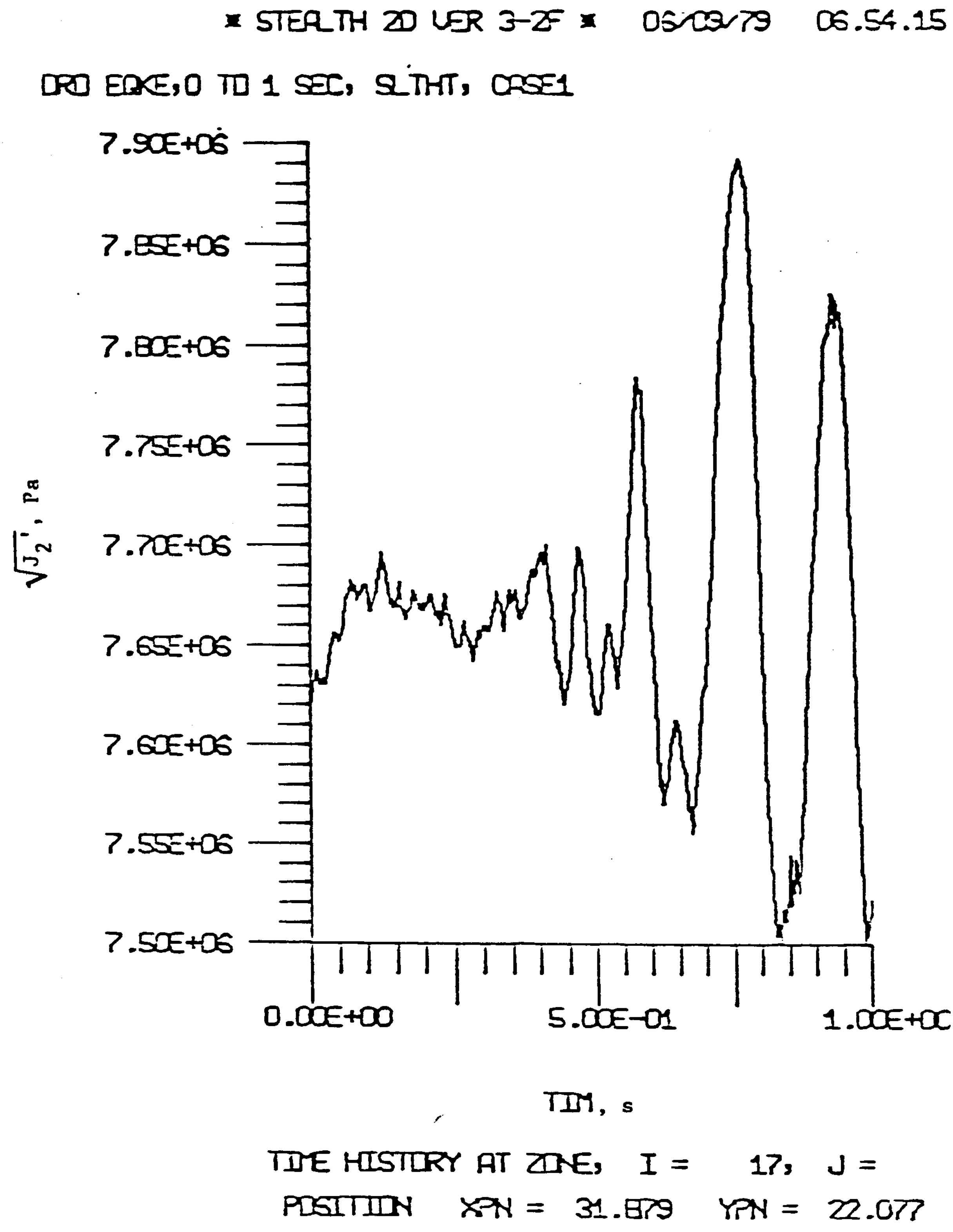

FIGURE 13. A Time-History of $\sqrt{J_2'}$ Near the Bottom Right Hand Corner of the Tunnel, Salt, Case 1

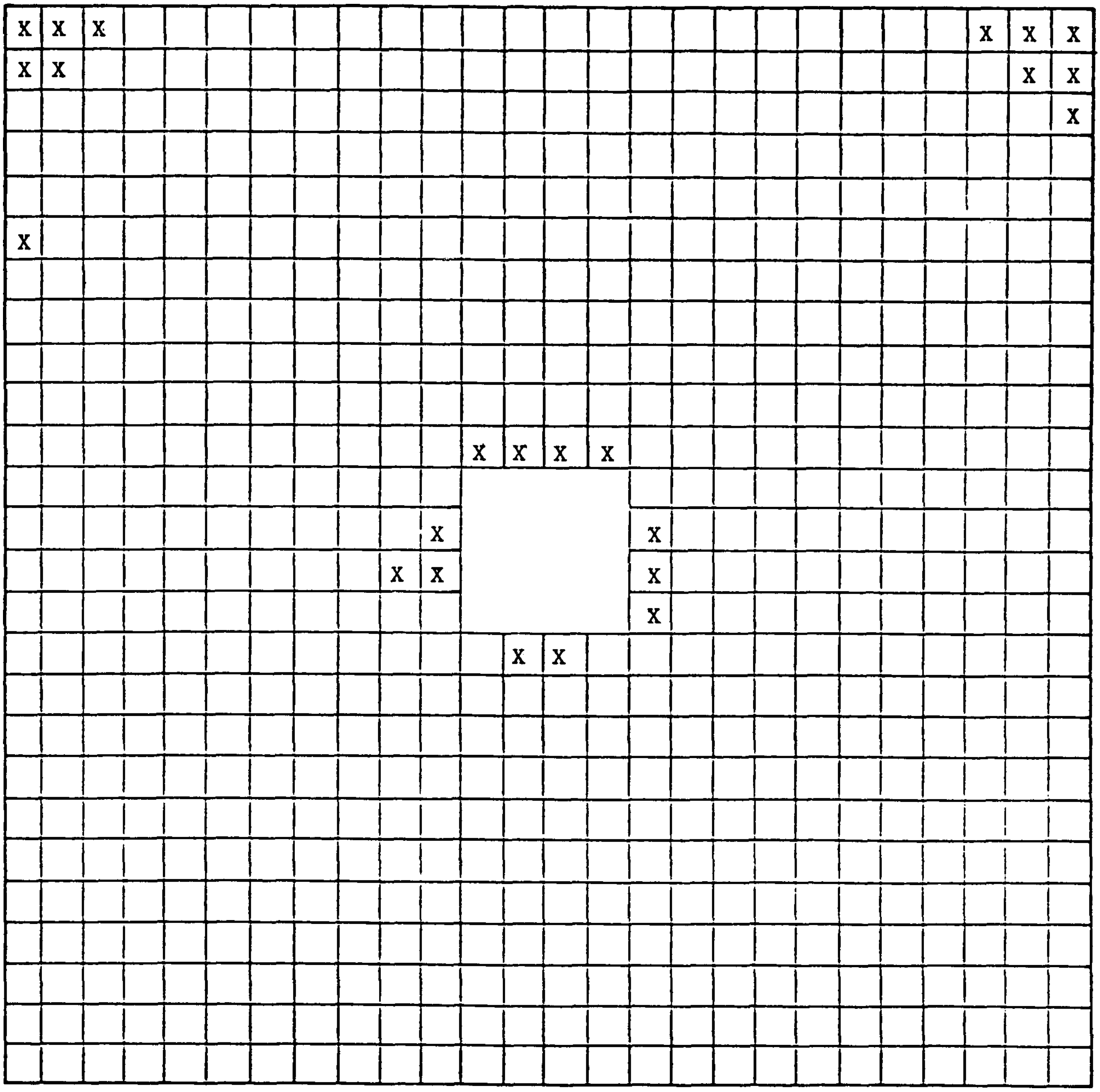

FIGURE 14. Zones with Cracks (indicated by an X) at the End of the Heating Phase, but Prior to the Earthquake in Salt, Cases 1, 2, and 3

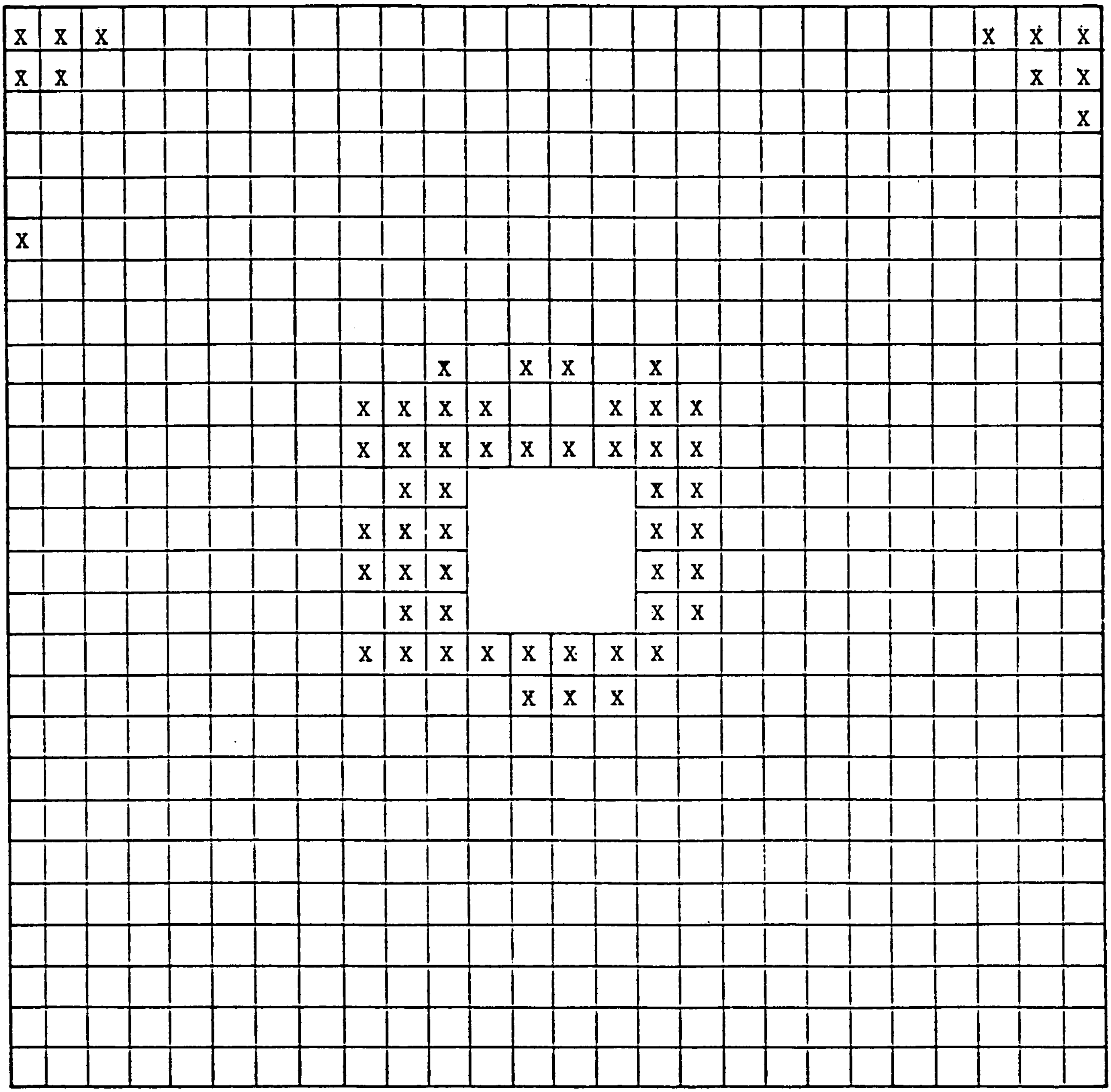

FIGURE 15. Zones with Cracks (indicated by an X) After 0.138 s of Earthquake Motion in Salt, Case 3

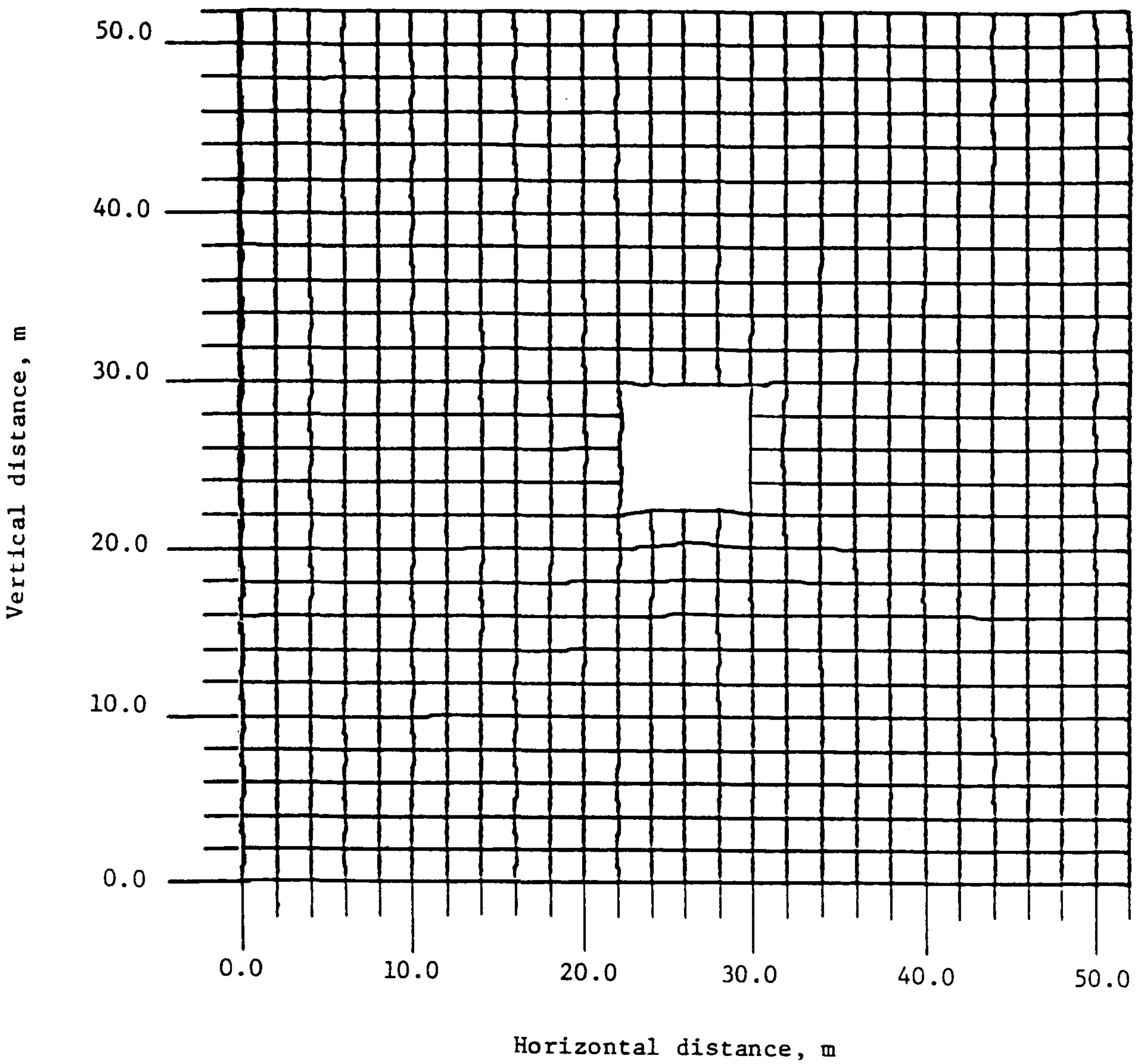

FIGURE 16. **Mesh Configuration Just Prior to the Earthquake for Cases 1, 2, and 3 in Salt**

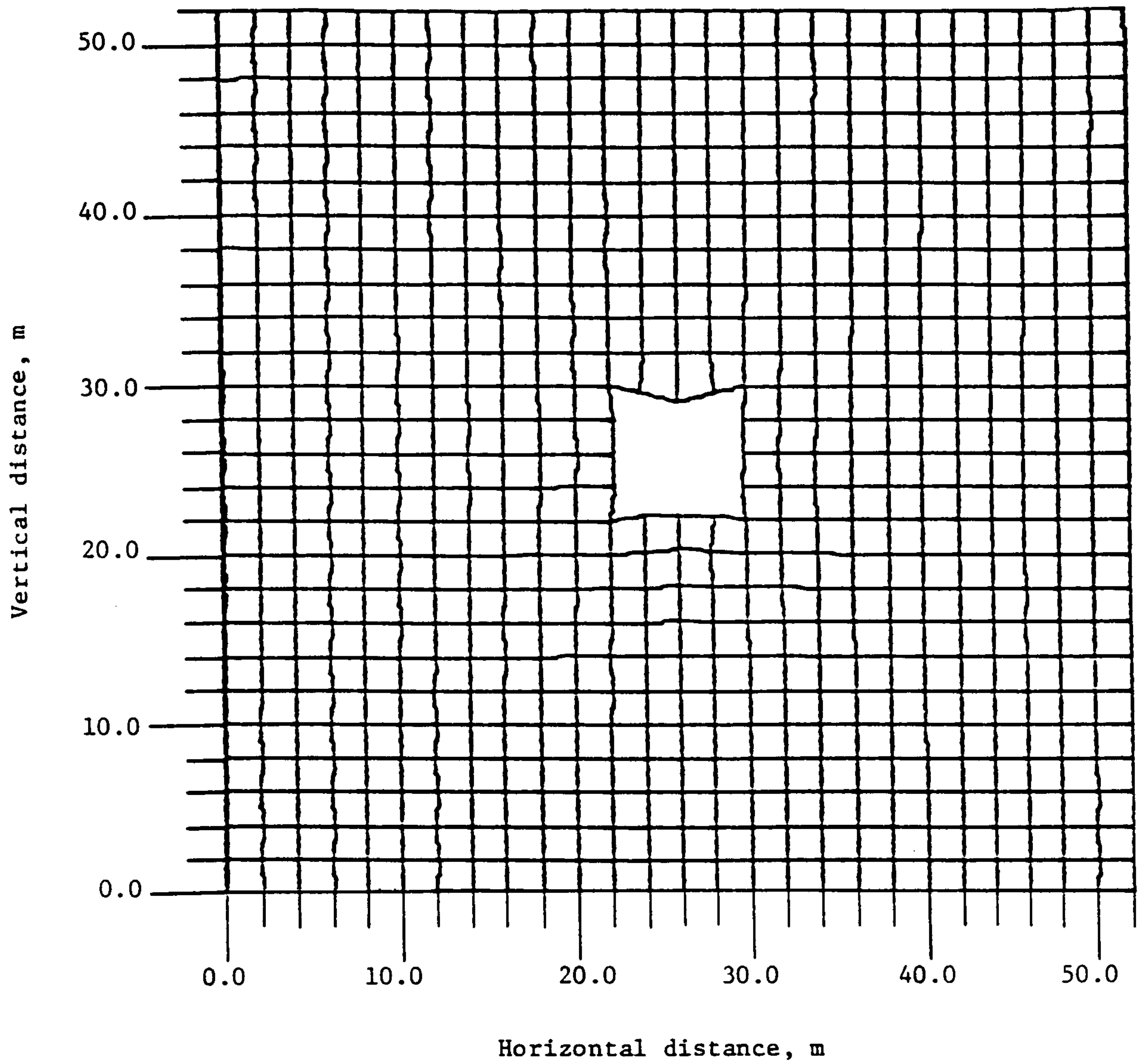

FIGURE 17. Mesh Configurations After 0.138 s of ERPM Motion in Salt, Case 3

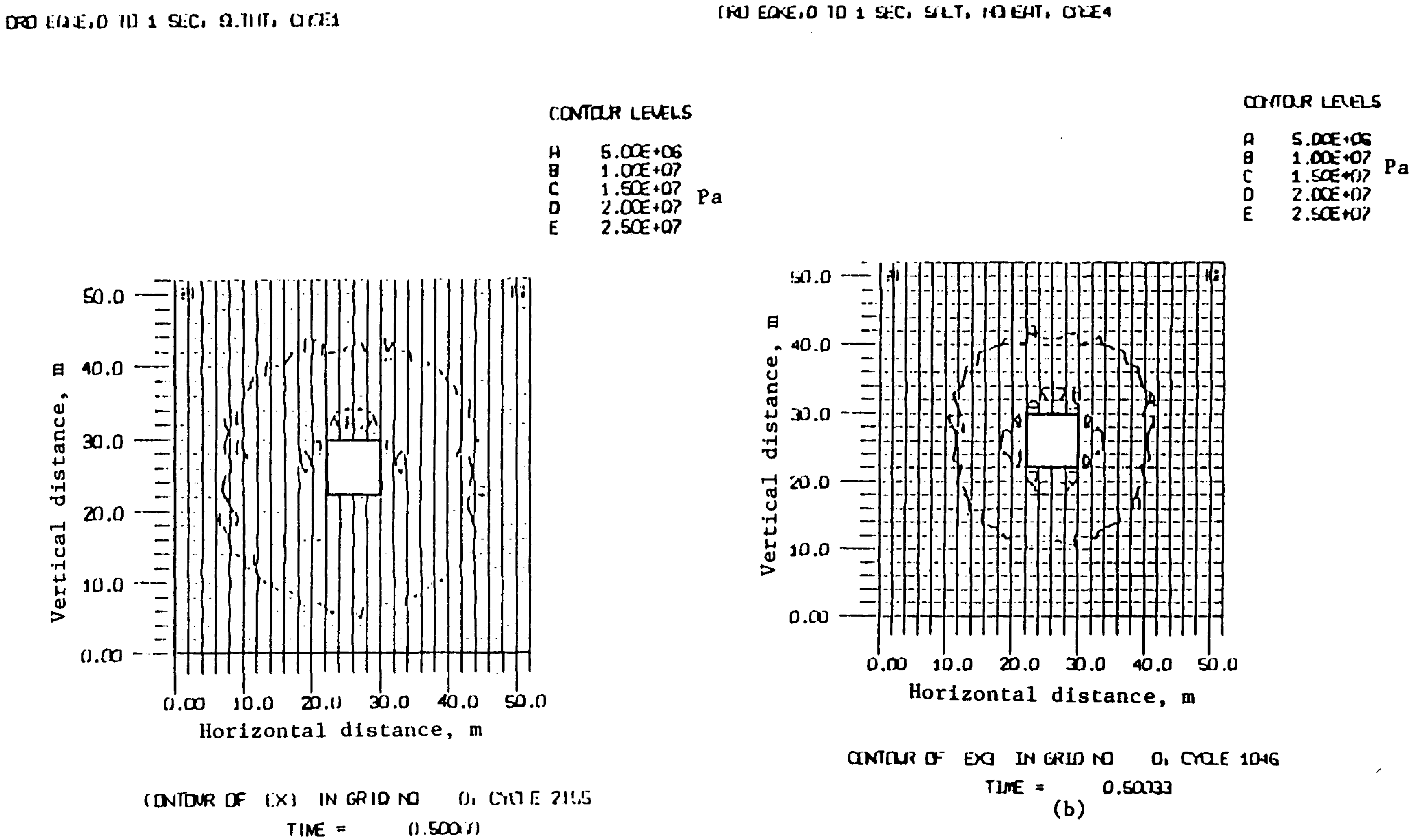

FIGURE 18. Contours of $\sqrt{J_2'}$ in Salt at 0.5 s: (a) Case 1, and (b) Case 4

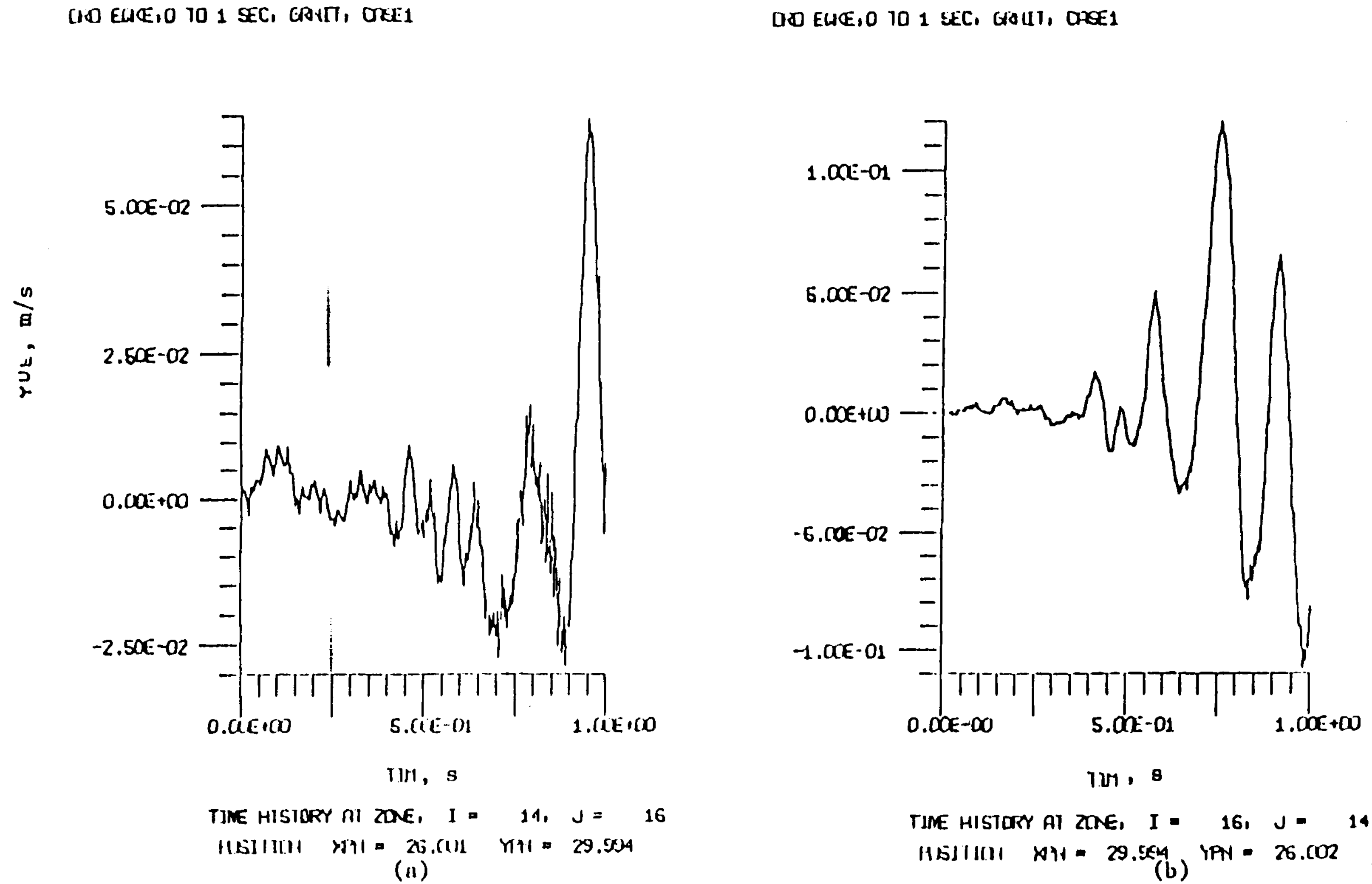

FIGURE 19. Velocity Time History at Locations 1 and 2: (a) Y-Velocity History at Location 1, and (b) X-Velocity History at Location 2

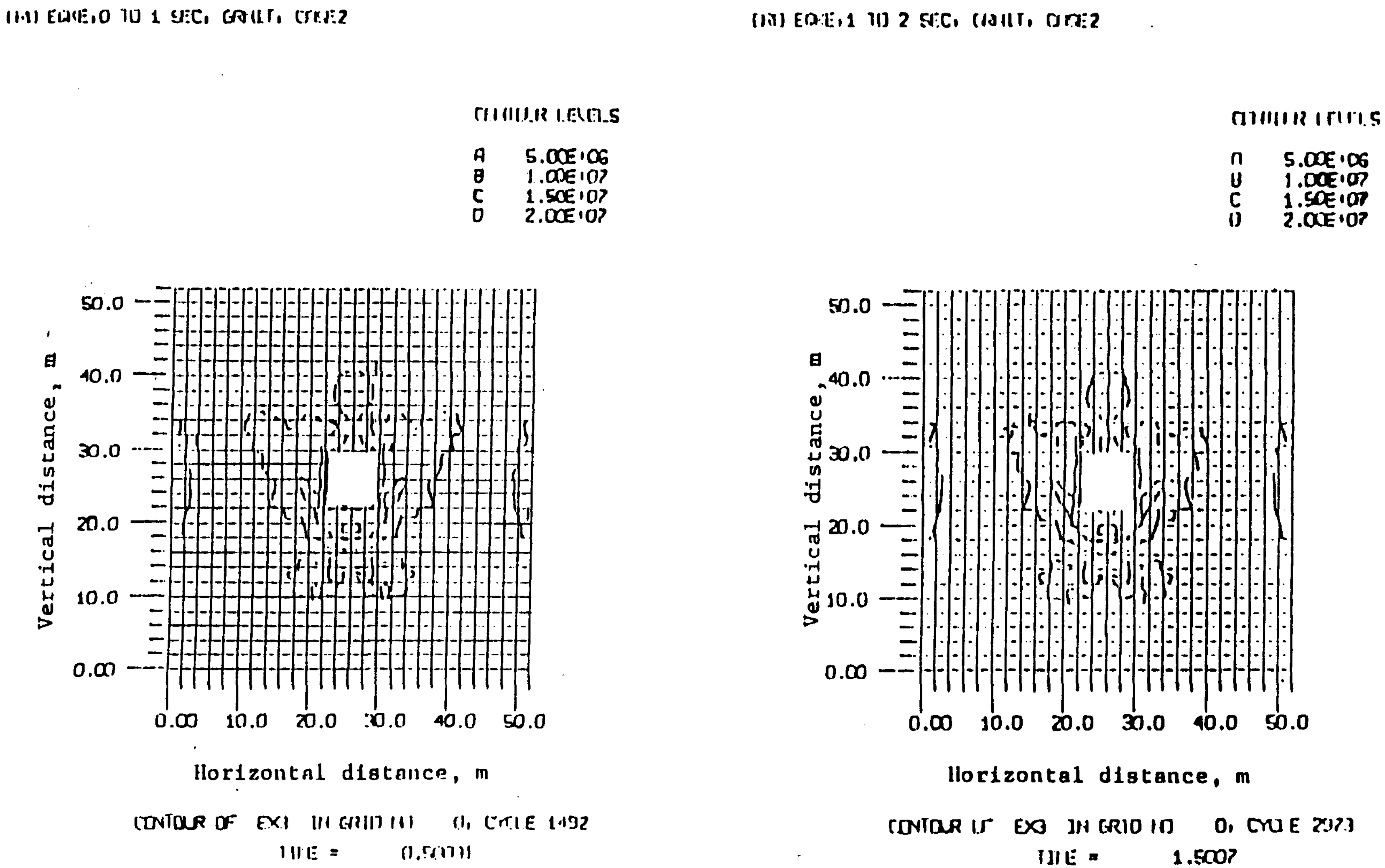

(a)

(b)

FIGURE 20. Contours of $\sqrt{J_2'}$ in Case 2 of Granite: (a) at 0.5 s; and (b), at 1.5 s

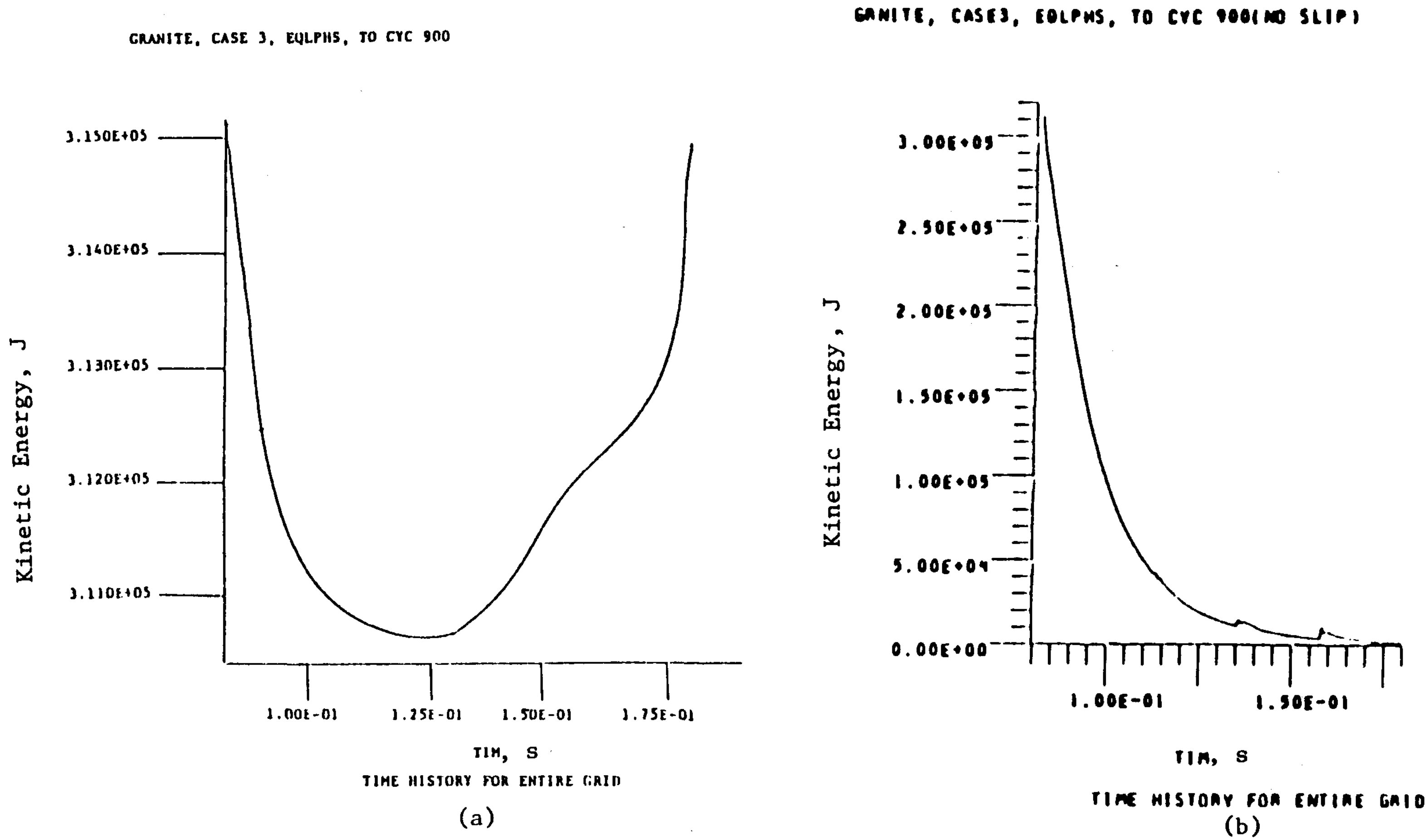

FIGURE 21. A Comparison of the Kinetic Energy Time History During the Equilibrium Phase in Case of Granite: (a) Slip Active, and (b) Slip Inactive

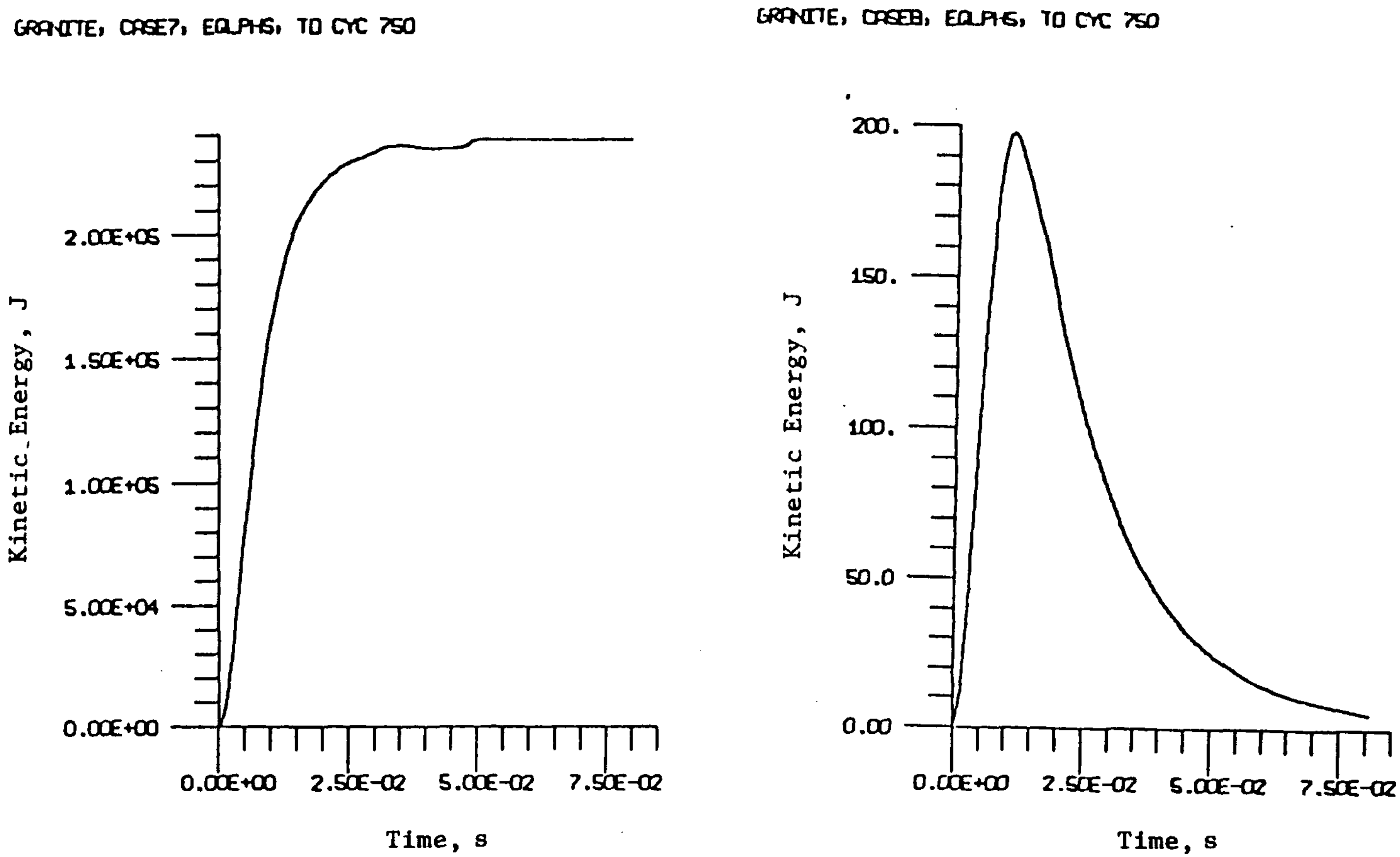

Time History for Entire Grid

(a)

Time History for Entire Grid

(b)

FIGURE 22. **A Comparison of the Kinetic Energy Time History During the Equilibrium Phase for Cases 7 and 8 in Granite: (a) Case 7 (unstable), and (b) Case 8 (stable)**

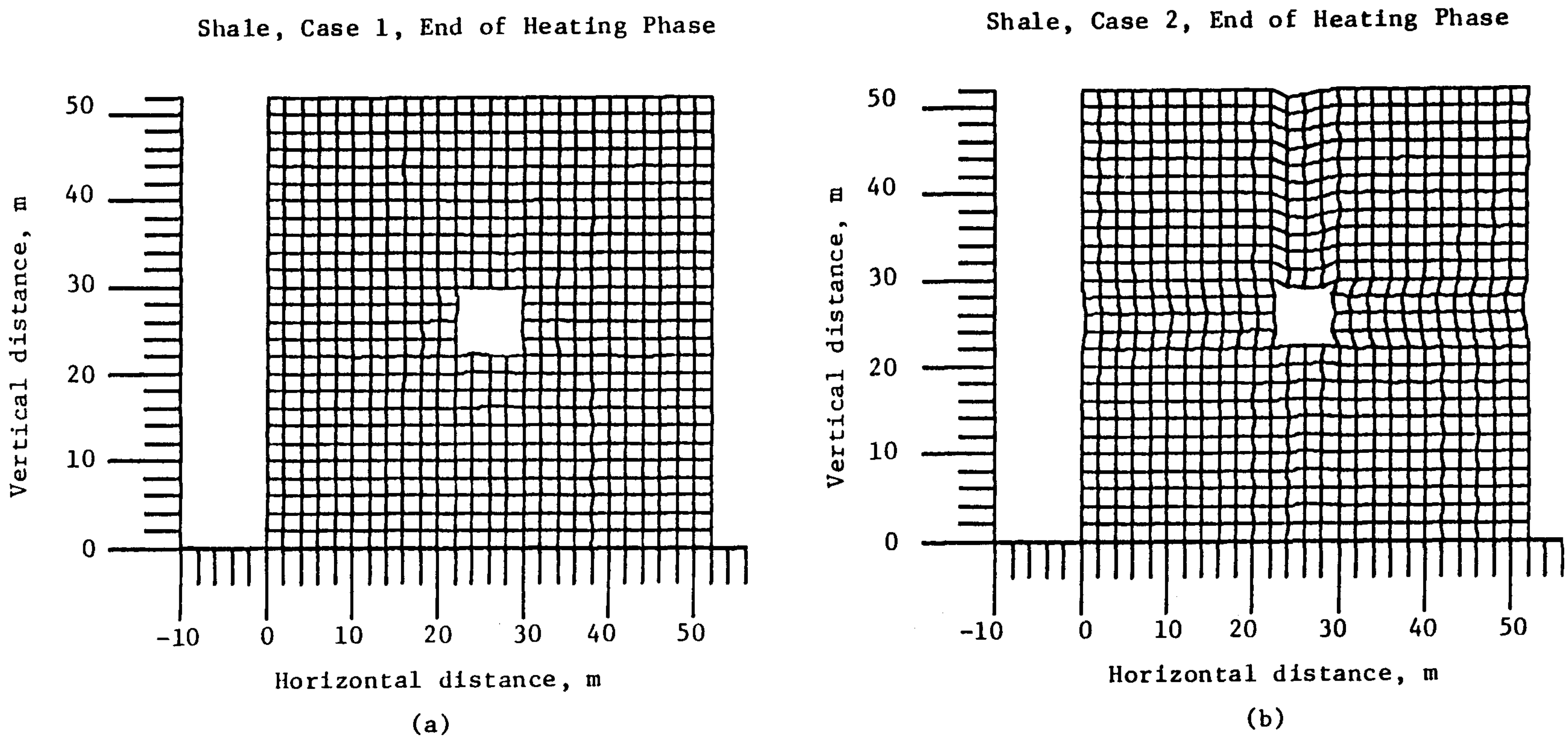

FIGURE 23. Mesh Plots at the End of the Heating Phase in Shale

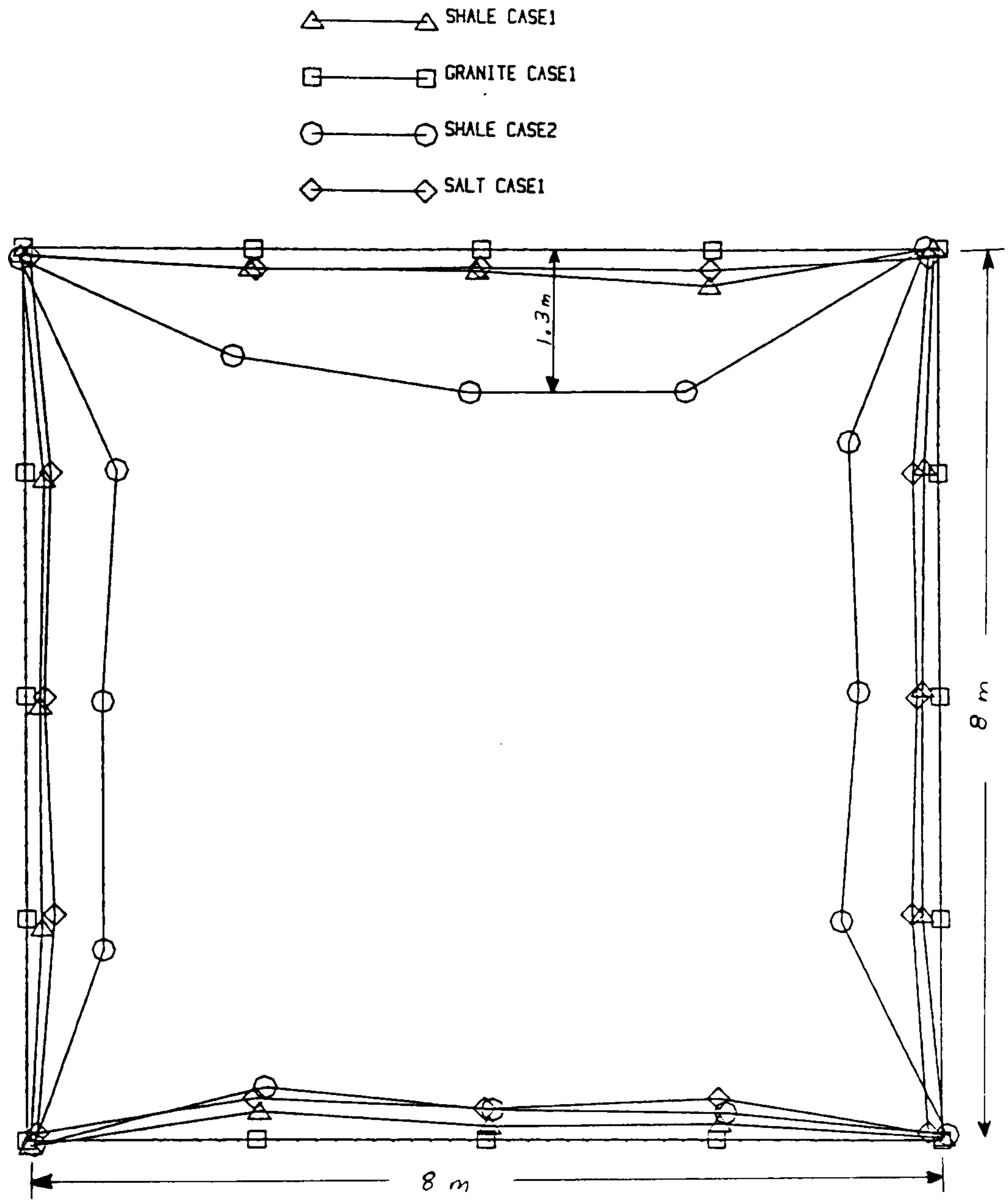

FIGURE 24. Tunnel Displacements at the End of the Five-Year Heating Period in Various Media (the Scale Factor between the Displacements and the tunnel dimension is unity)

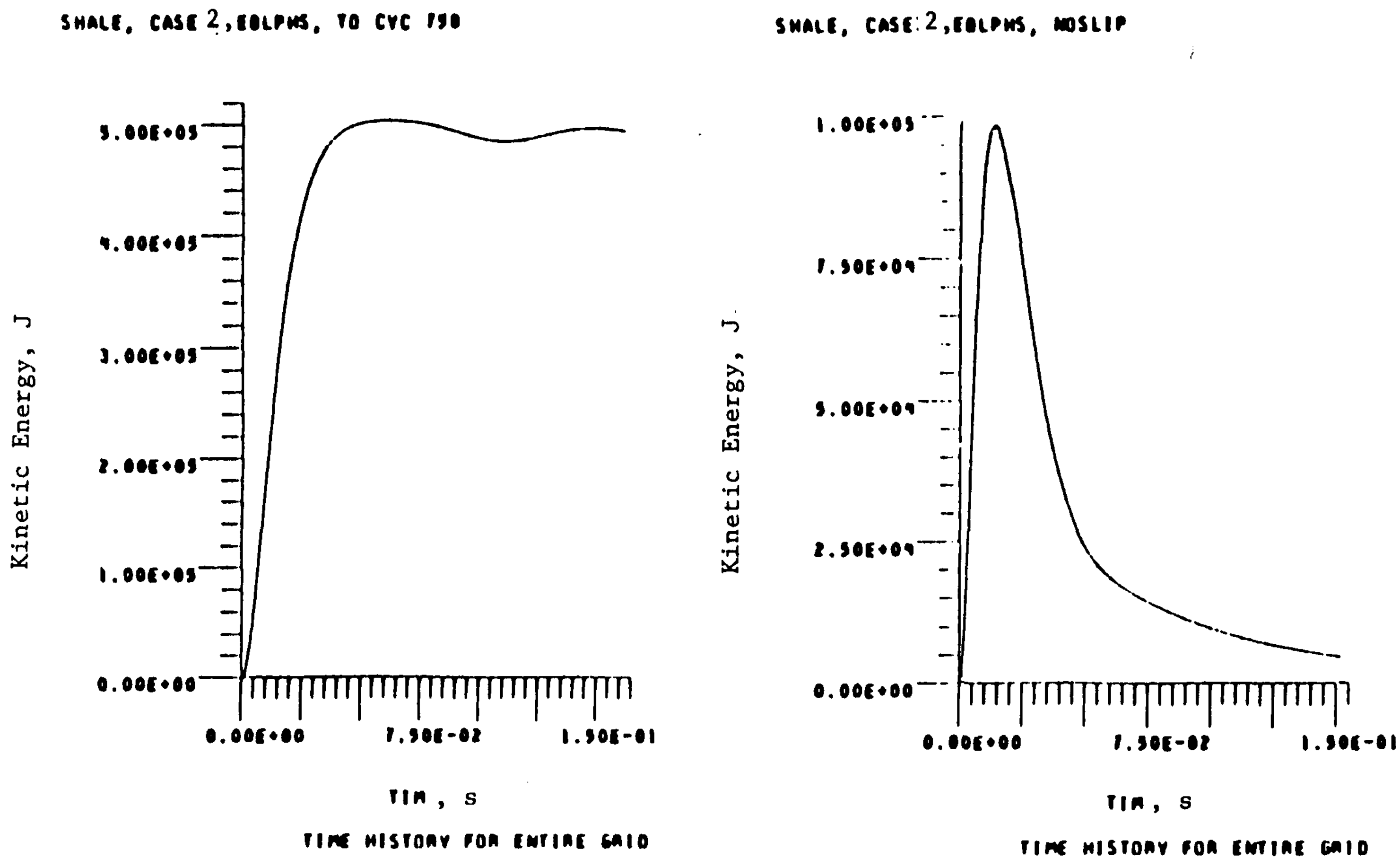

FIGURE 25. A Comparison of Kinetic Energy Time Histories in Shale During the Equilibrium Phase: (a) Slip Active, and (b) Slip Inactive

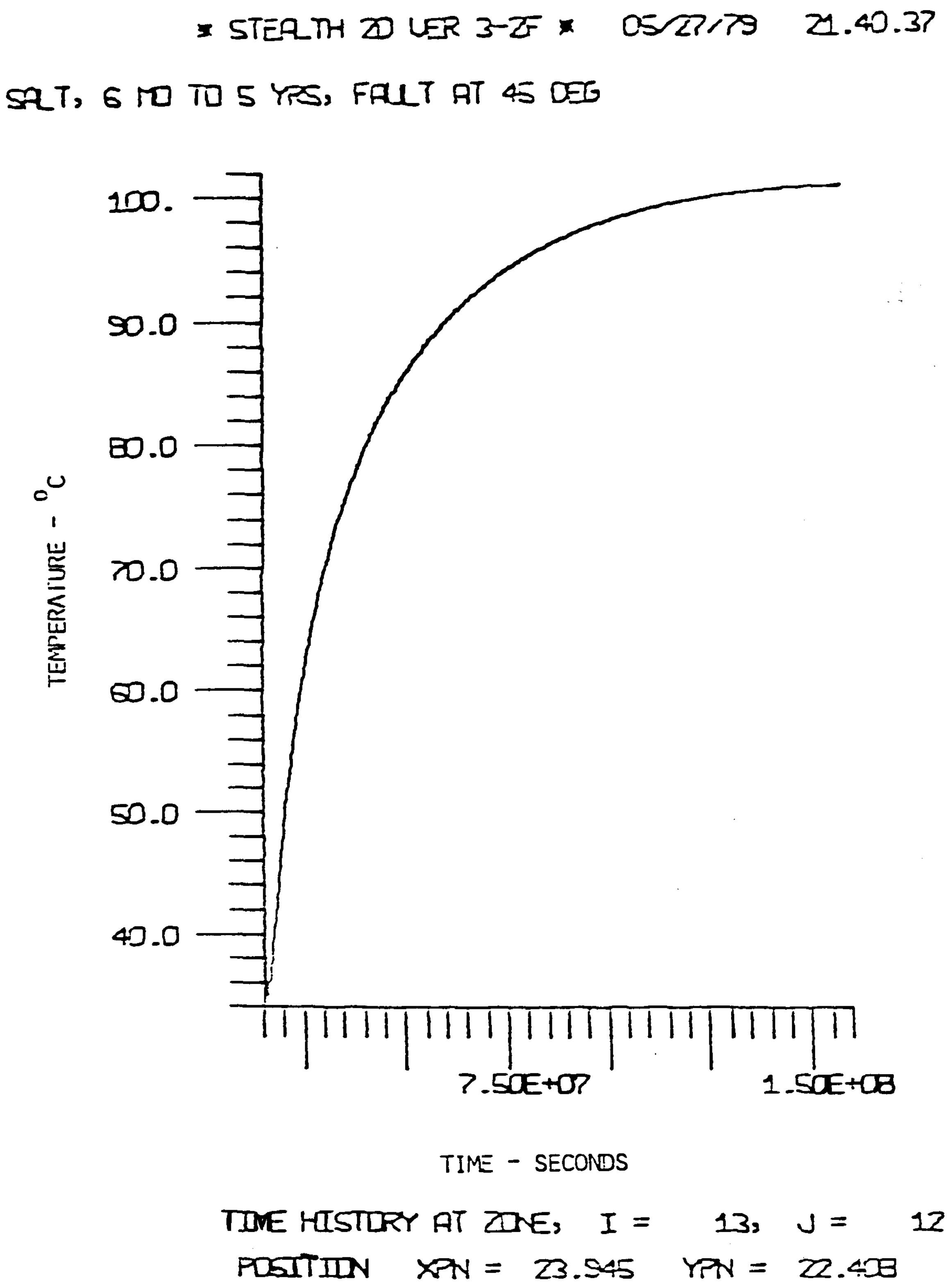

FIGURE 26. Temperature History Adjacent to the Heat Source in Salt (Case 5)

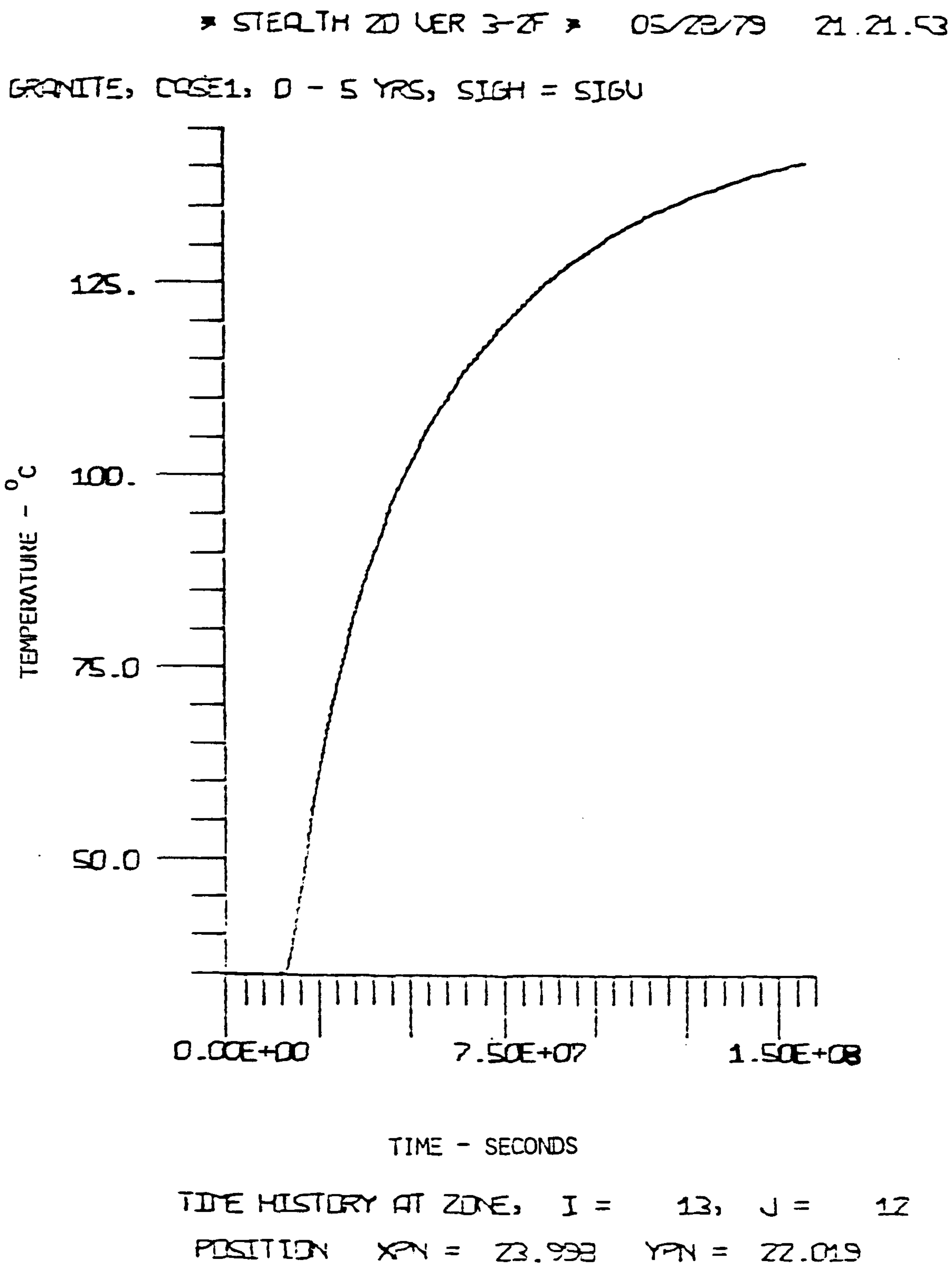

FIGURE 27. Temperature History Adjacent to the Heat Source in Granite (Case 1)

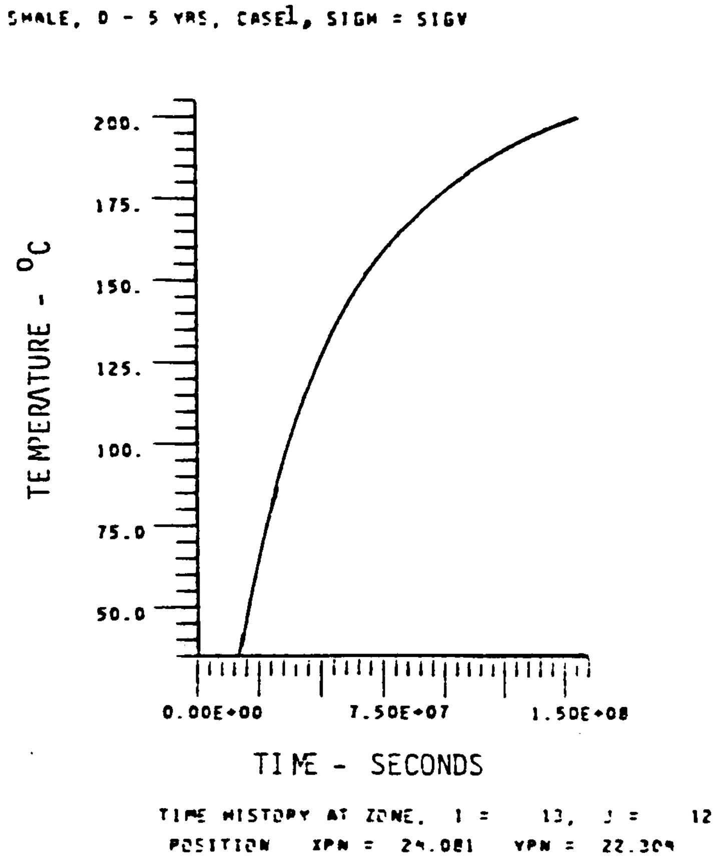

FIGURE 28. Temperature History Adjacent to the Heat Source in Shale (Case 1)

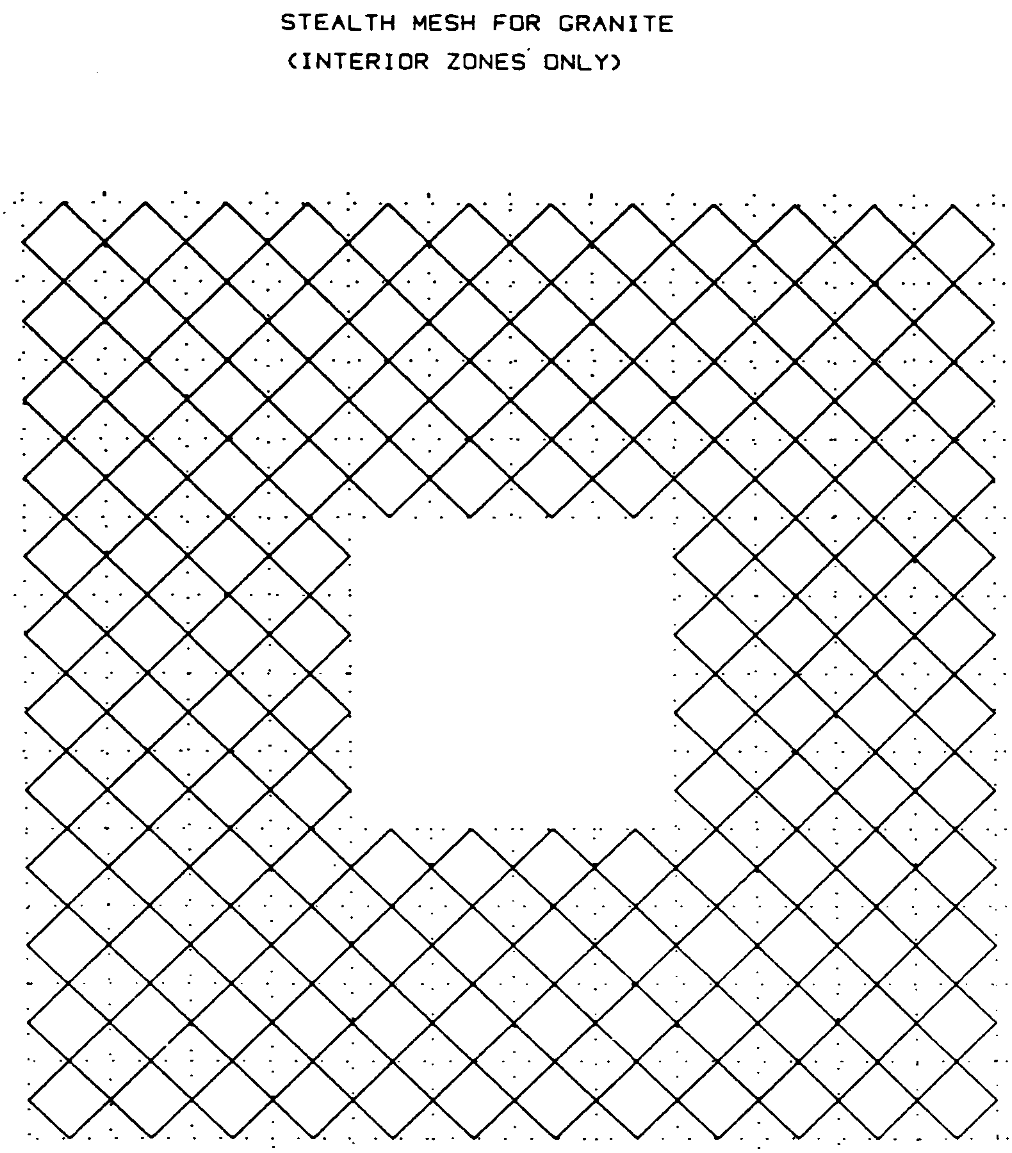

FIGURE 29. **Joint Pattern for Granite (solid lines) and Zone Boundaries (dotted lines)**

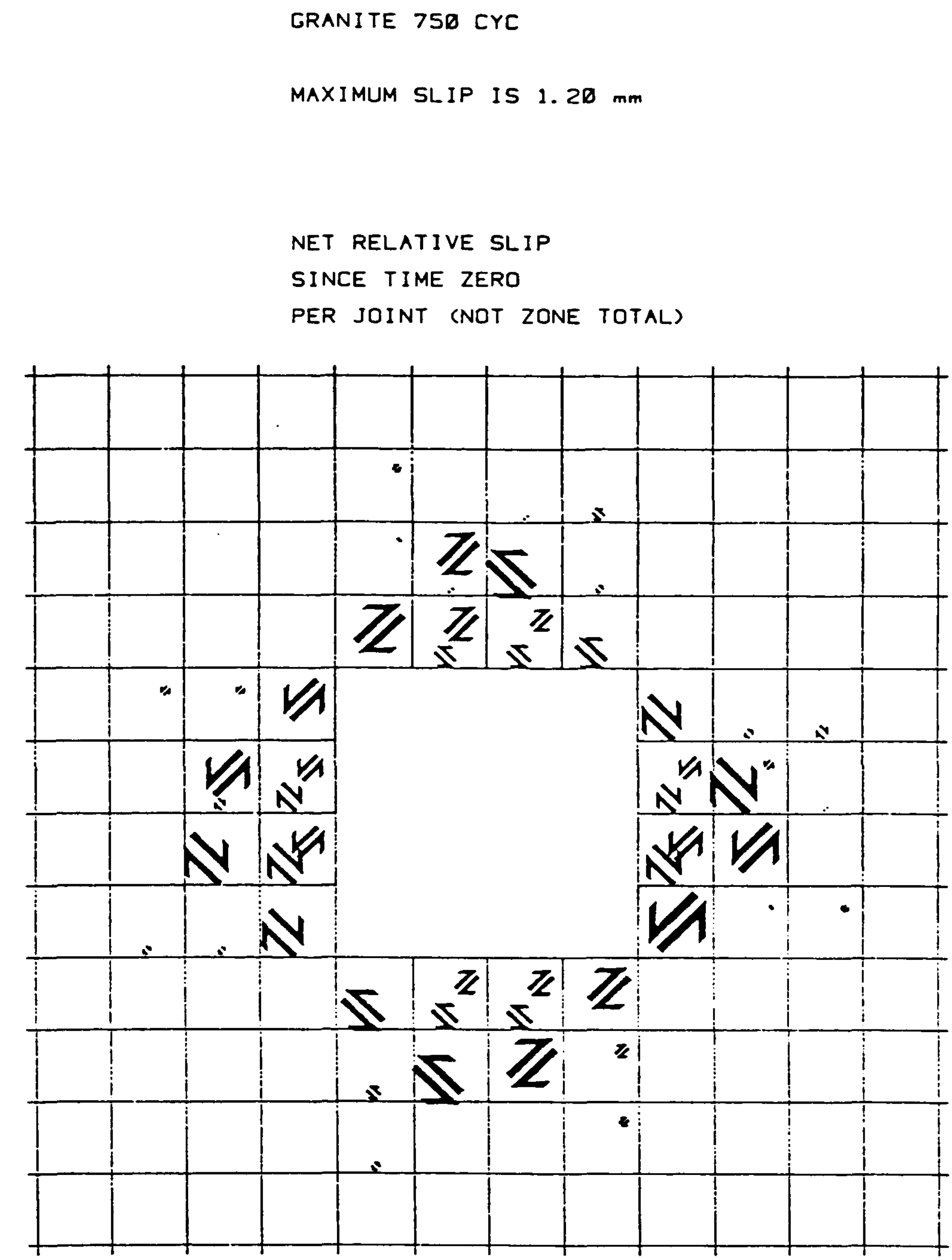

FIGURE 30. **Slip Pattern in Granite After Heating and Transition Phases, Stress Ratio = 1:1:1**

GRANITE 3 S ORO

MAXIMUM SLIP IS 1.20 mm

NET RELATIVE SLIP
SINCE TIME ZERO
PER JOINT (NOT ZONE TOTAL)

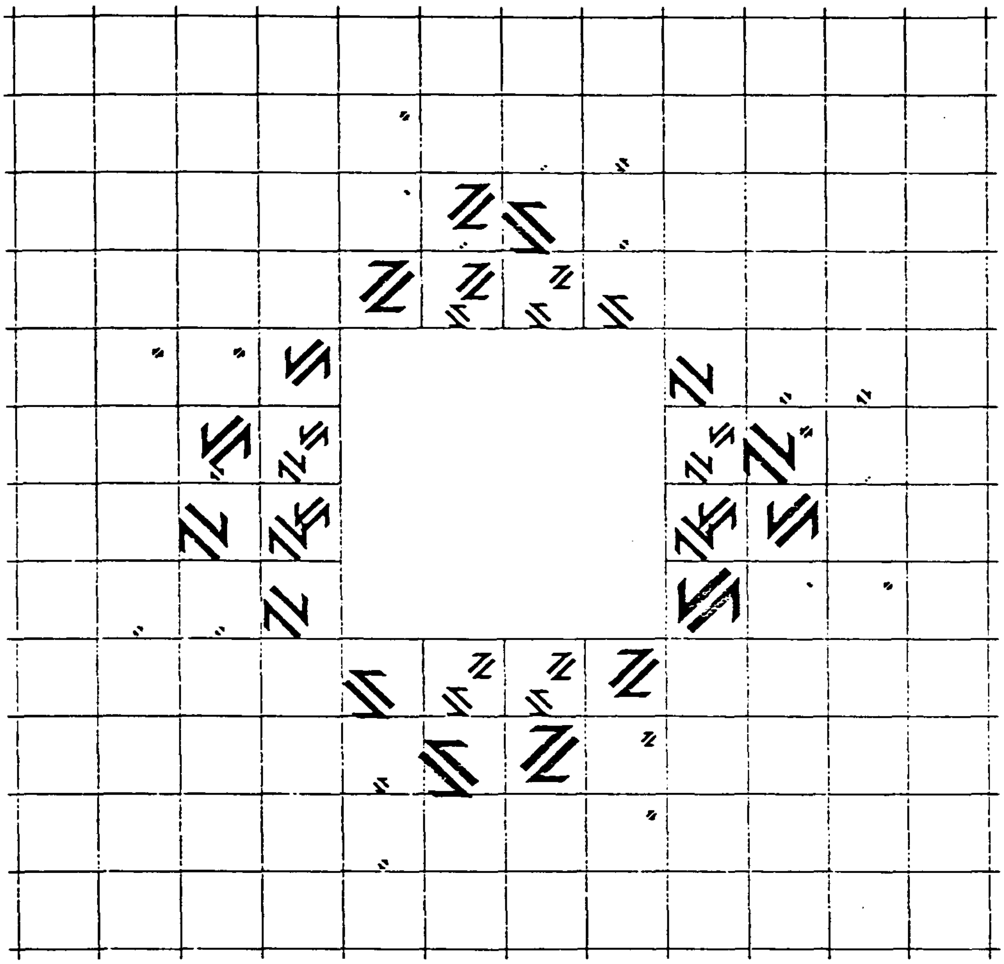

FIGURE 31. Slip Pattern in Granite After Oroville Earthquake, Stress Ratio = 1:1:1

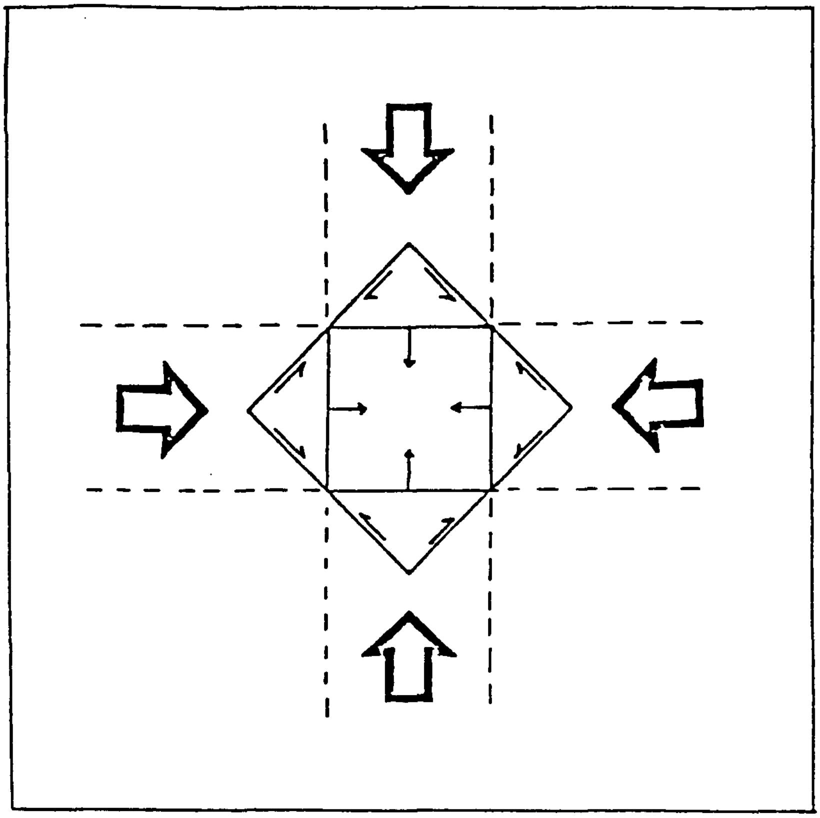

FIGURE 32. Double Direct-Shear Test Analogy for Granite

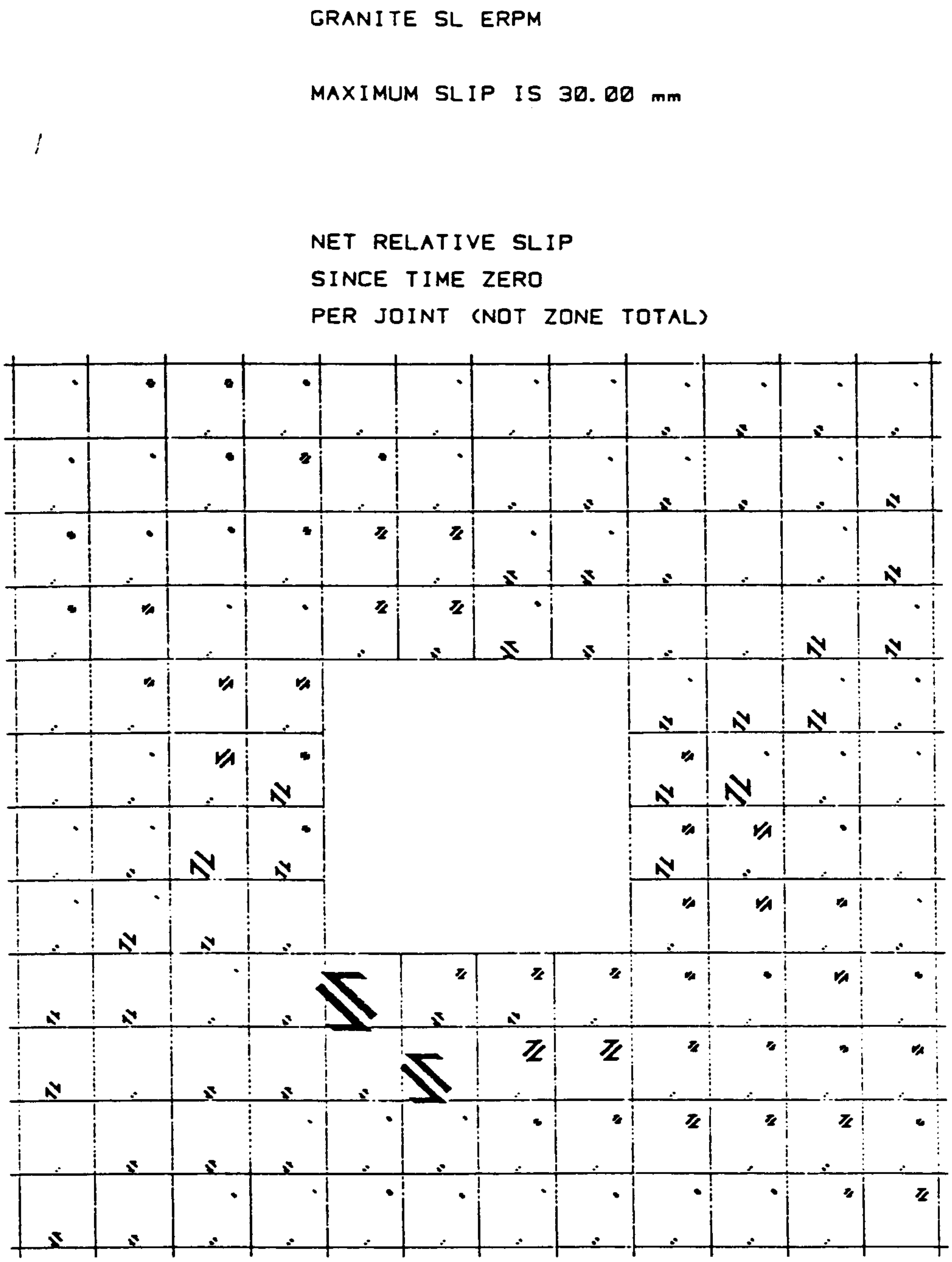

FIGURE 33. Slip Pattern in Granite (Case 6) After ERPM Earthquake (not entire record), Stress Ratio = 1:1:1

CASE 7 - TRNS

MAXIMUM SLIP IS 30.00 mm

NET RELATIVE SLIP
SINCE TIME ZERO
PER JOINT (NOT ZONE TOTAL)

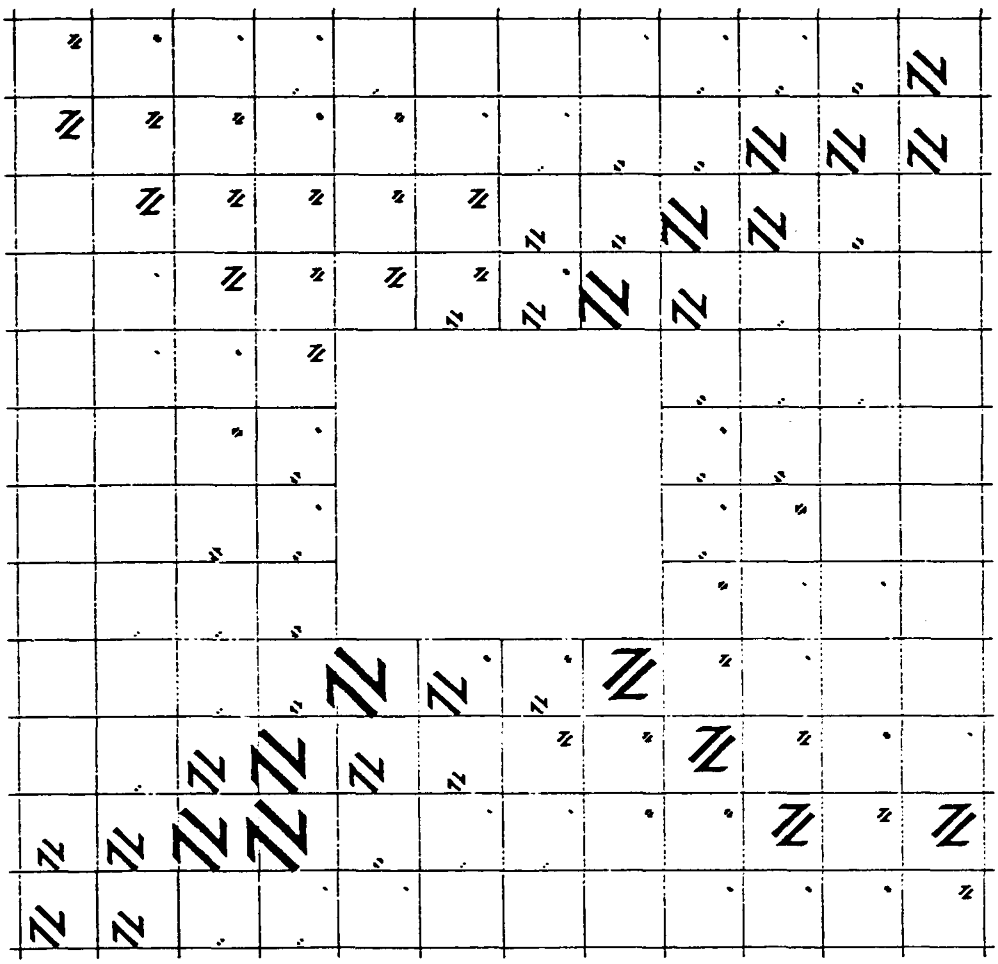

FIGURE 34. Slip Pattern in Granite (Case 7) After Heating and Transition Phases, Stress Ratio = 1:2:1

CASE 8 - TRNS

MAXIMUM SLIP IS 6.00 mm

NET RELATIVE SLIP
SINCE TIME ZERO
PER JOINT (NOT ZONE TOTAL)

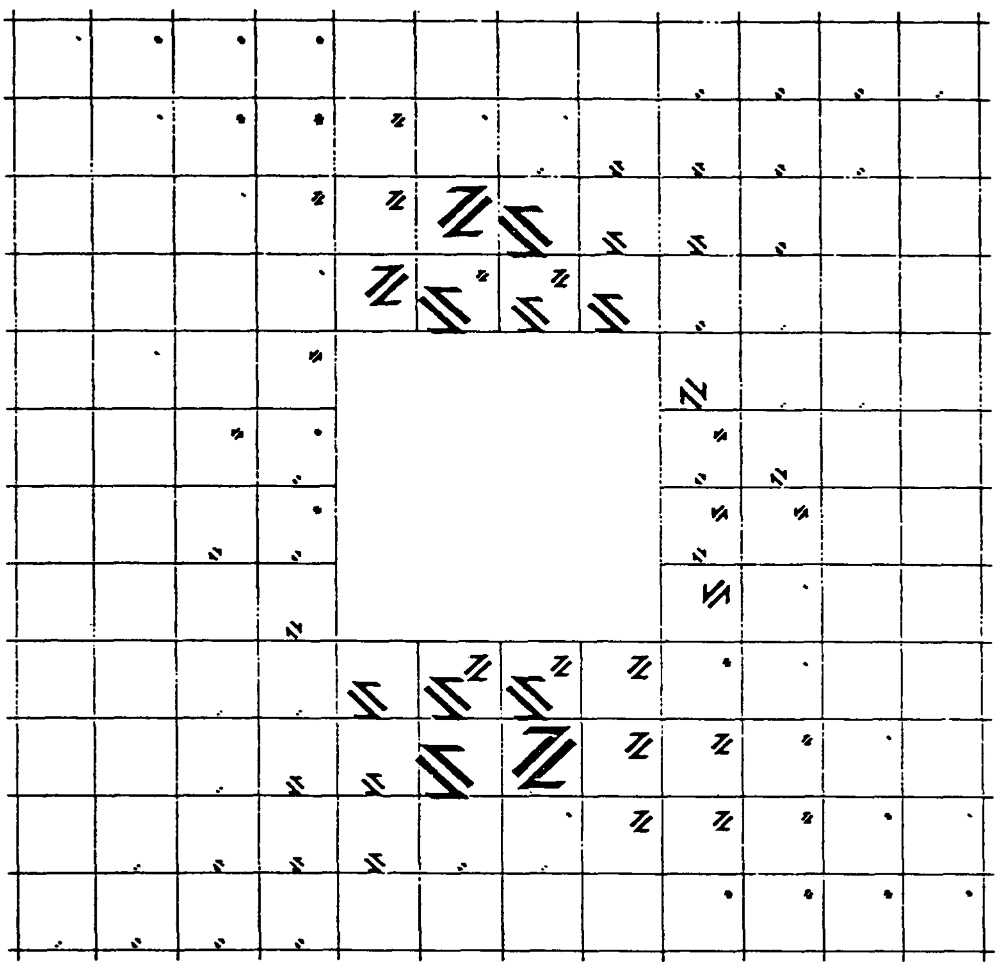

FIGURE 35. Slip Pattern in Granite (Case 8) After Heating and Transition Phases, Stress Ratio = 1:1.5:1.5

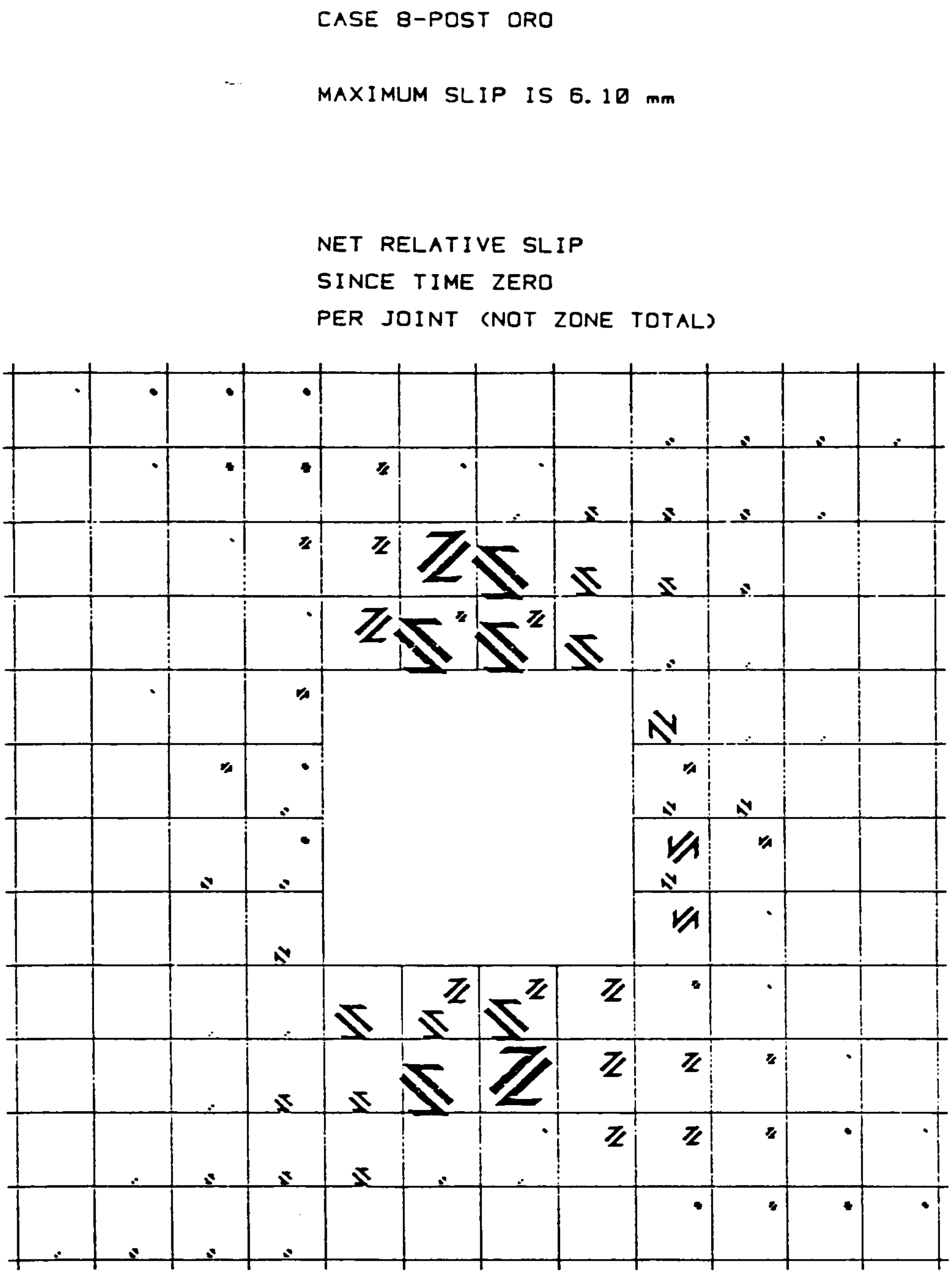

FIGURE 36. Slip Pattern in Granite (Case 8) After Oroville Earthquake, Stress Ratio = 1:1.5:1.5

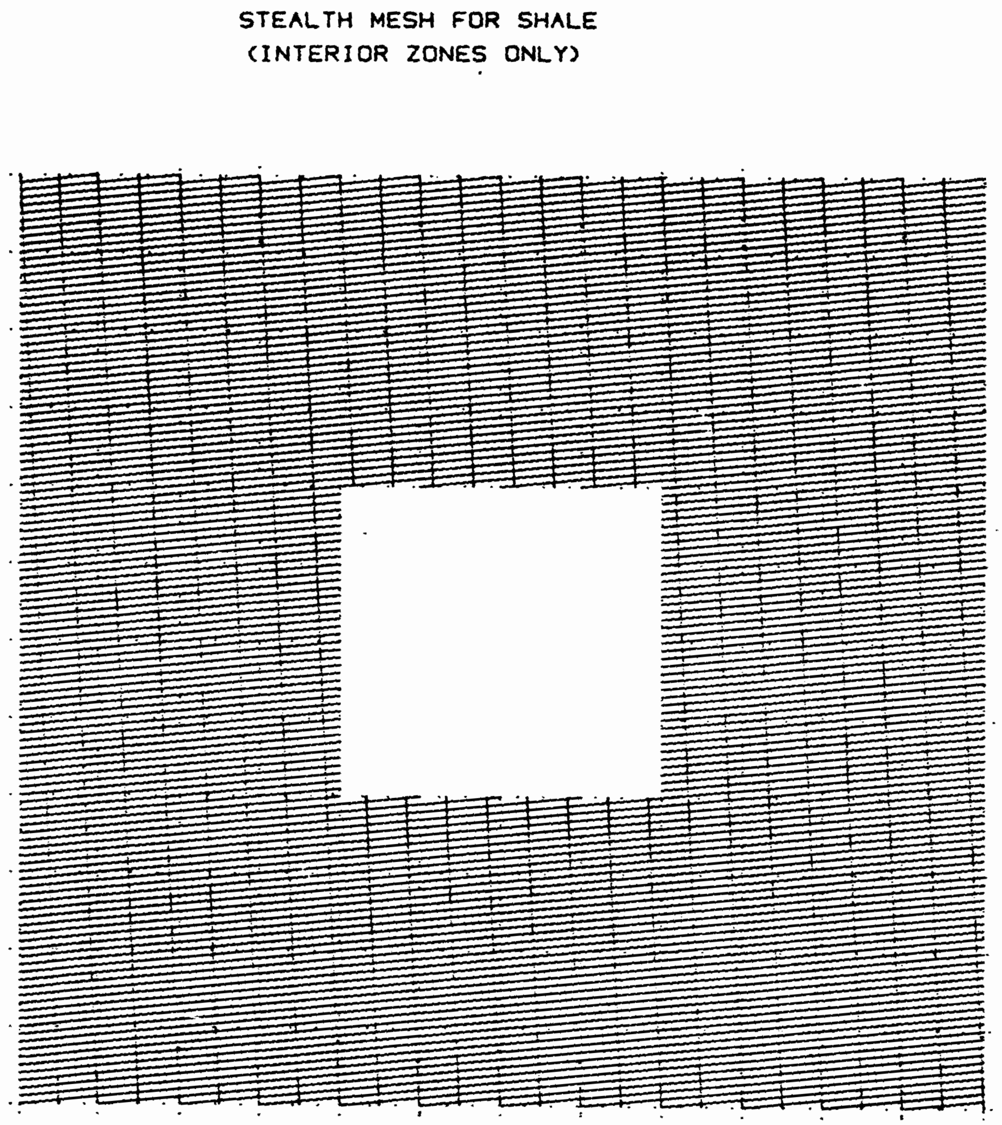

FIGURE 37. Joint Pattern for Shale (solid lines) and Zone Boundaries (dotted lines)

SHALE 800 CYC

MAXIMUM SLIP IS 49.00 mm

NET RELATIVE SLIP
SINCE TIME ZERO
PER JOINT (NOT ZONE TOTAL)

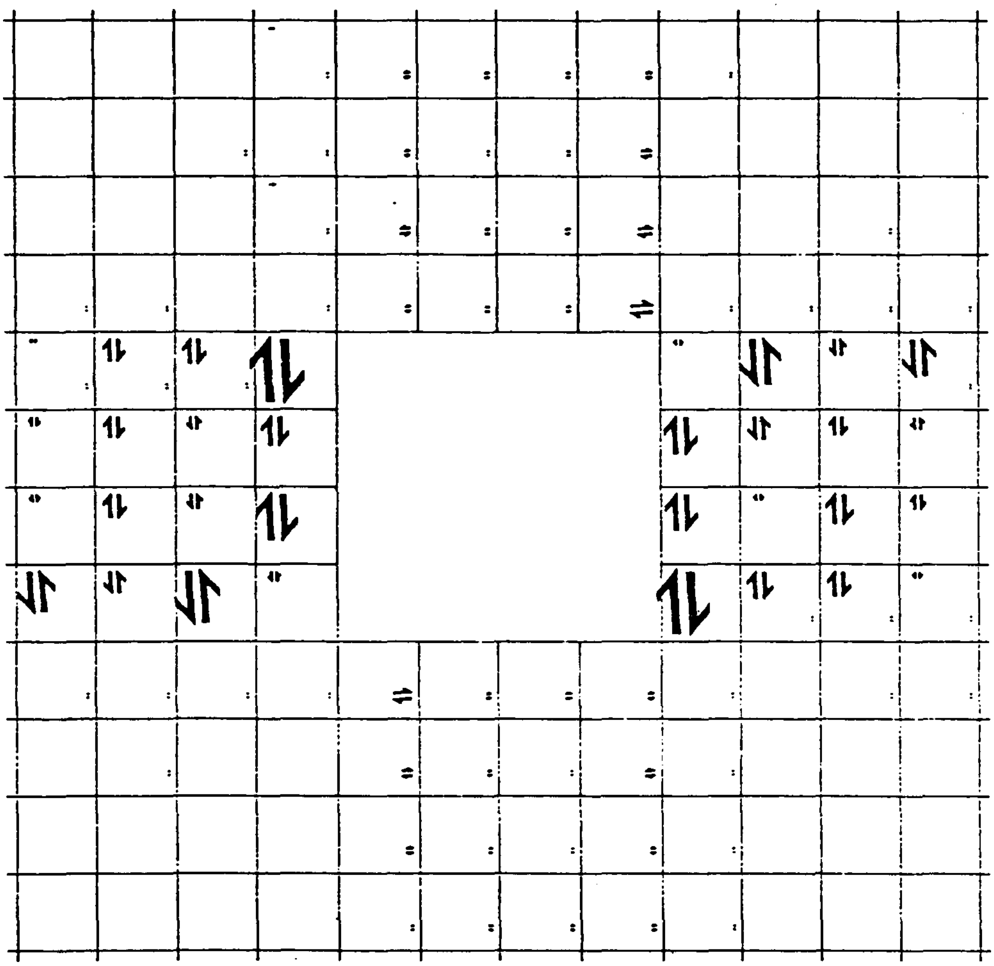

FIGURE 38. Slip Pattern in Shale (Case 1) After Heating and Transition Phases

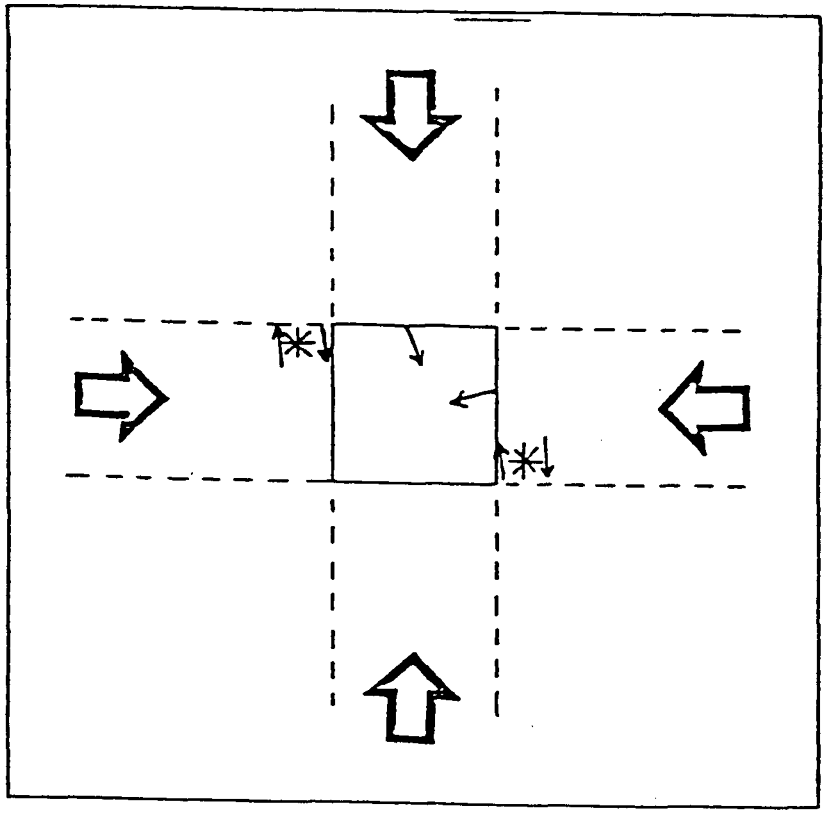

FIGURE 39. Double Direct-Shear Test Analogy for Shale

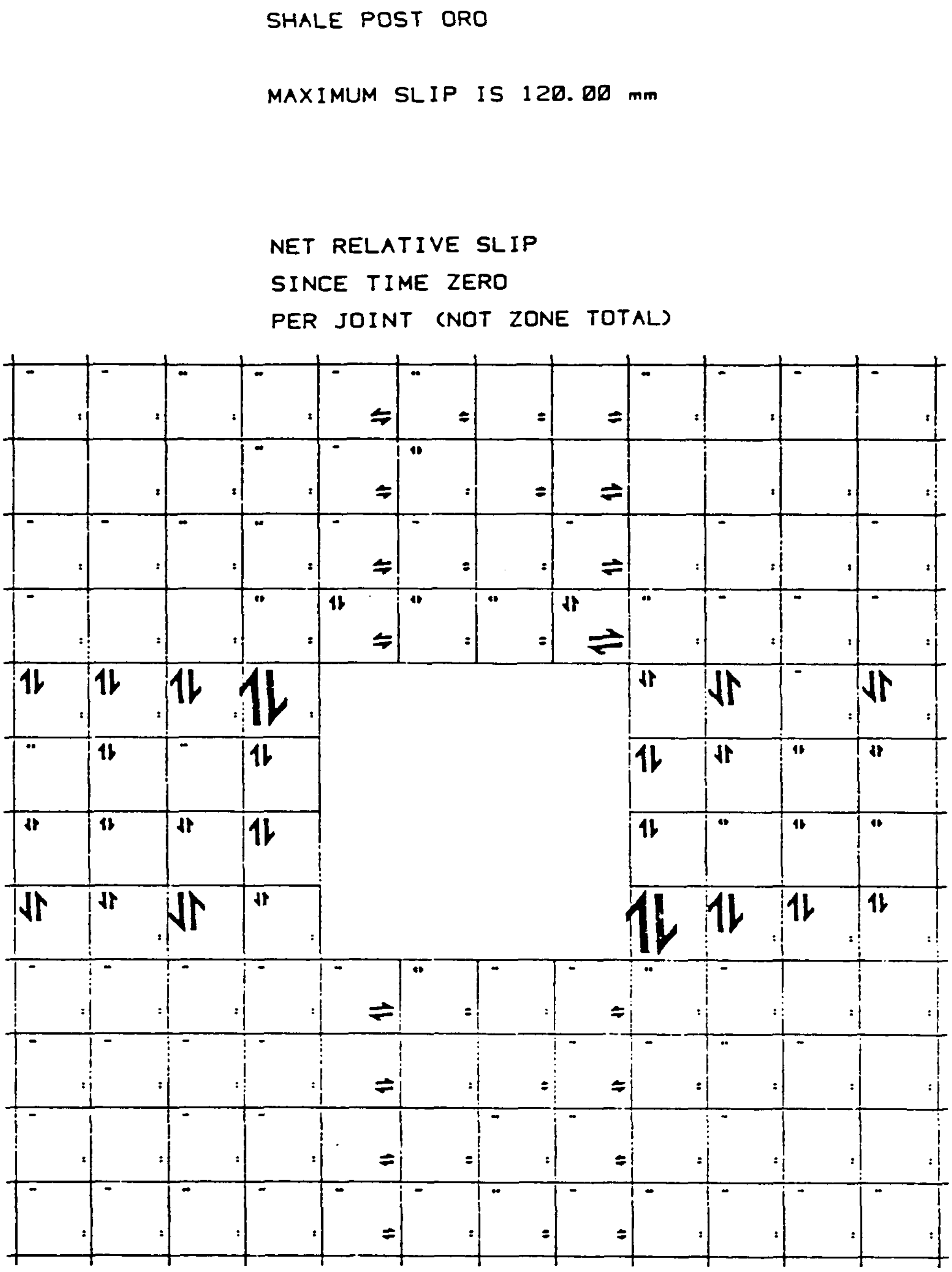

FIGURE 40. Slip Pattern for Shale (Case 1) After Oroville Earthquake (not entire record)

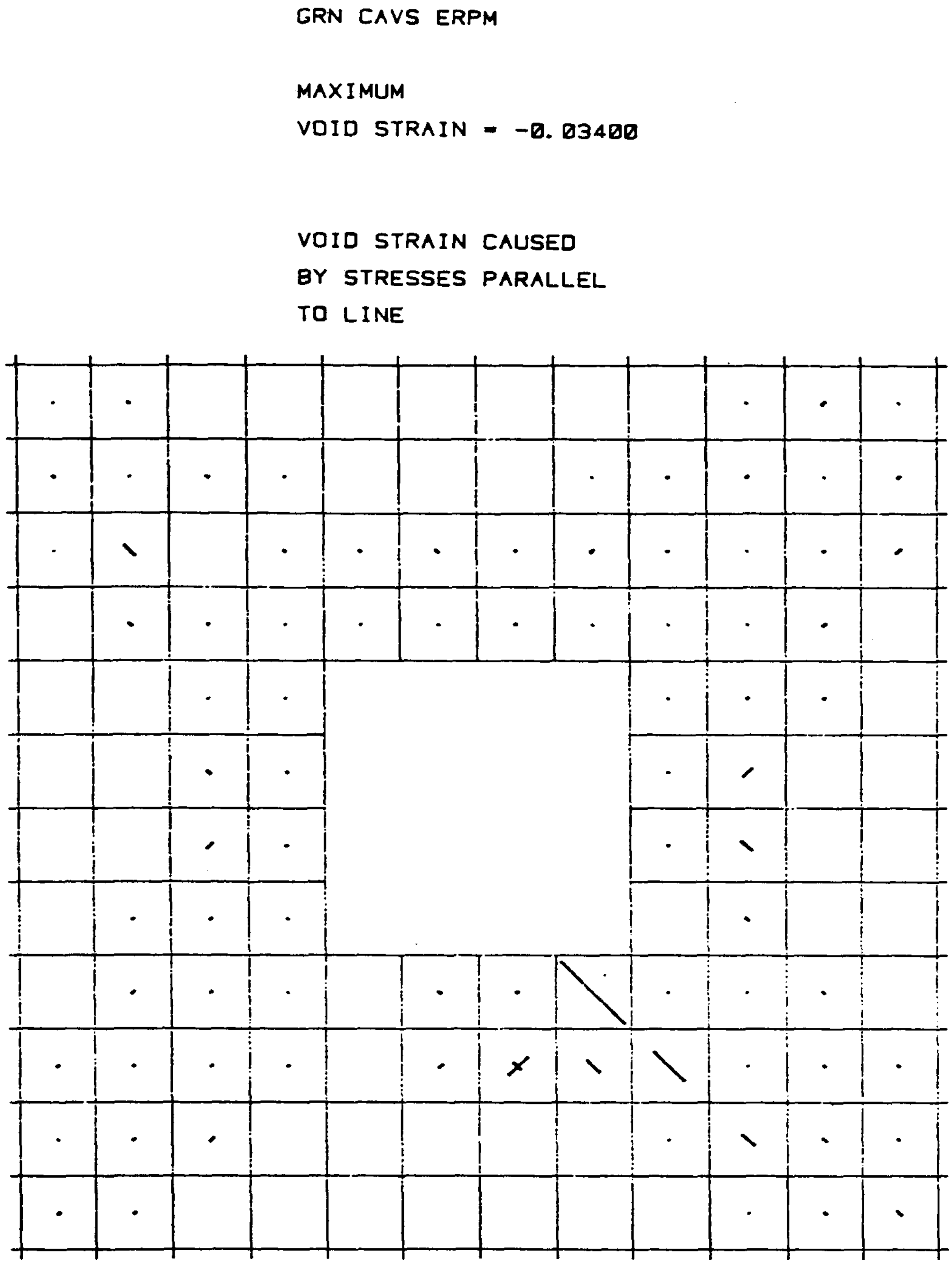

FIGURE 41. **Void Strain Pattern in Granite (Case 6) After ERPM Earthquake (not entire record), Stress Ratio = 1:1:1**

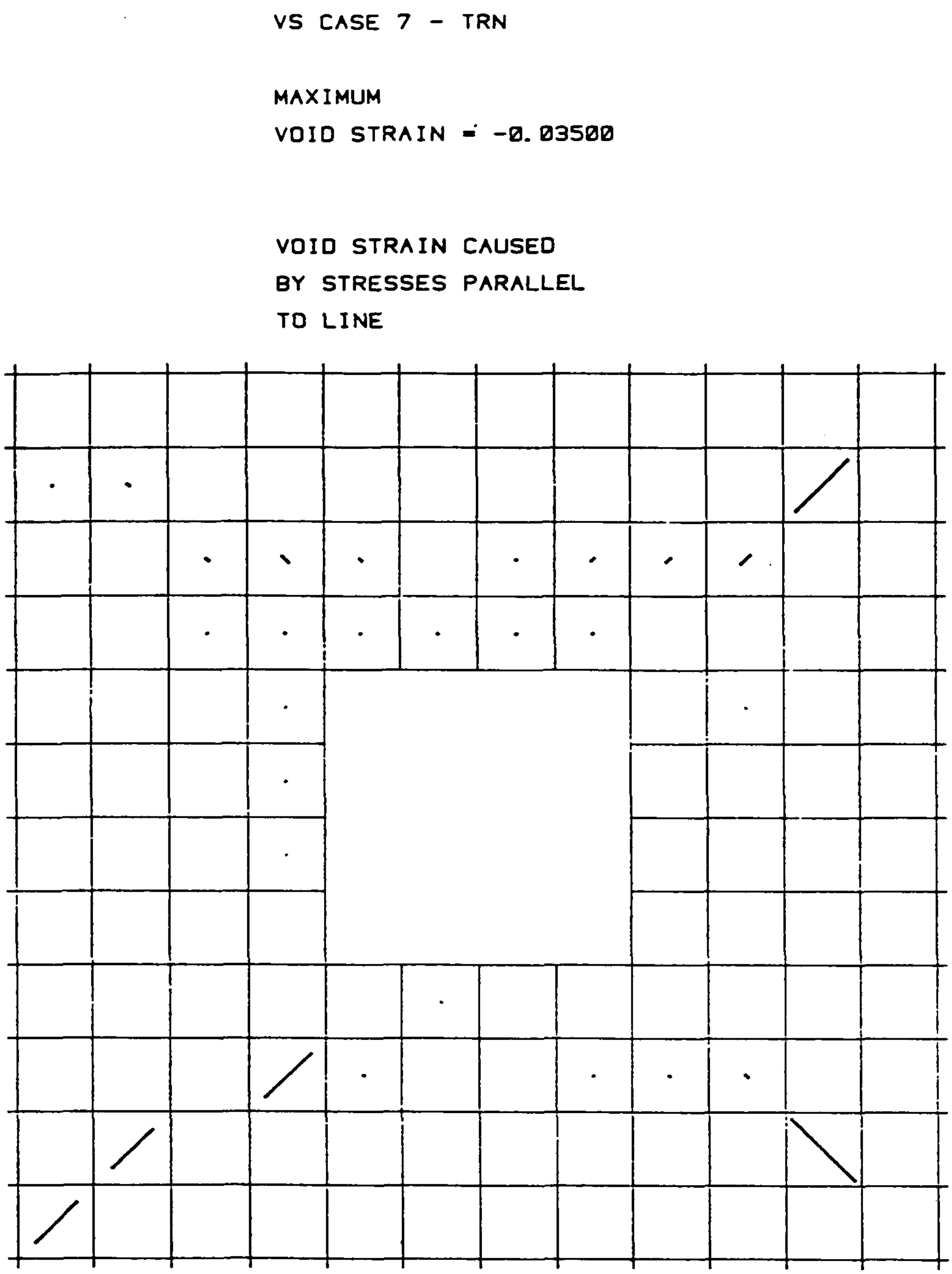

FIGURE 42. Void Strain Pattern in Granite (Case 7) After Heating and Transition Phases, Stress Ratio = 1:2:1

VS CASE 8 - TRN

MAXIMUM
VOID STRAIN = -0.00360

VOID STRAIN CAUSED
BY STRESSES PARALLEL
TO LINE

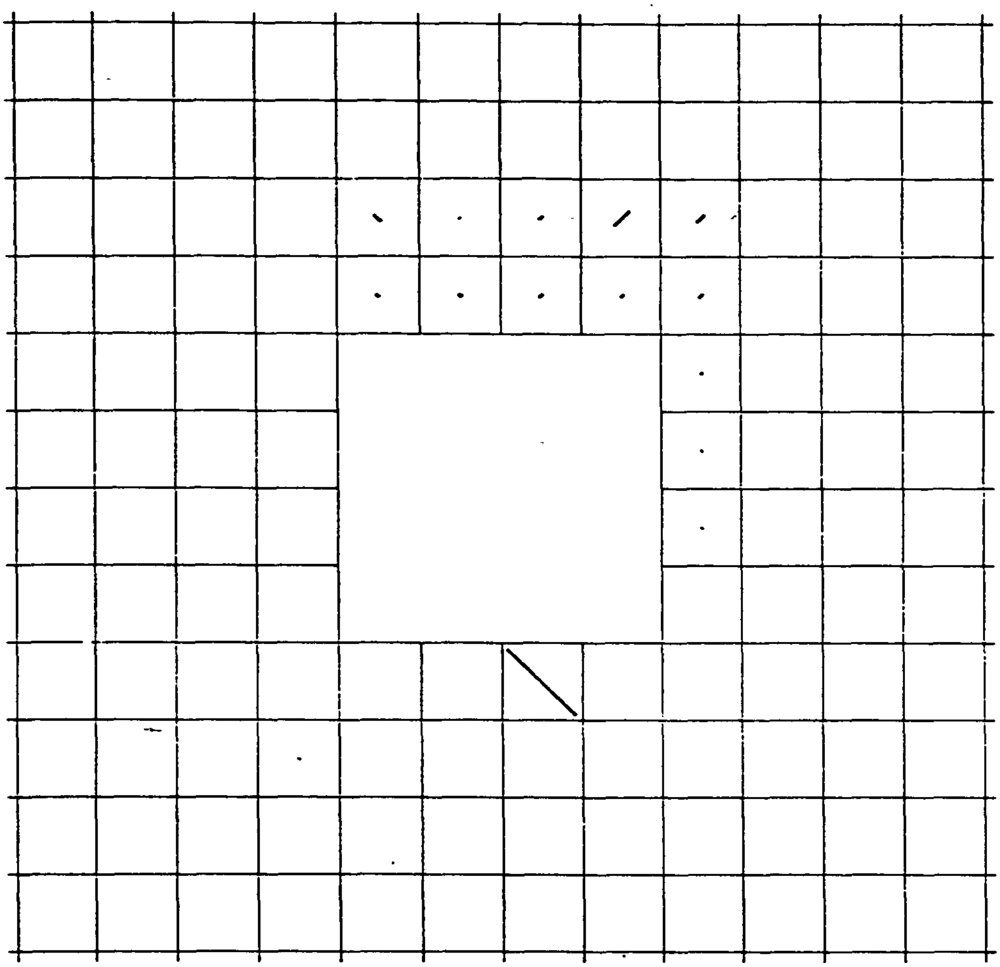

FIGURE 43. Void Strain Pattern in Granite (Case 8) After Heating and Transition Phases, Stress Ratio = 1:1.5:1.5

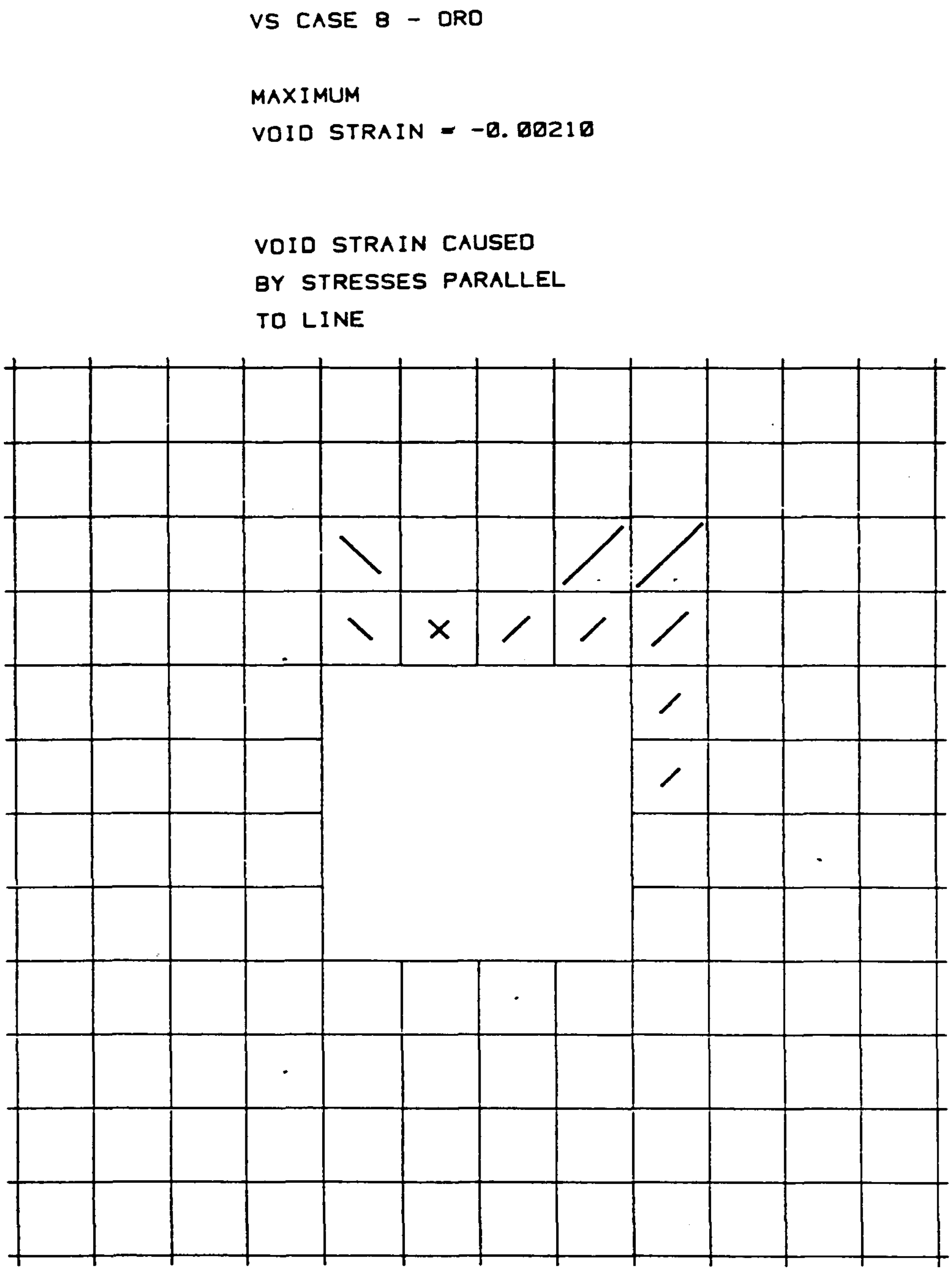

FIGURE 44. Void Strain Pattern in Granite (Case 8) After Oroville Earthquake, Stress Ratio = 1:1.5:1.5

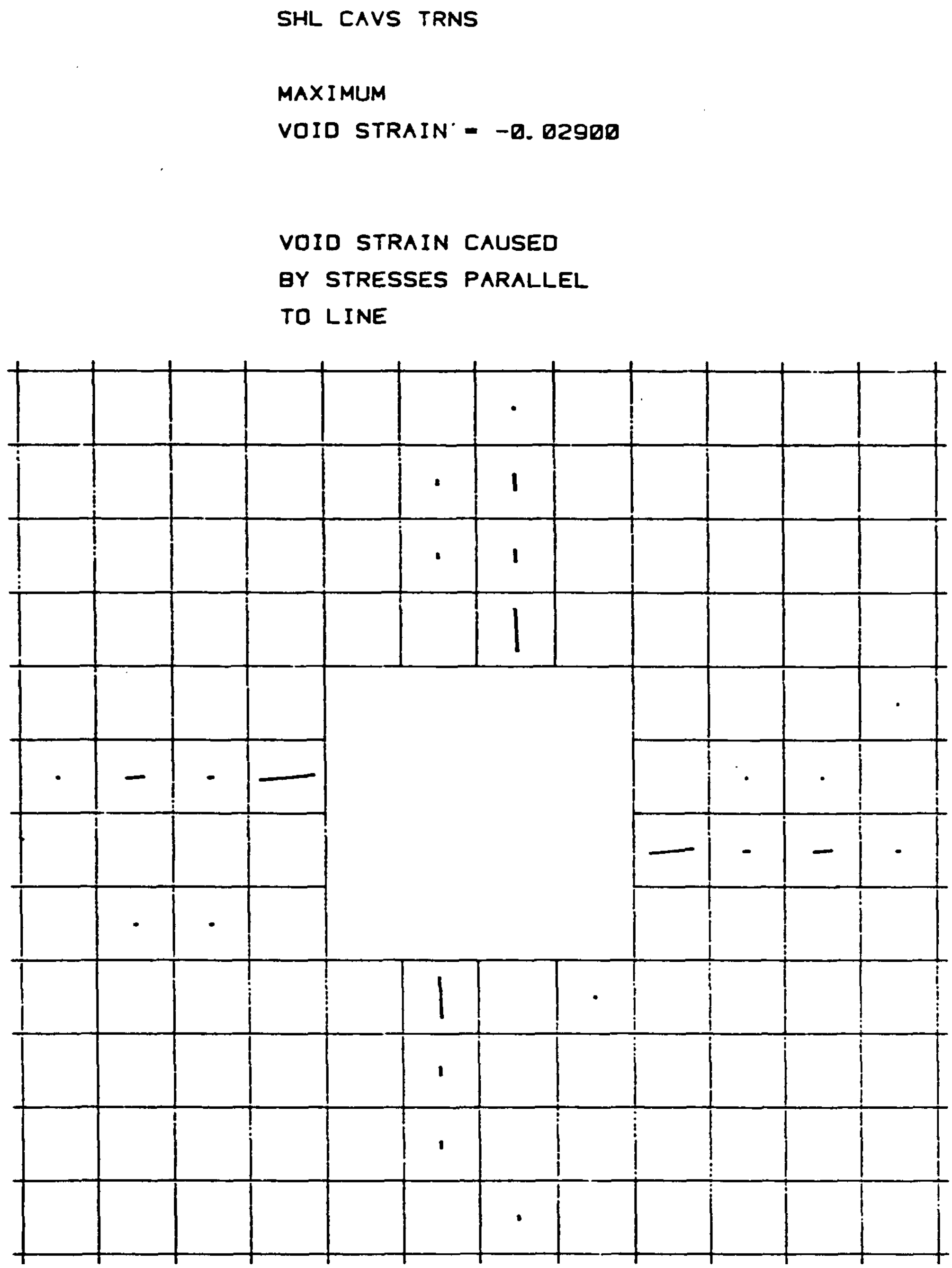

FIGURE 45. Void Strain Pattern in Shale (Case 1) After Heating and Transition Phases

SHL CAVS ORO

MAXIMUM
VOID STRAIN = -0.31000

VOID STRAIN CAUSED
BY STRESSES PARALLEL
TO LINE

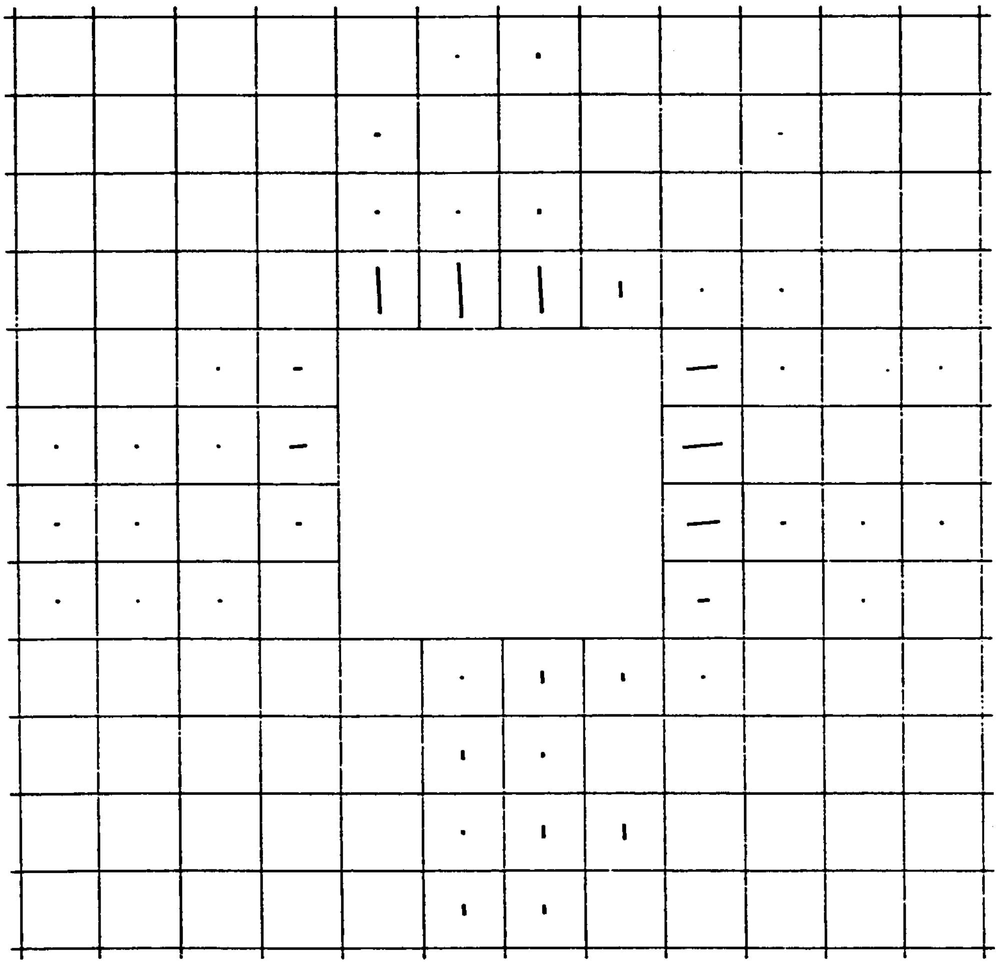

FIGURE 46. Void Strain Pattern in Shale (Case 1) After Oroville Earthquake (not entire record).

SALT CAVS ERPM

MAXIMUM
VOID STRAIN = -0.91000

VOID STRAIN CAUSED
BY STRESSES PARALLEL
TO LINE

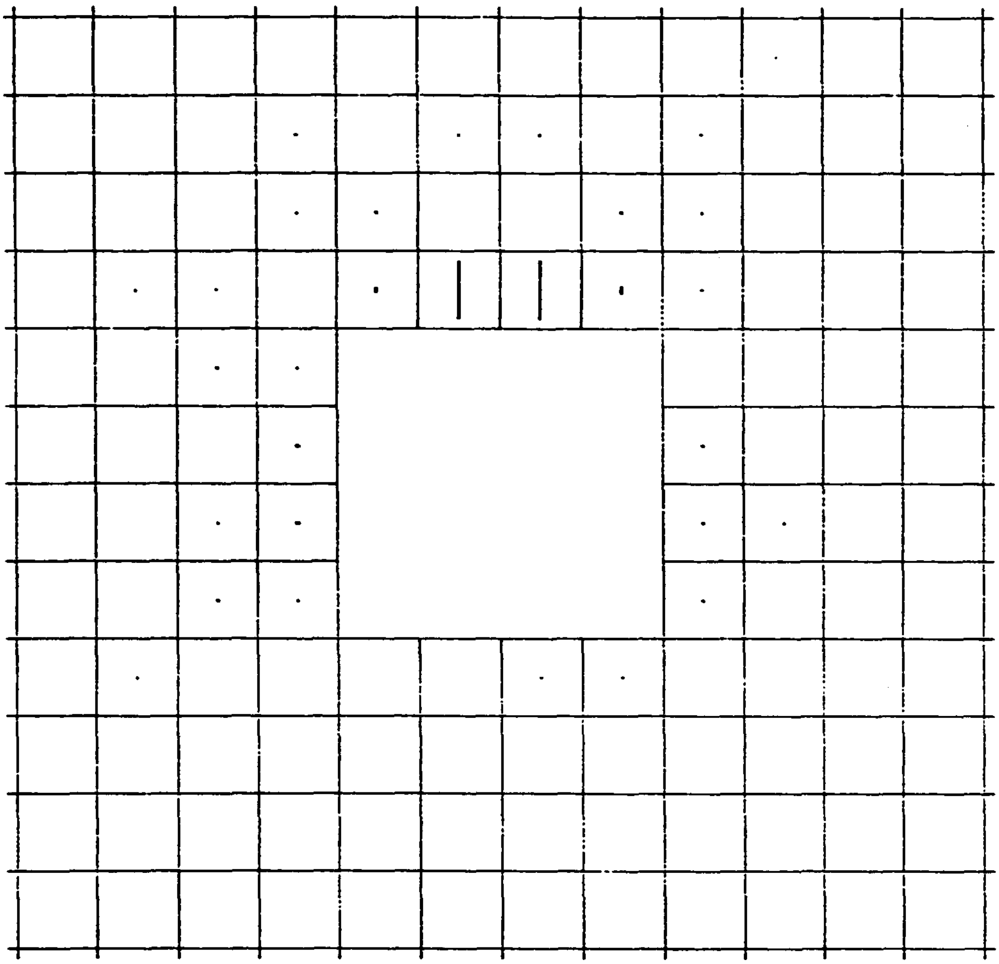

FIGURE 47. **Void Strain Pattern in Salt (Case 3) After ERPM Earthquake (not entire record)**

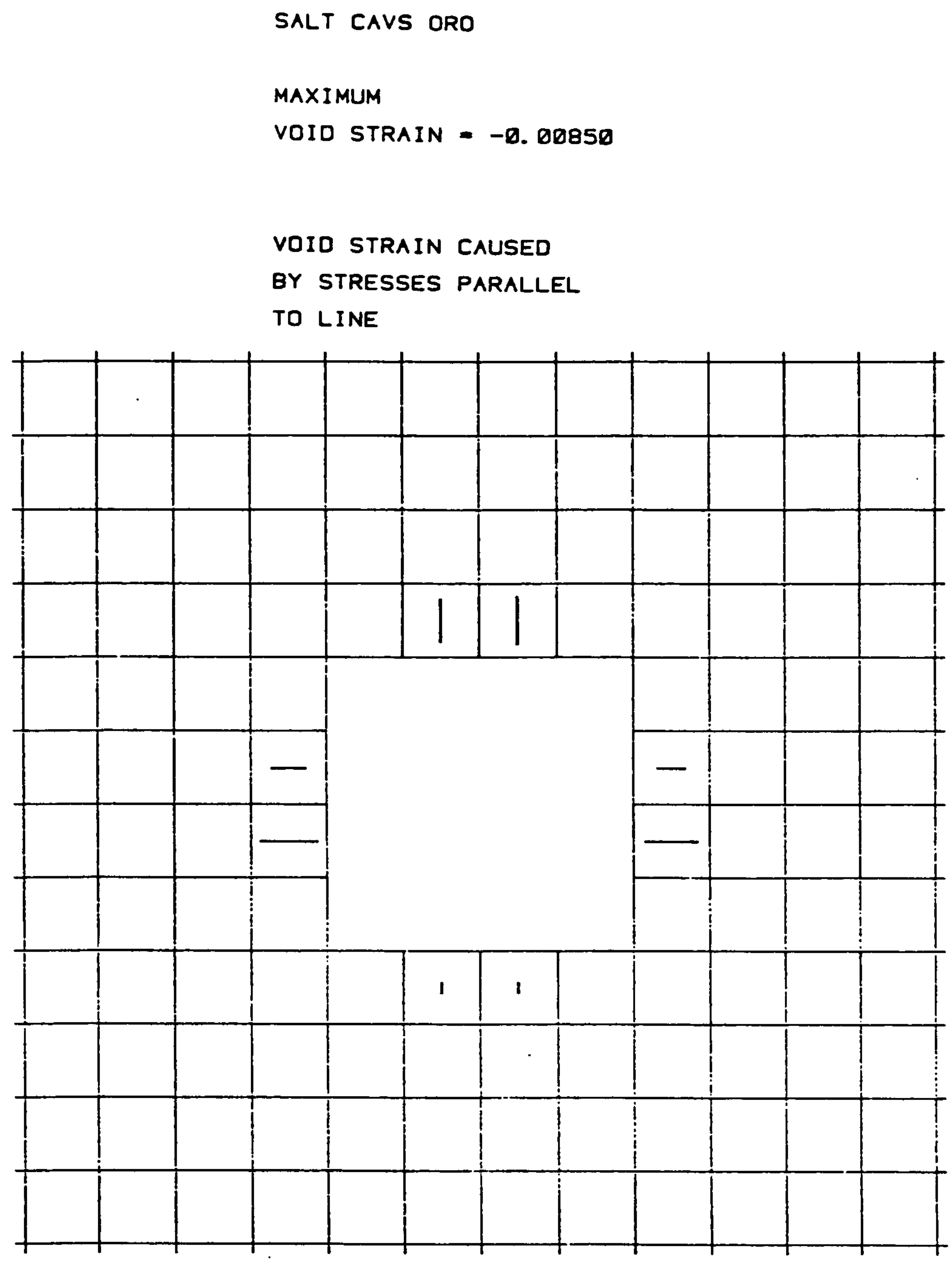

FIGURE 48. **Void Strain Pattern in Salt (Case 1) After Oroville Earthquake**

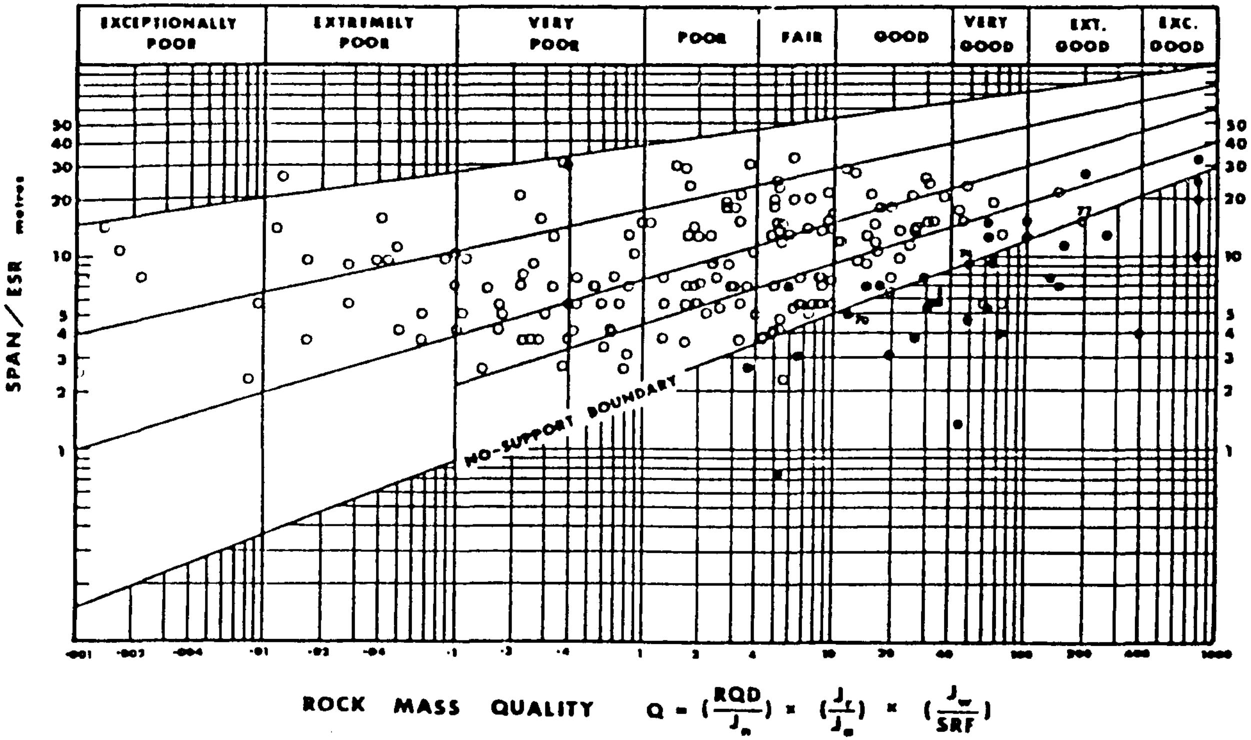

FIGURE 49. Analysis of Case Records Indicating Approximate Boundary Between Supported (o) and Unsupported Excavations (•) (Barton, 1975)

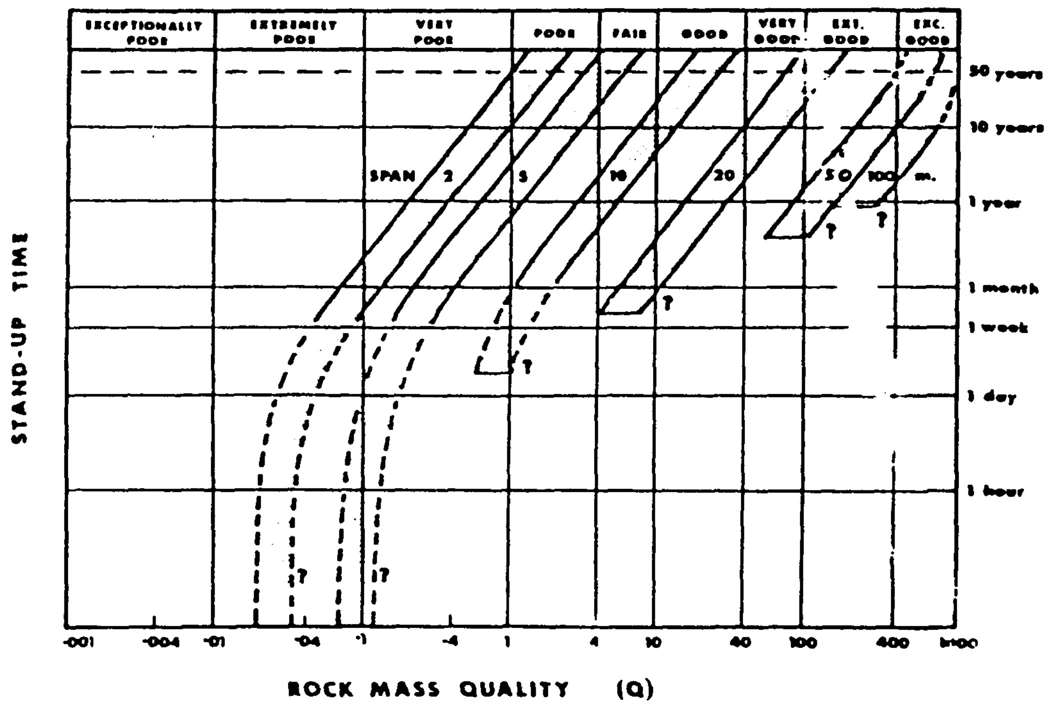

FIGURE 50. Estimate of Stand-up Time When the Span of an Unsupported Excavation is Increased Beyond the Maximum for Permanent Openings (Barton, 1975)

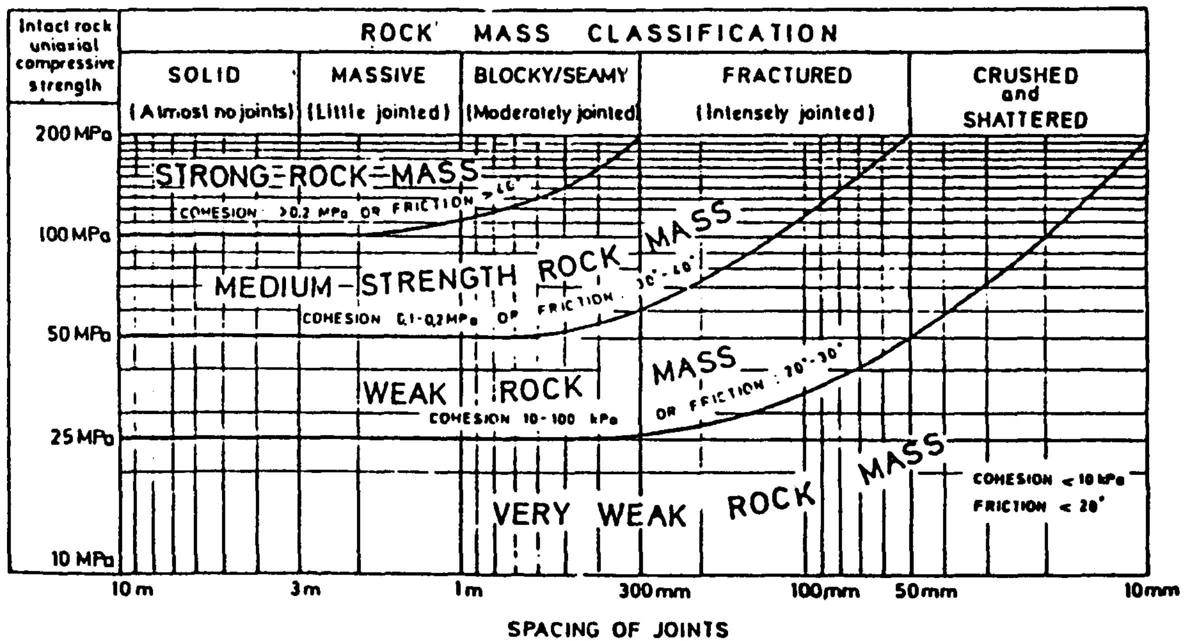

FIGURE 51. Strength Diagram of Jointed Rock Masses (Bienawski, 1973; Modified After Muller)

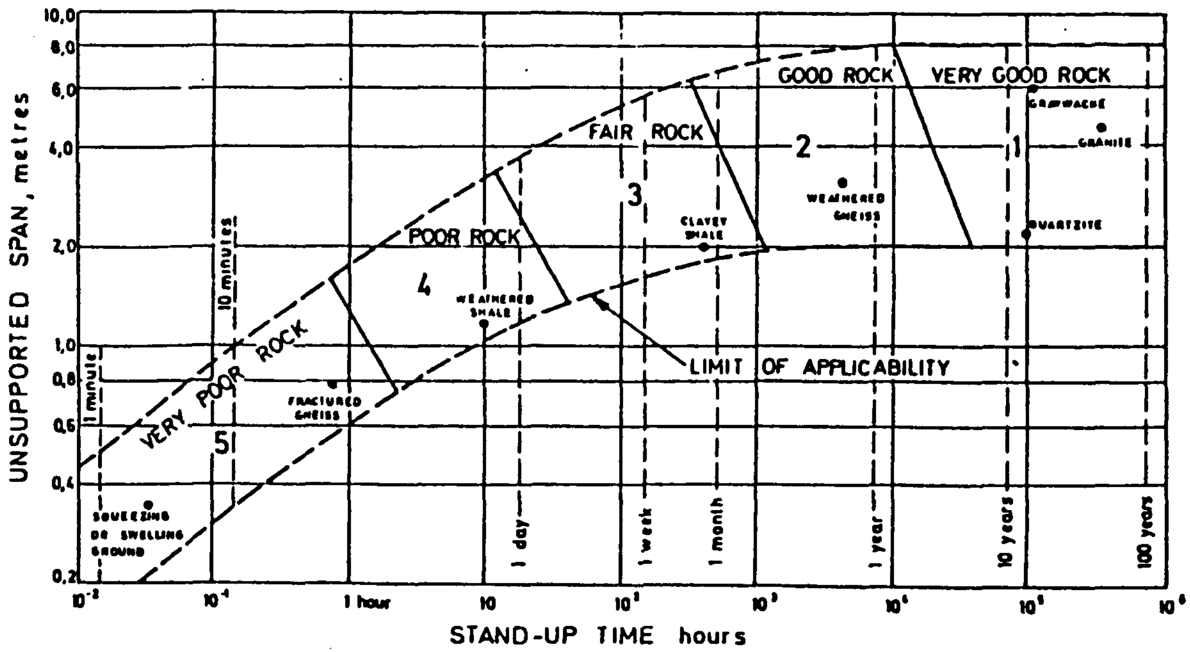

FIGURE 52. Rock Mass Classification for Tunnelling (Bienawski, 1973; Modified After Lauffer)

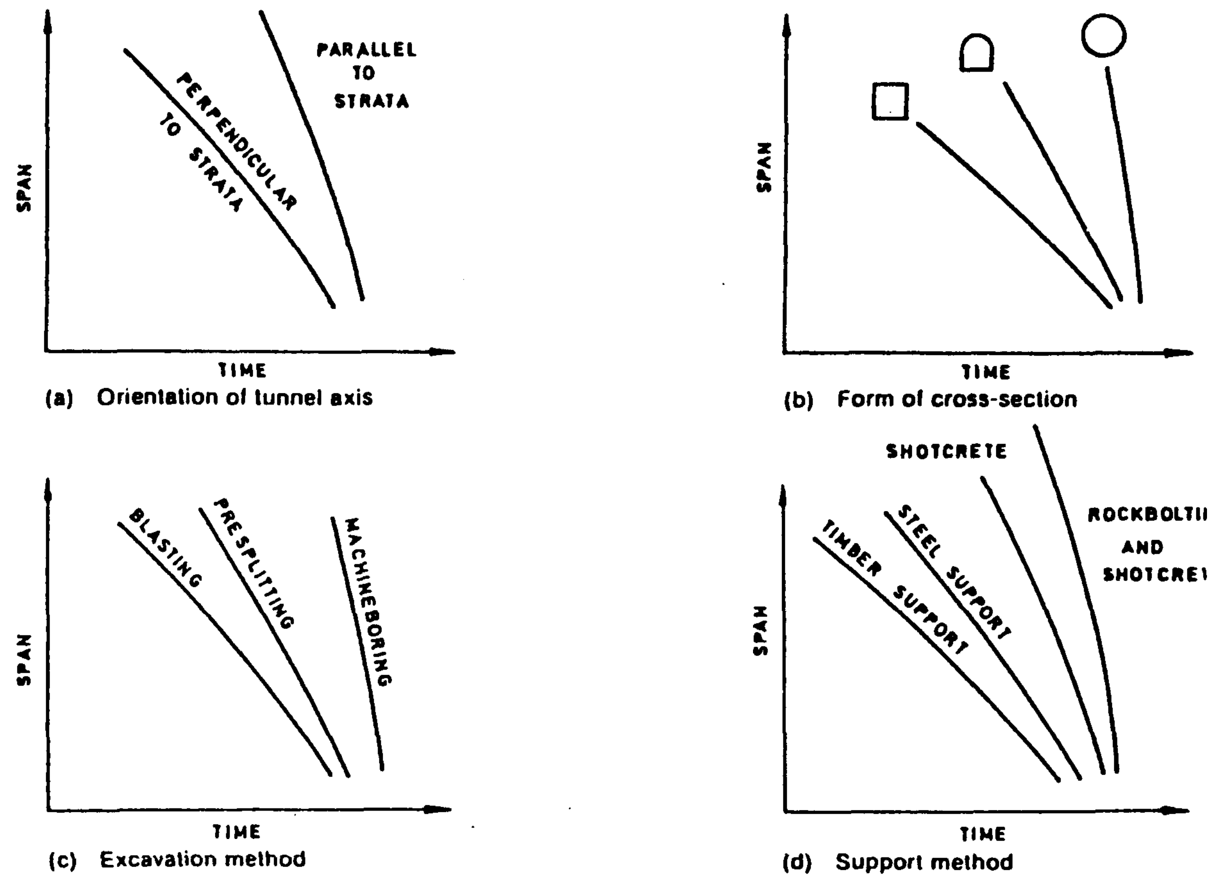

FIGURE 53. Factors Influencing Rock Mass Stability During Tunnelling (Bienawski, 1973; Schematically After Lauffer)